

Journal Pre-proof

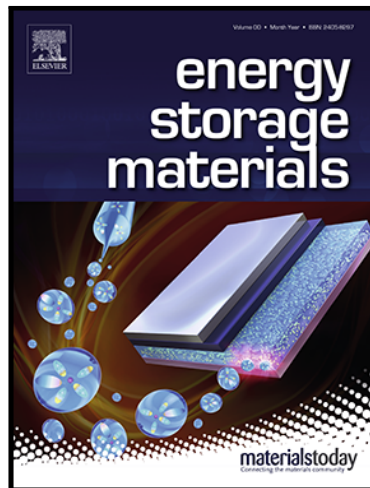
Diverting Exploration of Silicon Anode into Practical Way: A Review Focused on Silicon-Graphite Composite for Lithium Ion Batteries

Peng Li , Hun Kim , Seung-Taek Myung , Yang-Kook Sun

PII: S2405-8297(20)30438-4

DOI: <https://doi.org/10.1016/j.ensm.2020.11.028>

Reference: ENSM 1422



To appear in: *Energy Storage Materials*

Received date: 29 September 2020

Revised date: 10 November 2020

Accepted date: 17 November 2020

Please cite this article as: Peng Li , Hun Kim , Seung-Taek Myung , Yang-Kook Sun , Diverting Exploration of Silicon Anode into Practical Way: A Review Focused on Silicon-Graphite Composite for Lithium Ion Batteries, *Energy Storage Materials* (2020), doi: <https://doi.org/10.1016/j.ensm.2020.11.028>

This is a PDF file of an article that has undergone enhancements after acceptance, such as the addition of a cover page and metadata, and formatting for readability, but it is not yet the definitive version of record. This version will undergo additional copyediting, typesetting and review before it is published in its final form, but we are providing this version to give early visibility of the article. Please note that, during the production process, errors may be discovered which could affect the content, and all legal disclaimers that apply to the journal pertain.

© 2020 Published by Elsevier B.V.

Highlights

- Cooperation strategies of silicon-graphite anodes are systematically concluded.
- Lithium storage behaviors are summarized based on recent studies.
- The designed hybrid anodes are rationally classified and introduced.
- Current bottlenecks toward practical lithium ion full cells are unveiled.

Journal Pre-proof

Article type: Review Article

**Diverting Exploration of Silicon Anode into Practical Way: A Review
Focused on Silicon-Graphite Composite for Lithium Ion Batteries**

Peng Li^a, Hun Kim^a, Seung-Taek Myung^{b} and Yang-Kook Sun^{a*}**

^aDepartment of Energy Engineering, Hanyang University, Seoul 04763, South Korea

^bDepartment of Nanotechnology and Advanced Materials Engineering, Sejong University,
Seoul, 05006, Republic of Korea

*Corresponding author.

**Corresponding author.

E-mail addresses: smyung@sejong.ac.kr (S.-T. Myung), yksun@hanyang.ac.kr (Y.-K. Sun)

Abstract

With the increasing need for maximizing the energy density of energy storage devices, silicon (Si) active material with ultrahigh theoretical capacity has been considered as promising candidate for next-generation anodes in lithium ion batteries (LIBs). However, their practical application has always been hindered by suppressed electrochemical properties, which arise from large volume changes and deteriorated electrode architecture during cycling process. Notably, recent developments have demonstrated that silicon active materials incorporated with tough graphite frameworks are very promising electrode candidates for efficient lithium storage devices, taking advantage of the high theoretical capacity of Si and ultrahigh stability of graphite. In this review, the necessity of co-exploitation of silicon and graphite is

highlighted, and representative silicon-graphite anodes along with various approaches for composite construction are organized. Moreover, critical issues, challenges, and perspectives of the Si-graphite electrodes are also systematically concluded and presented. With a deep understanding of associated electrochemical processes, the component and structural optimization of Si-graphite anodes could be effectively enhanced.

Keywords: Graphite; Silicon; Practical anode; Electrochemistry; Lithium ion battery

1. Introduction

Energy and environment are the most important themes for the sustainable development of human society. The continuous consumption of coal, petroleum, and natural gas has resulted in a growing concern regarding environmental pollution and the depletion of mineral energy.[1, 2] Consequently, lithium rechargeable batteries, as a kind of clean energy resource, have attracted worldwide attention, which mainly composed of four components, *i.e.*, anode, cathode, separator and electrolyte; two electrodes are divided by the separator, and electrolyte allows lithium ions to shuttle back and forth between anode and cathode.[3] It has been almost 30 years since the commercialization of lithium ion batteries (LIBs) in 1991, which have already been applied in many areas, such as aerospace, medical instruments, and portable devices, and widely regarded as one of the best power sources for low-emission or zero-emission vehicles, including electric and hybrid cars.[4, 5] In the case of anode, graphite is commercially adopted as the electrode material due to its high conductivity, good reversibility and low cost. Nevertheless, since every six carbon atoms can hold only one lithium atom, graphite apparently has limited energy density, making it increasingly difficult to meet the ever-growing demand for high-performance rechargeable batteries, along with the updates in apparatus and improvement of living quality.[6]

Numerous attempts have been made to discover appropriate electrode materials with higher output capacity. The investigation of high performance alternative anodes with novel active materials has gained a significant amount of attention.[7] As each silicon atom can bind to around four lithium ions, the silicon electrodes in LIBs possess a high theoretical gravimetric capacity (4200 mAh g^{-1} for $\text{Li}_{22}\text{Si}_5$ at 415°C and 3579 mAh g^{-1} for $\text{Li}_{15}\text{Si}_4$ at room-temperature), making it one of the most promising alternative candidates.[8, 9] Besides, silicon is the second-most abundant element in the earth's crust with relatively low redox voltage and remarkable environmental benignity.[10] However, completely replacing traditional graphite with a Si electrode is still unrealistic because of its low conductivity,

insufficient electrode loading, and limited energy density. Furthermore, silicon electrodes also suffer from large volume change and sluggish ion diffusion, resulting in structural pulverization, electrical isolation, and stability decline during repeated charge/discharge processes.[11, 12]

In order to alleviate the foregoing challenges, various Si-based anodes with different modifications have been synthesized. Among these, the incorporation of silicon active materials in carbonaceous products (*e.g.*, carbon nanotubes and graphene) is considered as a widely applied process for anode enhancement, such as depositing silicon layer on the carbon surface, constructing porous silicon/carbon anode, wedging carbon nanotube into micron Si, and embedding nanosilicon into a carbon matrix, since carbon materials could not only buffer electrode disintegration, but also significantly increase the conductivity of silicon.[13-16] Nevertheless, the excessive formation of a solid electrolyte interface (SEI) layer due to the enlarged surface area and unstable structure could still partially offset the merits of engineered silicon.[17] Graphite, as a low-cost commercial carbon material with high tap density, low surface area, and stable physical and chemical properties, can significantly reduce unnecessary electrolyte decomposition on the surface of electrodes while maintaining satisfactory anode integrity.[18] Thus, designing an anode consisting of Si incorporated in a mature graphite backbone is expected to be an effective method for the alleviation of intrinsic disadvantages of Si-based anodes and attainment of satisfactory specific capacity and cycling stability.

There are already a few classical reviews about silicon based anodes which mainly concentrate on a variety of nanostructured active materials (*e.g.*, nanoparticles, nanowires, nanotubes and nanoflakes) or their corresponding carbon/silicon hybrid with good cycling durability and rate capability.[12, 19, 20] Different from previous reviews, we focus on an underneath tendency in recent years that the exploration of silicon anode are being diverted into practical way gradually, and silicon-graphite anode as a key point has been summarized

toward the widespread applications for next-generation lithium-ion battery.

In this review, the recent developments of Si-graphite composite anodes in LIBs are systematically concluded, and the commonly utilized synthesis techniques, lithium storage behaviors, and electrochemical applications of Si-graphite anode are organized and presented in detail, as depicted in Fig. 1. Finally, based on the insights gained through the review of existing literature, we make a comprehensive conclusion and deep discussion on the opportunities and trends for future research and application.

2. Preparation Strategies

2.1 Mechanical Ball Milling

Mechanical ball milling is a low-cost, scalable, and efficient technology for material preparation, which can significantly refine the particle size, improve powder activity, and enhance particle distribution uniformity.[30, 31] It has been widely applied in the synthesis of Si-graphite composite anodes with rationally designed microstructure for LIBs.[32] In 2015, Manthiram *et al.* proposed a facile, low-cost synthesis of silicon-based composite anodes with high tap density *via* a two-step mechanical milling process. As shown in Fig. 2a, SiO and Al powders were mixed and milled in a hardened stainless steel vial for 8 h at room temperature with the addition of an appropriate amount of elemental Ni powder, realizing a complete reduction of SiO to Si by the mechanochemical reaction with Al and partial formation of NiSi_2 phase.[21] The conductivity of result powder was then enhanced by milling with graphite for 15 min, producing carbon-coated micron-sized particles that consisted of aggregated nanostructured building blocks with an uniform dispersion of well-mixed Si/NiSi_2 nanocrystallites in amorphous Al_2O_3 matrix. To further promote its commercialization, a mesoporous $\text{Si}@\text{amorphous carbon/graphite}$ ($\text{Si}@\text{C/G}$) material was synthesized by Yang's group through acid etching of low-cost Al-Si alloy in 1 mol L⁻¹ HCl solution followed by ball-milling and heat treatment process together with graphite and sucrose at 800 °C for 4 h.[33] Owing to the introduction of the developed porosity, conductive graphite and integrate carbon

coating outside silicon, the volume expansion during the formation of Li-Si alloy phase could be successfully buffered. As the introduction of transition metal elements has been approved to be effective to strengthen the electrode stability, Zhang *et al.* tested the influence of cobalt addition in Si-graphite anodes, taking advantage of its good metal ductility and mechanical strength (Fig. 2b).[22] As expected, the uniformly distributed cobalt as well as the stable and conductive graphite was able to alleviate the voltage hysteresis of Si and provide better electrical contact upon cycling. In contrast to Si, SiO_x could further buffer the volume change of silicon active material since Li₂O and Li silicates could play a matrix role. Thus, ternary hierarchical Si@SiO_x/Ni/graphite composites were prepared *via* the ball milling method.[34] During the mechanical milling, nanosilicon embedded in the oxide particles were formed due to the mechanochemical reduction of Si monoxide by nickel, and the nickel/graphite matrix could play a role of a tough framework and electronic highway in assembled electrode. Besides, the milled nanoNi/graphite matrix in the cross-linked framework was able to stick well to active materials and further enhance the activity and utilization efficiency of the Si based particles. Fig. 2c demonstrates the obtained Si/graphite/carbon microstructure designed by Lee *et al.* through the milling of a mixture of nanosilicon/graphite/petroleum pitch followed by heat treatment in an argon atmosphere.[23] The resultant spheres were made up of nanosilicon and graphite flakes which were dispersed in petroleum pitch originated carbon matrix with good structural stability. In 2017, a Si/SiO_x/C microsphere was prepared by Yang *et al.* using a typical two-step ball milling process and the synergistic effect was explored.[35] First, a disproportionation reaction occurred during the ball milling of SiO, thereby forming the Si/SiO_x composite, which was then incorporated with graphite through intensive ball milling. As expected, there was a synergistic effect between Si/SiO_x and graphite with improved electrode integrity. Fig. 2d schematizes the preparation process of another unique Si/G@C anode. It includes ball milling process with N-hexane as a dispersant and coal tar pitch encapsulation process under argon atmosphere containing 5% H₂.[24] Interestingly,

through sufficient mechanical ball milling, a phosphorus-doped Si/graphite anode was cost-effectively obtained using phosphorus, Si, and graphite as the primary materials.[36] The modification of phosphorus was determined to be capable of suppressing the phase transition and reducing the charge transfer resistance of the anode, while graphite skin was able to desirably prevent Si from direct contact with the electrolyte, thereby further restraining the excess formation of the SEI layer. Recently, Rojo *et al.* mechanically milled nanosilicon and commercial graphite with a weight ratio of 37.5: 62.5 in a planetary mill; with the assist of 10 mL isopropyl alcohol during milling process, the agglomeration of silicon particles was found to be effectively prevented, producing a kind of stable silicon@graphite active material.[37] Waste silicon is another low-cost silicon source. In Fig. 2e, Xie *et al.* recycled the waste silicon with a particle size of less than 3 μm by electron beam melting, and then milled them together with ethyl alcohol in milling chamber for 14 h.[25] After cooperation with phenolic resin and graphite, Si-C/G anode was finally obtained, in which silicon particles (51 nm) interwoven well with carbon matrix. Generally, ball milling method is a very efficient way to cooperating silicon and graphite. Transition metal doping and mechanochemical reaction could be triggered during the intensive milling process. However, unsatisfactory morphology control and limited combination chemistry still suppress its application in the fabrication of silicon-graphite electrode.

2.2 Spraying Method

Apart from ball milling, spraying method is another widely adopted technique for Si-graphite anode synthesis.[38, 39] The spherical morphology and size of the designed sample was found to be easily adjustable under appropriate parameters for product synthesis, such as slurry concentration or jet rate. A kind of spherical Si/graphite@graphene composites were proposed by Gan *et al.* by dispersing and spraying graphene oxide, nanosilicon, and graphite in an alcohol solution using an output nebulizer, followed by pyrolysis at high temperature in inert atmosphere.[40] By comparing the impedance results of the samples with different

components, it could be found that graphene was capable of effectively optimizing the electron and ion transportation throughout the anode. To circumvent the limitations of pure Si, Chen and co-workers proposed a strategy of synthesizing the Si/graphite/pyrolytic carbon (SiGC) anode with industrial bulk Si, graphite, and sucrose as the primary materials (Fig. 2f).[26] The collected silicon-graphite product maintains peculiar core/shell structure, in which the carbon components could not only prevent direct contact of Si with the electrolyte, but also keep the integrity of electrode. Attempting to adopt transition metal elements into the silicon based electrode, Cho *et al.* proposed the synthesis of Fe-Cu-Si blended with graphite through a spray and pyrolysis process.[41] It was found microdroplets consisting of nanosilicon, iron nitrate nonahydrate and copper nitrate trihydrate could be suitably atomized and dried before calcination and graphite incorporation. As shown in Fig. 2g, the Si-based particles collected through aerosol spray drying of commercial silica water suspension exhibit an average size of 11 μm , as indicated by the particle size distribution (insert).[27] Each microsphere is composed of lots of 10-nm primary silica, implying that spray drying is very effective to aggregate nano-sized silica precursor, producing uniform microsphere. With impressive conductivity and good mechanical strength, carbon nanotubes are selected by Yang *et al.* to prepare a hierarchical porous Si/graphite/CNT@C anode with optimized synergetic effect *via* the spraying method (Fig. 2h). In the composite, low-cost pitch was verified to be capable of bonding CNT/graphite and Si particles together effectively.[28] By varying the ratio of pitch, the surface compactness and porosity development of final products could be easily adjusted. To further promote the uniform distribution of silicon active material, flake-shaped Si was prepared by Huang *et al.* as the active material dispersed by pyrolyzed carbon and natural graphite (Si/C@NG) (Fig. 2i).[29] During the spray drying process, flake Si and the polymer precursor were embedded into natural graphite, which was further assembled into larger secondary particles, and styrene-acrylonitrile copolymer was proved to be an appealing matrix to accommodate the sub-micron Si plates. Shao *et al.* also tried citric

acid as the organic precursor in porous Si-graphite composite based on spray drying and subsequent pyrolysis, wherein graphite served as the core and nanosilicon dispersed inside the citric acid acted as the shell.[42] This unique structure was found to be capable of effectively buffering the large volume expansion and shrinkage of the Si active material, thereby further enhancing the integrity of silicon-graphite anode. Spraying method is an environmentally friendly and relatively high-yield strategy for the preparation of silicon-graphite sphere. However, during the production, the thermal efficiency is not high enough, and the separation of gas and obtained silicon based sphere has high instrumental requirement.

2.3 Chemical Vapor Deposition

To further enhance the synergistic effect of Si with high theoretical capacity and graphite with impressive stability, great efforts have been made in exploring the application of chemical vapor deposition (CVD) in anode material synthesis, given that it could delicately tune the final products through adjusting the reaction rate, deposition temperature or precursor sources.[49-51] Fig. 3a demonstrates the synthesis procedure of edge-plane-activated graphite/Si nanolayer composites (SEAG) *via* the CVD method.[43] C₂H₂ and SiH₄ gases were applied as the carbon and Si precursors, respectively, and deposited on holey graphite constructed by catalytic hydrogenation reaction upon calcination at high temperature which was triggered by nickel catalyst formed on the surface. It was verified that the activated edge site could provide improved Li⁺ mass transfer. Besides, Kim *et al.* also prepared a type of copper silicide-coated graphite using a plasma-enhanced CVD method.[52] After carefully controlled sputtering, copper silicide particles (*ca.* 30 nm) were uniformly dispersed on the graphite, and the reversibility and integrity of anode materials could be effectively enhanced, making it a potential anode material in lithium secondary batteries, since copper was very beneficial to the electrical conductivity of silicon and copper silicide could play as the buffering matrix against drastic volume changes of silicon. Compared with traditional silicon particles, has some unique features, such as optimized volume change, enhanced cooperation

with carbon matrix and controlled product morphology.[53, 54] As exhibited in Fig. 3b, a graphite/Si nanowire anode is rationally designed in Cho's group. Spherical micelles bearing Ni ions on graphite were initially obtained *via* the selective complex formation and, thereafter, transformed to self-assembled Ni nanoparticles after polymer removal by heat treatment.[44] After exchange of catalyst from Ni to Au, Si nanowires could be grown in 3D-interconnected pores of graphite particles under SiH₄ flow. The CVD strategy could not only provide sufficient silicon accommodation but also verify good stability and conductivity. Moreover, a series of Si-metal-graphite composites were also prepared by the same group, and it was found that uniform silicon based particles could be easily formed.[55] Among the proposed Si-metal-graphite composites (*i.e.*, bare Si/graphite, Si-Cu/graphite, Si-Sn/graphite, and Si-Ni/graphite), Si-Cu/graphite showed the highest electrode potential due to the low impedance and effective buffer induced by the copper-silicide formation. To verify the isotropic volume expansion during lithium diffusion and increase the electrode integrity, amorphous Si nanoshell was successfully fabricated on artificial graphite in Lim's group by chemical vapor deposition.[45] It results the uniform deposition of silicon (orange) on graphite surface with clear Si/graphite interfaces identified in the following TEM test, as shown in Fig. 3c. CVD induced carbon shell with delicately tuned thickness is another significant protection for the anode stability. Fig. 3d shows the SEM and the high-resolution TEM images of the Si/C microsphere proposed by Guo *et al.*, which featured a nanosilicon/graphite core and a CVD-induced protective carbon shell.[46] It was revealed that graphite in the composite could effectively suppress the aggregation of nanosilicon, while the CVD-induced carbon shell could prevent the exposure of silicon active materials. To confirm the sufficient contact between silicon atoms and carbon buffer, Si-nanolayer-embedded graphite composite (SGC) was designed by Cho *et al.* through CVD using a scalable furnace (Fig. 3e).[47] During the two-step CVD process, Si nanolayer and pyrolyzed carbon were uniformly coated on a graphite substrate without excess voids, impurities or secondary phases shown on the

interfaces between graphite, Si layer and pyrolyzed carbon. Moreover, this gas deposition technique allows facile penetration of the Si precursor deep into the graphite framework, thereby realizing effective Si accommodation. Compared to CVD induced carbon shell, melted pitch with mixed organic polymers is much cheaper and easier to be manipulated. Thus, in 2019, Choi *et al.* coated melted pitch on the surface of Si nanolayer/graphite composite (SG) with even Si layer deposited on the surface of graphite, forming satisfactory carbon shell (Fig. 3f).[48] The formed pitch-based carbon shell maintains good mechanical properties and practically low cost. Notably, acetylene and sucrose were also used in carbon coating for comparison, but illustrated unsatisfactory electrodes damage with detached and rugged Si nanolayers identified on the graphite. Based on the aforementioned research works, it could be identified that CVD strategy is suitable to promote the distribution or protection of silicon active materials through silicon layer formation and carbon-shell encapsulation. Nevertheless, both gas sources (e.g. SiH₄, CH₄ and C₂H₄) and operation condition (> 900 °C) could inevitably hinder its sufficient reliability and further application.

2.4 Wet Processing Method

Wet processing is a type of facile, environmentally friendly, and scalable procedure for the synthesis of Si-graphite anodes, during which the Si active material, graphite, and other additives are thoroughly mixed and self-assembled in a solution. After solvent evaporation, centrifugation or filtration, the collected product can be applied in battery system after suitable modification or treatment. For example, Kim *et al.* designed and prepared a robust Si/carbon/graphite (Si-C-G) composite with coal tar pitch-based carbon layer coated on the surface of a Si/graphite particle (Fig. 4a).[56] Owing to the effective optimization of the electrical conductivity and alleviation of the mechanical stress originated from the nanosilicon volume change, the collected Si-C-G anode with a graphite core and nanosilicon/carbon shell could maintain enhanced structural integrity. As LiF is one of the main components of SEI formed on the silicon surface, Zhou *et al.* proposed the synthesis of the pitch-based carbon

and LiF comodified Si/graphite anode material (SGP@LiF). During the facile wet process, graphite was applied as the dispersion matrix, and LiF was used as the surface additive to promote SEI formation and reduce side reactions (Fig. 4b).[57] Besides, a similar Si/graphite/carbon (Si-G/C) composite was reported by He *et al.* wherein polyvinyl pyrrolidone (PVP) was used to promote the dispersion of nanosilicon in ethanol.[63] After the addition of pitch and graphite, the homogeneous suspension was evaporated prior to calcination. On the graphite surface, a Si layer with a thickness of hundreds of nanometers was observed through energy dispersive x-ray spectroscopy (EDS) analysis, while a carbon layer with a thickness of approximately 250 nm, coated on the outermost surface, was also identifiable. The as-expected microstructure apparently imply that PVP could act as ideal dispersant during Si-graphite synthesis. Additionally, graphene could also optimize the combination of silicon and graphite through wet processing (Fig. 4c). The modified Si could first assemble with graphene oxide (GO) through van der Waals interactions, which was then added to the graphite suspension dropwise for further electrostatic assembly with the help of mutual attraction of heterochemical charges.[58] Obviously, GO is like the “glue” between silicon active powder and graphite backbone, which is much better than the nanosilicon/graphite product prepared by just evaporating the nanosilicon suspension and graphite in methanol shown in Fig. 4d.[59] Although nanosilicon was uniformly coated on the surface of natural graphite with rough morphology and increased surface area, the combination is not tight enough during repeated charge and discharge process. In order to avoid segregation of silicon nanoparticles and enhance the contact between silicon and graphite, a polymer-blend of poly(sodium 4-styrenesulfonate) (PSS) and poly(dially dimethylammonium chloride) (PDDA) was explored (Fig. 4e).[60] As expected, the negatively charged Si coated with PSS could repel each other and effectively bond with the positively charged graphite modified by PDDA. Furthermore, the PSS-PDDA could also act as robust artificial solid-electrolyte interphase after thorough carbonization. Additionally, inspired by

the improved integrity of core-shell silicon-graphite anode, Liu *et al.* proposed a double core-shell carbon/silicon/graphite anode material. As can be seen in Fig. 4f, the MCMB particles was surrounded by 1 μm of silicon particles with amorphous carbon film at the boundaries.[61] These two selected carbon material, *i.e.* MCMB and amorphous pitch, could build a superior stable matrix to relieve the mechanical stress of Si.[61] Considering polyaniline (PANI) could provide for additional flexibility and chemical stability, Schulz *et al.* further applied PANI in the silicon-graphite anode in large scale.[62] It was found that there was a beneficial electrostatic attraction between silicon and graphite (Fig. 4g), which promoted stable self-assembly and further emphasized the promising potential of PANI in commercial Si-graphite production. Wet process remarkably simplified the synthesis of silicon-graphite composite. In addition, the requirements for the precursors are nearly eliminated, which makes it suitable for large-scale application. Nevertheless, through wet process, the diversity of microstructures is relatively limited, taking the obtained products mentioned in this section into account.

2.5 Other Methods

Apart from the abovementioned methods, several other effective strategies have also been explored and applied in Si-graphite anode preparation. For instance, Zhang *et al.* reported a facile electrochemical etching strategy for the preparation of porous Si/C-graphite electrodes with mitigated thickness swelling. As illustrated in Fig. 5a, the porous Si exhibited thin crystalline walls formed around pores, which demonstrated alleviated expansion and provided stable electrochemical performance when mixed with graphite at an appropriate weight ratio.[64] Arc-melting is an effective strategy to transform single silicon into significantly buffered state. Through this method, Park *et al.* prepared a kind of Si-Ni alloy-graphite composite, wherein the Si alloy (Fig. 5b), as an intermetallic compound, contained two different phases (*i.e.*, active Si and inactive NiSi and NiSi₂); the active silicon was the key component for lithium storage while the inactive phase could act as buffer and conductivity promoter.[65] By varying the ratio of Si and nickel, products with different active components

could also be obtained. However, this method is relatively time-consuming and expensive compared to hydrothermal method which is a facile and popular way for the synthesis of Si-based anodes.[70] Through the cost-effective hydrothermal approach, Jeong *et al.* prepared a kind of hard carbon-coated nanosilicon/graphite composite followed by high-temperature heat treatment as demonstrated in Fig. 5c.[66] In contrast to its counterpart prepared by simply mixing the hard carbon, nanosilicon and graphite, the designed product significantly maintained good structural integrity under a repeated charge/discharge process. Lee *et al.* synthesized granulated Si oxide nanoparticles through plasma treatment, which was further combined with graphite for anode application (Fig. 5d).[67] The plasma treatment was conducted at ultrahigh temperature attained by compressing the plasma-forming nozzle at high voltage. During this treatment, the oxygen content in the final Si active materials could be precisely controlled by changing the injected oxygen flow. Compared with plasma treatment, magnesium reduction is much more practical for scalable preparation of silicon based electrode. Wei *et al.* reported a type of Si nanostructures *in situ* formed within the confined gallery region of graphite which was synthesized by tetraethoxysilane hydrolysis and magnesium reduction. As can be seen in Fig. 5e, carbon and silicon were dispersed within the cross section of porous expanded graphite/silicon composite (PG-Si), and the diffraction rings of silicon with polycrystalline nature could also be clearly identified.[68] Notably, since magnesium is a kind of highly active metal, the amount of magnesium should be carefully controlled during the reduction reaction. To further optimize the electrode stability during repeated cycling, ultrafast laser processing is carried out, as shown in Fig. 5f. It enables precise ablation without significant heat impact and provides free spaces for volume changes, thereby leading to a significant decrease in volume change within the electrodes.[69] After cycling, the laser-generated artificial free spaces were filled with the electrode material, thus guaranteeing the reduction of mechanical stress and preservation of the shape of current collector. Additionally, electrolysis was likewise exploited in Si-graphite anode preparation by

Yang's group, during which graphite was modified by milling to improve its chemical reactivity, and then electrolyzed together with SiO₂ (Fig. 5g), thereby leading to a reduction of Si on the surface and lateral side of graphite.[18] Ultimately, the graphite/Si@carbon composites could be collected after spheroidization and carbon layer coating. Nevertheless, electrolysis method is not yet widely adopted owing to the unsatisfactory efficiency and tedious procedure hard to be manipulated. Various silicon based active materials that have been applied in LIBs are described in Table 1.

3. Lithium Storage Behaviors

The electrochemical behavior of silicon-graphite composite electrode is concluded in Fig. 6. As illustrated in Fig. 6a, Gasteiger *et al.* investigated the relative SEI volume of silicon-graphite electrodes with different silicon ratios.[79] Normalized to the pore volume of the pristine electrodes, the approximation could give a semi-quantitative measure of the volume of electrolyte decomposition. Apparently, the silicon ratio could significantly influence the produced SEI volume after cycling. The 20 wt% silicon electrode consisted of a nearly contiguous graphite backbone structure, which enhanced the overall electrode stability and suppressed electrolyte decomposition.[79] When the silicon ratio was further decreased to 5 wt%, the distribution of silicon could be further optimized, in which tough graphite particles successfully formed reliable framework (Fig. 6b).[80] The volume expansion of silicon nanoparticles encountered during the lithiation was rationally reduced and accommodated by the carbon scaffold, thus preventing the delamination of the electrode upon repeated cycling, as exhibited in Fig. 6c.[81] Generally, there was no chemical bond between silicon active materials and graphite particles. But, based on the exploration of Choi and his coworkers, silicon and carbon matrix could be chemically connected through the assistance of amphiphilic binder, as illustrated in Fig. 6d.[82] Thermally renatured DNA (reDNA) was responsible for hydrophobicity *via* the heterocyclic aromatic components to bind with

graphite, while alginate (ALG) favorably connected with hydrophilic Si particles (Fig. 6e).

Taking such physicochemical advantages of the amphiphilic binder, the connection between Si and graphite could be remarkably enhanced. To clarify the lithium storage behavior in graphite, Kang *et al.* investigated the potential profile consisting of multiple single and two-phase regions (Fig. 6f).[83] It is assumed that the curve might be represented by three phases: stage 1 LiC₆, stage 2 LiC₁₂, and stage 3 LiC₃₂, and the regions between the single phases consisted of a two-phase region as one stage grew at the expense of the other. Generally, raw graphite aligned with high orientation is not a desirable anode candidate, while shuttle-shaped graphite obtained through facile vibration-rod milling could provide enhanced rate performance, considering that the edge-plane surface of some randomly stacked shuttle-shaped graphite matches the current flow direction. Nevertheless, the rolling and pressing processes adopted in industrial production, which are intended to increase the conductivity and tap density, always lead to sluggish lithium intercalation at high current densities. Thus, spherical graphite prepared through intensive milling, in which small pieces are folded into compact spherical particles, has gained significant attention given that the optimized morphology verifies the random orientation and promotes a uniform spread on copper foil (Fig. 6g).[84] In theory, Li storage could be based on the following equation: $6C + xLi + xe^- \rightarrow Li_xC_6$ ($0 < x < 1$), in which large particle size and high current density suppresses graphite lithiation, thereby resulting in a low x . In terms of Si, at high temperature (415 °C), four different phases could be manifested, *i.e.*, Li₁₂Si₇, Li₇Si₃, Li₁₃Si₄, and Li₂₂Si₅, whereas only two transformation phases could be found in the Si lithiation process at room temperature (4Si + 15Li⁺ + 15e⁻ → Li₁₅Si₄) (Fig. 6h).[85] During the initial lithiation process, a high concentration of Li atoms is accumulated in the Li_xSi/Si front to overcome the high activation energy needed for breaking up the crystalline Si; notably, only amorphous Si-Li phase could be obtained since the formation of the equilibrium phases is kinetically hindered. In addition, Fig. 6i summarized the phase transformations during cycling, and implied that Li₁₅Si₄ was the

most highly lithiated phase at room temperature.[85] Aiming to further understand the lithium-silicon reaction, Cui *et al.* *in situ* observed the lithiation and delithiation behavior of silicon nanospheres.[86] Notably, it revealed a two phase mechanism in the first lithiation process according to the structural evolution in TEM test (Fig. 6j), which was suggested to be as a result of the rate-limiting effect during Si-Si bond breaking. Moreover, different from the isotropical lithiation in amorphous silicon, there was an anisotropic lithiation process in crystalline silicon. As shown in Fig. 6k, Si nanopillars with three axial orientations were prepared and lithiated, leading to different expansion orientation into cross, ellipse and hexagonal shapes, respectively. This interesting phenomenon might be ascribed to anisotropic interface reaction rates influenced by the bond density at different surfaces.[85] Significantly, the stress evolution was unveiled in detail by Mao and coworkers, as illustrated in Fig. 6l.[87] When lithiation was started, the formation of Li_xSi on the surface counteracted part of the tensile stress. During further lithium reaction, the overall stress transformed from tension to compression, and the magnitude reached 0.3 GPa.[87] Owing to the increased thickness of outmost Li_xSi layer, stress detection was blocked to some extent at the end of lithiation. Subsequently, the in plane deformation and fracture during lithium storage process was further analyzed by Komvopoulos's group.[88] After full lithiation, large plastic strains gradually grew along the (100) edges due to the constrained volumetric expansion, while plasticity was continued to be accumulated as a pair of perpendicular deformation bands which could be introduced to construct high-plastic-strain bands at larger scales (Fig. 6m). As shown in Fig. 6n, the crack and damage was not significant during the first few cycles, but gradual and cumulative. The dominant feature was two orthogonal directions of developed crack and isolated small squares that formed a regular repetitive pattern on the electrode surface.[88] Furthermore, it also accounted for the formation of square cavities after 50 cycles. After repeated charge/discharge, it was reasonably identified by Wetjen *et al.* that the silicon density dramatically decreased and accumulated fluorine and oxygen originated from

electrolyte decomposition wrapped the entire silicon, which could deteriorate the electrode integrity (Fig. 6o).[89] With regard to the Si-carbon anode, there is usually an increased thickness after cycling, which mainly includes three parts, *i.e.*, the expanded Si active material, electrolyte decomposition-induced SEI layer, and internal electrode cracks. Generally, the crack does not destroy the working anode directly; however, it could isolate the active materials from electrical connection (Fig. 6p). Additionally, as illustrated in Fig. 6q, the interfaces among solid particles were not as clear as those in pristine electrodes as a result of SEI formation.[90] Although the SEI layer might prevent the exfoliation of the graphite electrode, it can block the interparticle electron pathway between the Si-Si and Si-graphite, further jeopardizing the electrochemical performance. Considering the stable physicochemical properties of graphite, silicon part plays an important role in the optimization of electrode with suppressed crack, limited SEI formation and electrode volume expansion. Huang *et al.* found that there was a strong particle-size-dependent fracture behavior of Si nanoparticles during the first lithiation.[91] Surface cracking related to the developed hoop tension in the surface could not be identified due to the insufficient amount of strain energy in nanoparticles smaller than 150 nm (Fig. 6r). Consequently, physics of stress generation and surface cracking could be roughly controlled by tuning the silicon particle diameter and flaw size.[91] Previous studies have indicated that the erosion of Si particles by hydrofluoric acid (HF) which derives from the hydrolysis of LiPF₆ based electrolyte plays an important role in the deterioration of electrochemical performance, making it significantly essential to enhance the cross-linking strength and elastomer properties of interfacial SEI.[93-96] Notably, Grey and coworkers also found that, after repeated charge/discharge, the Li-ion diffusion could be restricted to surface regions as a result of SEI delamination and dense electrode structure.[92] As illustrated in the schematic image in Fig. 6s, In the early stages of cycling, lithium could access the entire porous electrode structure. However, with continuous volume expansion and contraction in pronounced SEI growth during later stages of cycling, dense structure and

increased tortuosity nonnegligibly impeded the diffusion of Li-ion through the bulk of anode, leading to undesirably limited lithiation. Thus, the lithium storage behaviors is not only related to the morphology, diameter and microstructure of separated silicon and graphite but also influenced by the design and stability of hybrid composite. Furthermore, other parameters, such as current rates, working temperature, binder engineering and electrode modification, could also give rise to disturbance to some extent.

4. Electrochemical Performance of Silicon-Graphite Anode

4.1 Graphite/SiO_x (0<x<2)

Despite its impressively high theoretical capacities, Si is still confronted with challenges, such as inevitable volume expansion and unstable SEI coating. To address the challenges of pure Si active materials in anodes, various strategies have been explored.[100-102] Among them, with tunable oxygen content, SiO_x has been extensively investigated owing to its relatively superior electrochemical performance, given that the Li₂O and Li silicate could effectively alleviate mechanical stress during lithiation.[103-105] Amorphous SiO has been applied in various technical areas for many years. In terms of its utilization as the anode in LIBs, two main models have been proposed to date, *i.e.*, the random-bonding model and random-mixture model.[106] According to the random-bonding model, SiO is a single-phase material with randomly distributed Si-Si and Si-O bonds. In terms of random mixture model, SiO is a multiphase mixture with tiny domains of Si and SiO₂ randomly mixed together.[107] In addition, based on previous conception and results obtained from angstrom-beam electron diffraction, an interface clusters mixture model was proposed by Hohl *et al.*, wherein Si and O exist in clusters of Si and SiO₂ surrounded by a variety of suboxide-type tetrahedral coordinates at interface regions.[108] As compared with the 300% volume expansion of Si, SiO_x-based anode shows a relieved volume change (approximately 160%) with decreased theoretical capacity of around 2500 mAh g⁻¹, which is already sufficient, considering the specific capacity of the cathode (approximately 200 mAh g⁻¹).[109] Pitch has always been

used as a “binder” to enhance electrode integrity and cycling stability, as found in previous studies, owing to its low-cost, abundant resources, high electric conductivity, and good cladding performance. For example, Xu *et al.* proposed a facile and scalable fabrication technique for the synthesis of the SiO_x -graphite composite with SiO_x , graphite, and pitch as the active material, backbone, and adhesion agent, respectively. When used as the anode in an LIB, the resultant composites provide good lithium storage capability (645 mA h g^{-1}) at high mass loading (3.5 mg cm^{-2}), impressive charge/discharge performance (approximately 90 % retention after 500 cycles), and acceptable rate properties (Fig. 7a).[72] Owing to its high tap density and good structural durability, the SiO_x /carbon anode could still provide stable cycling even at high pressing density (1.3 g cm^{-3}). In addition to the combination with pitch, carbon nanotube has also received considerable interest because of its excellent physicochemical property, such as high mechanical strength, impressive electrical conductivity, and good structural flexibility. As shown in Fig. 7b, a type of Si monoxide/graphite/carbon nanotube (SiO/G/CNT) was prepared by Yu *et al.*, in which Si monoxide with a diameter ranging from 2 to 3 μm and a graphite sphere (16 μm in diameter) were combined *via* in-situ grown CNT.[97] Although SiO/G demonstrates a good initial discharge capacity of 855 mAh g^{-1} , the capacity retention is still unacceptable with a capacity loss of 55% after only 50 cycles. Notably, the CNT modified SiO/G with initial lithiation/delithiation capacities of 790 and 513 mAh g^{-1} , revealed a desirable cycling stability (96.5% capacity retention after 100 cycles). The CNT induced enhancement was mainly ascribed to the effective volume buffer and optimized electrical conductivity. The oxygen content in SiO_x could significantly determine its lithium storage capacity. To investigate the optimum stoichiometry, Lee *et al.* synthesized various SiO_x particles to compare their electrochemical performance. Although the initial specific capacity and coulombic efficiency (CE) decreased with an increase in x due to the formation of irreversible products (*e.g.*, Li_4SiO_4), the volume expansion could be significantly suppressed to approximately 60% when the x is optimized as 1.06. Blended SiO_x /graphite

composite was then attempted and provided impressive capacity retention (76% after 200 cycles) and satisfactory CE (99.99%) (Fig. 7c).[67] Furthermore, transition metal particles could also be used in the preparation of high-performance SiO-based anodes, such as the Si oxide-nickel-graphite composite proposed by Wang *et al.*, wherein nanosilicon with abundant electrochemical activity was formed during the reduction reaction with nickel. SiO/Ni/graphite composites exhibit a black color, which is different from the brown color of SiO and SiO/Ni.[34] When used as the anode, pure SiO revealed obvious drawbacks, such as high voltage polarization and low working stability. The initial coulombic efficiency (ICE) of SiO/Ni/graphite (65.3 %) remarkably increased compared with that of the pure SiO anode (48.5 %), revealing the enhanced conductive pathway induced by the Ni/graphite cooperation. Notably, after 100 cycles, SiO/Ni/graphite composite exhibited much better capacity retention (742.3 mAh g^{-1}) than those of SiO (142.4 mAh g^{-1}) and SiO/Ni (409.3 mAh g^{-1}), verifying that nickel addition could realize the effective prevention of electrode disintegration during cycling (Fig. 7d).[34] Aiming to produce more electrochemical active sites, Si/SiO_x/graphite was prepared *via* thorough milling of SiO and graphite. The charge/discharge performance of the obtained Si/SiO_x/graphite with various weight ratios of Si/SiO_x to graphite (*i.e.*, 5:1, 5:2, and 5:3) was tested, and the results are shown in Fig. 7e.[35] It indicated that the increase in the graphite ratio could promote the cycling stability of Si/SiO_x/graphite, whereas the reversible capacity inevitably decreased with high carbon content. With regard to Si/SiO_x/C-1 (5:1) and Si/SiO_x/C-2 (5:2), the carbon was unable to sufficiently mitigate the volume change of Si/SiO_x. Si/SiO_x/C-3 (5:3) could be treated as the optimal product in further studies, exhibiting desirable specific capacity, *i.e.*, 881 mAh g^{-1} in the 1st cycle and 726 mAh g^{-1} in the 500th cycle (Fig. 7f).[35] In order to further improve the lithium storage capability, TiO₂ was applied by Ming *et al.* to further exfoliate graphite, constructing SiO_x/TiO₂@MLG composite with the assist of van der Waals force (Fig. 7g).[98] The as-prepared SiO_x/TiO₂@MLG with a spheroid-like structure delivering an extremely high capacity of 1484 mAh g^{-1} and a long

lifespan beyond 1200 cycles at 2 A g^{-1} has a potential to be utilized in the LIBs in practical applications.[98] In 2020, Zhang *et al.* presented a facile and mature strategy to encapsulate SiO_x nanoparticle into the defect-enriched graphite flake (GF-4) assisted by solid diluent 4-aminophenol, which could prevent the aggregation of the graphite flakes and excessive formation of defect carbon during the milling process, and further consolidate the layered sandwich structured $\text{SiO}_x/\text{C}/\text{GF-4}$ composite.[99] Owing to the excellent structural compatibility and high diffusion rate of lithium ions guaranteed by the 3D electronic and flexible framework, the $\text{N-SiO}_x/\text{C}/\text{GF-4}$ composite displayed an impressive cycling performance (525.2 mAh g^{-1} over 500 cycles at 1 A g^{-1}) and superior rate performance (334 mAh g^{-1} at 5 A g^{-1}) (Fig. 7h). Although the lithium storage performance of SiO_x could be significantly enhanced though rational designation and modification, there are still several bottlenecks hindering its scalable commercialization. Generally, there is an unsatisfactory ICE owing to the irreversible consumption of excess lithium during the formation of lithium oxide. Besides, with the increase of oxygen content, the deteriorated conductivity of SiO_x could not be ignored and should be compensated by various modifications of conductive components.

4.2 Graphite/Si-Metal Alloy

Recently, graphite-cooperated Si-metal alloy has been critically explored for anode commercialization.[114] As an effective way to mitigate the volume change of Si, the preparation of metal silicide alloys could further dilute the active Si and buffer the volume change of Si during lithiation.[115, 116] For instance, in Fig. 8a, a novel Si-metal based anode with void space and abundant nanosized FeCuSi alloys was designed by Chea and co-workers.[41] As exhibited in the high-angle annular dark field in a scanning transmission electron microscope (HAADF-STEM) results, the FeCuSi had a spherical structure in which Si nanoparticles adhered to metal silicide were embedded. Based on elemental mapping, the Fe (red) and Cu (yellow) were evenly distributed in the Si (cyan) particle (Fig. 8b).[41] When

blended with graphite and used in a standard electrode, the FeCuSi/graphite composite was capable of providing high areal capacity (3.44 mAh cm^{-2}) and tap density (1.6 g cm^{-3}). Moreover, as compared with the other two commercial Si-based anodes (*i.e.*, carbon-coated SiO_x and Si embedded in the FeSi_2), the FeCuSi-based anode showed the highest initial coulombic efficiency (91.4%) and cycling stability (98% capacity retention after 50 cycles). Because of the inactive buffer effect and high conductivity, the Ti-Si system has likewise been attractive for anode application. Lee *et al.* presented a Ti-Si composite material with an alloy core and porous Si shell which was finally incorporated with graphite for practical use. Charge/discharge performances of blended electrodes containing C/Si composite and graphite with two different particle sizes (SG1 or SG2) was compared in Fig. 8c; SG1 with a graphite size of $7 \mu\text{m}$ appeared to perform better than SG2 ($12 \mu\text{m}$) as the number of cycles increased, revealing that the size of graphite particles should be paid more attention in future research.[110] Furthermore, Si-Ni alloy was also explored by Park *et al.* for further enhancing the electrochemical performance of Si-based electrodes. As shown in Fig. 8d, fine Si-Ni particles were uniformly dispersed on the surface of graphite, and the porous microstructure was capable of mitigating the volume change during cycling, providing a large discharge capacity of 1430 mAh g^{-1} .[65] Notably, there was an irreversible capacity loss of 300 mAh g^{-1} in the first cycle, which could be ascribed to the formation of solid electrolyte interfaces on the surfaces of the electrodes. In addition, a carbon-coated Si-Cu/graphite anode was synthesized by Zheng *et al.*, with the aim of taking advantage of the buffering effect of graphite and inert Cu_5Si alloy. When it was tested in a half cell, the capacity of the Si-Cu/graphite electrode increased continuously in the first 40 cycles, implying a continuous activation process.[117] Furthermore, after 80 cycles, there was still a high reversible capacity of 410 mAh g^{-1} , verifying the good buffering effect of Si-Cu alloy and graphite framework. Through mechanical ball milling of pulverized commercial FeSi_6 with graphite for 6 h in argon atmosphere, Yang *et al.* obtained a kind of FeSi_6 /graphite composite consisting of an

electrochemically active silicon phase and inactive phases FeSi₂ distributed uniformly in the graphite matrix.[111] Profiting from the buffering effect of the inactive FeSi₂ phase and graphite layers, FeSi₆/graphite anode offers a high lithium storage capacity (795 mAh g⁻¹) with a retention of 76% after 50 cycles (Fig. 8e).[111] In order to further understand the Si-Fe alloy and fulfill stable silicon-graphite anode, Chen *et al.* investigated the electrochemical performance of FeSi₂/Si@C composite collected *via* ball-milling of Fe, Si, and graphite powders. As shown in Fig. 8f, core-shelled structure of the nanocomposite can be visualized from the cross-sectional TEM image of a single particle; there is a 5-8 nm thick outer layer with the lattice fringes of 0.326 nm, corresponding to the d spacing value of the (002) plane of hexagonal graphite.[112] It is noteworthy that the FeSi₂/Si@C composite demonstrated a stable long cycling performance and high reversible Li storage capacity. Specifically, for FeSi₂/Si@C composite, an enhanced specific capacity of 940 mAh g⁻¹ could be remained after 200 cycles, corresponding to an impressive capacity retention of 93 %, whereas the capacity of the bare FeSi₂/Si alloy rapidly droped to 600 mAh g⁻¹ after 90 cycles, leading to an unsatisfactory retention of 43 % (Fig. 8g).[112] Such desirable electrochemical performances were attributed to the FeSi₂ phase in the alloy core and the outer graphite ductile layer with mechanical stress significantly accommodated and desirable electrode conductivity maintained. Then, a reasonable multi-metal modification was carry out by Sougrati *et al.*, proposing a nanostructured Ni_{0.14}Sn_{0.17}Si_{0.32}Al_{0.037}C_{0.346} composite in which spherical silicon particles with a typical size of around 150nm (varying from 20 to 400 nm) were embedded in a shapeless and complex matrix originated from intensive milling of element Si, Al and graphite powders and Ni_{3.4}Sn₄ intermetallic precursor (Fig. 8h).[113] Due to the effective buffering of anode volume change by the Ni and C components, high lithium storage capacity (920 mAh g⁻¹) with a good durability for 280 cycles could be achieved during the lithiation of both Si and Ni_{3.4}Sn₄ phases.[113] To enhance mechanical stability, embedding silicon into a non-active matrix seems to be effective to accommodate volume expansion induced by the

formation of Si-Li, preventing the coalescence of active material during cycling. Besides, the modification of metallic phases could optimize the electric conductivity within the electrode. But, graphite combination is also an essential component for the fulfillment of tough electrode with high energy density, satisfactory areal capacity and reliable cycling stability.

4.3 Graphite/nanosilicon

Watermelon-Like Structure. Nowadays, the watermelon-like Si/C structure is a widely accepted combination wherein nanosilicon particles are dispersed as the “watermelon seed” and carbon materials act as the “watermelon flesh”; thus it allows nanosilicon, which is uniformly embedded in the carbon matrix, to be buffered effectively during lithiation. For instance, Qian *et al.* prepared hierarchical graphene-scaffolded Si/graphite composites denoted as Si/G/GF (Fig. 9a).[13] The hierarchical-structured anode was determined to be capable of providing a reversible capacity of 445 mAh g⁻¹ at 372 mA g⁻¹ after 300 cycles, implying a capacity fading ratio of only 0.07 % per cycle. When the current densities were increased to 2976, 3720, and 5580 mA g⁻¹, there was still good capacity retention (236, 186, and 124 mAh g⁻¹, respectively). To further assess practical use, the full cell with an obtained Si/G/GF as the anode and commercial LiFePO₄ as the cathode was further assembled and tested at 170 mA g⁻¹. It exhibited an initial lithiation/delithiation performance of 154/118 mAh g⁻¹ and maintained a capacity retention of 70% after 100 cycles.[13] It could be concluded that the porous structure with fast ion penetration channel and mitigated Si aggregation induced by the graphene and graphite framework was of vital importance for the realization of impressive lithium storage performance. Phenolic resin and flake graphite were further explored by Gan *et al.* as the “watermelon flesh”. Related characterization proves that the nanosilicon had a homogeneous distribution on the surface and in the interior of the graphite, which consequently provided reversible capacities of 640.5, 613.4, and 447.5 mAh g⁻¹ at 100, 200, and 500 mA g⁻¹, respectively.[74] During the following test, the Si/C composite was observed to be capable of maintaining high capacity retention (more than 95 %) at 500 mA g⁻¹

after 40 cycles. Phenolic resin revealed its effectiveness in filling the gap between silicon and graphite, guaranteeing the integrity of obtained anode. Moreover, Su *et al.* designed a spherical graphite/Si@reGO composite consisting of nanosilicon and flake graphite enwrapped by flexible graphene (Fig. 9b).[118] As expected, the proposed composite was capable of delivering a high reversible capacity of 575.1 mAh g^{-1} with an initial coulombic efficiency of 74.5%, and the capacity retention was approximately 73.1% after 50 cycles. The added graphene had been proved to be effective in improving the turbulence of composites and preventing the exacerbation of Si agglomeration. The obtained Si/graphite@graphene anode was also reported and charge/discharged at various current densities, showing slightly decreased capacities (820.7, 803.3, 789.8, and 766.2 mAh g^{-1} at 50, 100, 200, and 500 mA g^{-1} , respectively).[40] The Nyquist impedance data of the Si/graphite and the Si/graphite@graphene composite were also compared. As a result of the effective attachment induced by graphene incorporation, Si/graphite@graphene was found to be capable of delivering lower charge transfer resistance. As an alternative ternary silicon-graphite anode, Si/G/C was also designed and prepared by Liu *et al.* with nanosilicon uniformly dispersed and supported on the graphite scaffold along with a polyacrylonitrile-derived amorphous carbon coating (Fig. 9c).[119] Compared with Si/C and Si/G, the ternary composite exhibited considerable discharge capacity (832 mAh g^{-1} at 200 mA g^{-1}) and good cycling performance (400 mAh g^{-1} after 200 cycles at 500 mA g^{-1}).[119] It fully embodied the advantages of synergetic effect of designed ternary anode. CNT is a kind of electrode additive enhancing the conductivity and electrode strength. Thus, Yuan *et al.* prepared a Si/graphite/carbon nanotube (Si/G/CNT) composite with Li storage performance systematically analyzed. Although the Si/G anode demonstrated a high initial specific capacity of 2032 mAh g^{-1} , the capacity after only 35 cycles was decreased to 903.5 mAh g^{-1} , indicating a low capacity retention of 57%, whereas the final Si/G/CNT exhibited a reversible capacity of 1363 mAh g^{-1} , and provided a high retention rate of 86 %. Besides, the charge-transfer resistance of the Si/G/CNTs electrode

was 65Ω , which was much lower than that of the Si/G composite (111Ω), further revealing the importance of CNT integration in decreasing the anode resistance.[78] In order to further improve the practicality of designed silicon-graphite electrode, Paik *et al.* investigated the application of sucrose and prepared sucrose coated silicon/graphite granule (C@SGG).[120] Similar with watermelon, the silicon active particles was uniformly dispersed in the carbon matrix constructed by graphite flakes and sucrose based carbon (Fig. 9d).[120] To evaluate the long cycling performance, C@SGG was charged and discharged at 1 C rate, showing an outstandingly capacity retention of 71% over 500 cycles and great potential to be applied in practical batteries (Fig. 9e). To summarize briefly, in the watermelon-like silicon based active materials, the nanosilicon was deeply embedded in the “watermelon flesh”, avoiding unsatisfactory deformation of electrodes during repeated lithiation, large exposure of silicon and continuous consumption of electrolyte. Furthermore, graphite as part of carbon matrix could guarantee an enhanced tap density and satisfactory anode integrity even upon high-pressure pressing. These features unquestionably provide the rational designed silicon-graphite anode with promising application potential.

Core-Shell Structure. A core-shell structure is another typical nanosilicon/graphite microstructure, wherein graphite, as the core, can provide Si-based layers with a large adhesion surface. Generally, the Si coating layer is a mixture of Si and polymer-based carbon, which is used as a “binder” to enhance structural stability. As shown in Fig. 9f, a hard carbon-enhanced nanosilicon/graphite (HC-nSi/G) composite was reported, and the elemental mapping revealed that nanosilicon was uniformly embedded in the carbon shell.[121] The electrode with 10% binder and 11.4% Si showed a relatively low reversible capacity (638.6 mAh g^{-1}), but a satisfactory capacity retention of 92.1% after 150 cycles, whereas the anode with 10% binder and 14.6% Si exhibited a higher lithium storage capacity (769.2 mAh g^{-1}) and much lower capacity retention (75.2%). When the binder content was increased to 20%, the capacity retention of the composite anode with 14.6% silicon could be enhanced to 84.1%

(Fig. 9g).[121] Thus, the binder and Si contents could significantly influence electrode stability and, subsequently, control the electrochemical performance of the composite anode. Another core-shell-structured graphite/Si-porous carbon (Si/C) composite was also rationally designed (Fig. 9h). The graphite/Si-porous carbon anode composed of a dense core and a porous shell delivered a high initial reversible capacity of 723.8 mAh g^{-1} with an impressive capacity retention of 94.9% after 100 cycles (Fig. 9i).[42] It was found that sufficient Si buffers and abundant channels for electrode/electrolyte interaction to maximize electrolyte penetration and electron transportation were of vital importance for good electrical conductivity, high stability during SEI formation, and reliable structural integrity.[42] Notably, Kim *et al.* further reported that adjusting the Si content of core–shell Si-C-G anode constructed by coating pitch mixed with Si on the surface of graphite could effectively vary the electrochemical behavior (Fig. 9j).[56] In particular, Si-C-G-20 with the highest Si content (21 %) had an initial lithiation/delithiation performance of $1009/805 \text{ mAh g}^{-1}$, corresponding to a capacity loss of 20.2 %. [56] When the content of Si was reduced, there was enhanced efficiency and decreased reversible capacity; Si-C-G-10 and Si-C-G-15 composites were determined to be capable of exhibiting more stable charge/discharge performance at 0.2 C for 50 cycles (87.8% and 83.8% retention, respectively) than Si-C-G-20 (81.7% retention) which continuously suffered from capacity fading because the carbon buffer was unable to relieve the mechanical stress induced by the high amount of Si particles (Fig. 9k).[56] Wu *et al.* found that controlled etching of graphite precursor with the assist of KOH could further promote the structural integrity of developed nanosilicon-graphite composite with porous graphite/nanosilicon core and a pitch coating carbon shell (Si/PG/C).[122] In the collected Si/PG/C, nanosilicon was filled inside the pores of etched graphite, which was then encapsulated by amorphous carbon. The PG constructed by alkali-etching and carbon shell prepared by pyrolysis of heavy oil realized a 3D conductive network and stable skeleton for silicon accommodation, which could effectively enhance the lithium storage reversibility

(approximately 400 mAh g⁻¹) (Fig. 9l) and cycling performance (380.7 mAh g⁻¹ after 40 cycles) (Fig. 9m).[122] It is encouraging that core-shell structured nanosilicon-graphite anodes have been proved to be reliable structural designation with satisfactory electrochemical properties, making full use of the graphite with ultrahigh physicochemical property and nanosilicon with high lithium storage capability and partially mitigated volume change by decreased particle size.

Quasi-Sandwich Structure. The quasi-sandwich structure was created based on the unique three-layered graphite-Si-carbon microstructure for the first time, wherein the Si nanolayer is tightly adhered on the surface of the graphite and coated by the outermost carbon buffer layer. The favorable electronic performance was ascribed to the structural compatibility of the quasi-sandwich composite, and the unique Si-based anodes were expected to provide impressive Li storage properties. In Fig. 10a, a type of Si-G/C composite was constructed *via* a scalable evaporating process. After heat treatment, a quasi-sandwich structure with a thin Si layer between the graphite and amorphous carbon layer was obtainable.[63] The electrochemical property of the Si-G/C anode with a carbon content of 10.5% was tested, providing a moderate reversible capacity of 820.8 mAh g⁻¹ and enhanced ICE of 87.6%. These values were much higher than those of pure Si (*i.e.*, 1767 mAh g⁻¹ and 76 %, respectively). When the carbon content was increased to 21.9% and 34.3%, the Li storage capacity was slightly decreased to 784 and 759.2 mAh g⁻¹ with improved ICE of 88.5% and 90.6%, respectively. Therefore, the carbon layer was verified to have great enhancement on surface protection in assembled LIBs. Additionally, Cho *et al.* also designed a Si nanolayer/graphite composite using silane gas and acetylene as the precursor of Si layer and the outermost carbon layer, respectively (Fig. 10b).[43] When used as the anode in LIBs, the collected anode delivered excellent cycling performance for 50 cycles with remarkable capacity retention of 99.3% at 1.75 mA cm⁻², owing to the uniform Si nanolayer and highly conductive graphite capped with a nickel catalyst. Significantly, considering that the anode

with nickel silicide showed lower reversible capacity (435 mAh g^{-1}) and inferior capacity retention (88%), it could be implied that blocking the formation of nickel silicide during CVD process was essential for the cycling stability of the proposed anode (Fig. 10c).[43] In addition, quasi-sandwich structured graphite/Si nanolayer/pitch coating layer composite (SGC) was also investigated (Fig. 10d and e).[48] Tetrahydrofuran was used as a compatible and volatile solvent for the promotion of the homogeneous distribution of pitch on the surface Si-graphite particle. Thanks to the rational design, the SGC was effectively tolerant of the volume change of Si with the electrode swelling remarkably restricted to 48%, which was lower than the commercially acceptable limit (55%).[48] Furthermore, the SGC demonstrated a high capacity retention of 81.9% after 200 cycles at a rate of 0.5 C (Fig. 10f), verifying the effective optimization of the silicon pulverization and SEI accumulation during prolonged cycling. Quasi-sandwich like silicon-graphite composite is a kind of new emerging designation. The collected composite achieves close contact between silicon and graphite, successfully suppressing the exfoliation and pulverization of silicon active material during repeated lithiation/delithiation. Besides, this quasi-sandwich structure fundamentally optimizes the distribution of silicon in graphite matrix.

4.4 Graphite/microsilicon

Generally, nanosilicon is an expensive raw material for anodic use in LIBs.[124] Moreover, other inevitable problems (*e.g.*, agglomeration) make it relatively unsuitable for large-scale industrial application.[125] Thus, research on low-cost Si has attracted significant attention, among which micron Si with low cost, simple preparation process, and similar electrochemical properties to those of nanosilicon, has become a promising candidate for Li ion storage.[126] For instance, a type of porous Si/C anode with 5 to 10% micron Si, obtained through electrochemical etching, was designed and used in LIBs, and it exhibited excellent cycling stability and rate performance.[64] The electrode tested at a practical loading of 3 mAh cm^{-2} was determined to be capable of maintaining high capacity retention of 82% after

450 cycles with a low initial electrode swell (less than 20%) and acceptable end-of-life swelling (around 56%). When assembled into a typical calendered electrode, it exhibited a capacity of 2.5 mAh cm^{-2} and 2.1 mAh cm^{-2} at 0.06 and 0.4 mA cm^{-2} , respectively (Fig. 11a).[64] Cheap microsized Si powder with a particle size of approximately $10 \mu\text{m}$ was also used as the raw material for a Si/graphite/pyrolytic carbon (SGC) composite (Fig. 11b).[26] When applied as the anode in LIBs, an impressive specific capacity of 818 mAh g^{-1} at 0.1 A g^{-1} was achieved. Remarkable rate capability (458 mAh g^{-1} at 2 A g^{-1}) and excellent cycling stability (610 mAh g^{-1} at 0.5 A g^{-1} for 300 cycles) were also demonstrated for the SGC anode, which were much higher than those of the SG comparative anode (370 mAh g^{-1} at 2 A g^{-1} , 54.3 % retention after 300 cycles).[26] The delicately engineered microsized Si, highly conductive carbon buffer, and unique composite microstructure significantly contributed to the impressive Li storage properties. Taking advantage of the highly porous micron Si, Kim *et al.* synthesized a microsized porous Si/carbon composite with graphite blended (mpSi-Y/C@Gr) and investigated its application in LIBs. As shown in Fig. 11c, the specific capacities of the mpSi/C products were 3.1 to 3.7 times higher than those of graphite, while the volumetric capacity of graphite was only 50% to 60% of those of mpSi/C.[71] Furthermore, mpSi-Y/C@Gr was able to deliver a good rate performance, which was evaluated at various currents (100 to 10000 mA g^{-1}) for delithiation and a fixed current (100 mA g^{-1}) for lithiation. The reversible capacity at 10 A g^{-1} reached up to 87% of that at 100 mA g^{-1} , thereby revealing excellent rate capability.[71] The combined effect of graphite with ultrahigh physical stability and porous micron Si with high Li storage capacity was believed to contribute to the performance of the hybrid electrode.[127] The dealloying of micron Si-metal alloys was recently investigated by Sohn *et al.* as a facile strategy for the preparation of porous Si-based anodes with high electrochemical performance.[123] The Si-graphite composite (3D porous Si/Gr) demonstrated good specific capacity, remarkable cycling retention, and impressive rate performance. In particular, 3D porous Si/Gr was able to

maintain a reversible capacity of 436 mAh g⁻¹ after 120 cycles, while the Si-alloy/Gr exhibited a low specific capacity of only 349 mAh g⁻¹ at 125 mA g⁻¹, which might have been due to the relieved volume change of the 3D porous Si/Gr (Fig. 11d).[123] Furthermore, the volumetric energy density of the 3D porous Si/Gr with an ICE of 81% was *ca.* 156 mAh cm⁻³ larger than that of Si-alloy/Gr. Besides, microsized Si modified by boron and CNT were incorporated with graphite matrix (B-Si/CNT@G) by Sun *et al.* through solid state transformation and mechanical milling.[76] The optimized conductivity induced by CNT wedging and heteroatom doping and unique microstructure effectively contributed to the improved Li storage performance. When it was cycled at 225 mA g⁻¹, a good reversible capacity of 460 mAh g⁻¹ was obtained by B-Si/CNT@G after 115 cycles, whereas the pure graphite showed a low specific capacity and bare Si-G composite delivered a poor cycling stability (Fig. 11e).[76] It was worth noting that high mass loading (11.2 mg cm⁻²) was achieved, providing a high areal capacity of 5.2 mAh cm⁻². The superior electrochemical property, satisfactory mass loading and areal capacity, and stable cycling performance rendered the B-Si/CNT@G composite a promising anode for LIBs. Since Al-Si alloy is a kind of cheap and abundant industrial silicon precursor, Yang *et al.* designed a kind of mesoporous Si@carbon/graphite (Si@C/G), which showed an improved Li storage capability compared with pristine Si@C/graphite. This rationally designed anode not only delivered high initial lithiation and delithiation capacities (1267.0 and 985.6 mAh g⁻¹, respectively), but also provided good cycling retention (79.4% after 150 cycles) (Fig. 11f).[33] This research paves a reliable way for the industrial application of low-cost silicon based anodes. Flake-shaped sub-micron sized silicon (Si) firstly explored and enwrapped by pyrolyzed carbon and natural graphite (NG) was synthesized by Huang *et al.*, forming a kind of hierarchical anode (Si/C@NGs) (Fig. 11g).[29] The electrochemical performance of the obtained Si-graphite anode was systematically investigated further, and the reversible capacity of the final product was determined to be 483.3 mAh g⁻¹ in the second cycle, 461.7 mAh g⁻¹ after 50 cycles, and 428.1

mAh g⁻¹ after 100 cycles, much higher those of the bare Si electrode (69.9 mAh g⁻¹) and natural graphite (349.4 mAh g⁻¹) (Fig. 11h). It further proved the importance of suitable Si loading (6.7%) and rational microstructural fabrication.[29] Interestingly, Han *et al.* compared several different carbonaceous materials (artificial graphite, flake graphite and soft carbon) as carbon sources to combine with silicon active materials originated from thorough etching of Fe-Si alloy.[128] Notably, a well-distributed mixture coated by phenolic resin based amorphous carbon could be successfully formed when artificial graphite was applied as the carbonaceous material (Si/C-AG). Since the pore structure of porous silicon could guarantee a rapid Li-ion diffusion and well-coated carbon layer could enhance the formation of stable SEI, the proposed Si/C-AG delivered the highest reversible capacity (445 mAh g⁻¹ at 0.5 A g⁻¹) with a high retention of 94% after 200 cycles.[128] To sum up, micro-sized silicon/graphite based anodes shed light on commercialization of low-cost silicon-graphite anode without sacrificing the lithium storage capability. Through rational modification by heteroatom or carbon nanomaterials, the conductivity of the collected graphite-microsilicon anodes could be significantly optimized, and the buffer effect of graphite framework could also be underlined. The detailed comparison of electrochemical performance of typical Si-graphite composite anodes in LIBs is provided in Table 2.

5. Current Issues towards Practical Full Cell

Thermal and Compression Durability. In automotive application, lithium ion cells are generally packaged in rigid constraints to maintain battery pack dimension.[141] Thus, there usually be an increased temperature and external pressure on active materials in LIBs. The increased temperature could significantly induce gassing and rapid consumption of organic additives (e.g. FEC), forming a resistive SEI layer with high impedance.[142] In order to enhance the high temperature long-term cyclability, Figgemeier's group proposed a NMC622/Si-Gr pouch cells with 1 wt% (2-cyanoethyl)triethoxysilane (TEOSCN)

incorporated.[136] The pouch cell without TEOSCN was swelled with accelerated decomposition of the electrolyte under increased temperature, resulting in apparent capacity decay, while no sign of swelling was observed for the cell modified by TEOSCN attributed to the regulated electrode-electrolyte interface, evidencing the optimized thermal durability (Fig. 12a). Moreover, Arnold *et al.* suggested a link between compressive stress and battery performance degradation.[143] In 2020, more recent research about silicon-graphite/NMC622 pouch cells was carried out by Sutter's group, and its mechanical behavior under an external compressive load could be found in Fig. 12b. There was a dramatic rise in cell pressure during the first 50 cycles at 45 °C as a result of the increased pressure growth rate due to the thermally activated side reactions. Besides, the averaged pressure during each cycle increased with successive cycles, which is of vital importance for modeling the pressure evolution.[137] Significantly, it is reasonable to verify that pressure behavior should be labeled as a key factor in designing battery packs.

Silicon Content and Compatibility. Owing to the inevitable volume change, the silicon content in Si-graphite composite is always limited, which to some extent suppresses the effective capacity improvement. For instance, Mu *et al.* successfully prepared a kind aluminum shell full cells with Si/G@C-G and NCM523 as anode and cathode, respectively (Fig. 12c). Although, as expected, it exhibited stable cycling performance for 100 cycles and high ICE of 83.7%, the content of silicon in the composite was only 8 wt%. Aiming to increase the silicon content and further enhance the silicon-graphite compatibility, Karuppiah *et al.* prepare a Si nanowires-grown-on-graphite one-pot composite (Gt-SiNW) *via* a simple and scalable route.[138] When the content of silicon was 32 wt%, an optimal capacity and durability (87% capacity retention after 250 cycles at 2C rate) was obtained. The uniform distribution of SiNW and the graphite flakes alignment could effectively prevent electrode pulverization during cycling, resulting in very low electrode swelling (*ca.* 20%) (Fig. 12d). In addition, calendering-compatible macroporous architecture for silicon-graphite composite was designed

in Cho's group.[139] As shown in the cross-sectional images (Fig. 12e), the Si layer on conventional carbon-coated Si-graphite composite (CSG) was delaminated from the graphite surface and aggregated with each other during the lithiation process, and the drastic swelling and exfoliation of Si layer could also lead to a undesirable side reaction with the electrolyte. In contrast, the designed ultrathin Si-coated macroporous carbon-graphite architecture with outermost carbon covering (C/Si@MPC-G) had negligible swelling even after full lithiation without any trace of Si delamination. (Fig. 12f).[139] It further realized excellent lithium storage capability with high energy density of 932 Wh L^{-1} and stable cycle life of over 200 cycles, implying the effectiveness and importance of silicon-graphite compatibility.

Protection of Electrode/Electrolyte Interface. Capacity deterioration is the major concern in silicon-graphite cells, which is remarkably more serious than that in bare graphite based cells. Lithium ion loss to the SEI that forms on the electrode/electrolyte interface assumes the main responsibility for capacity fade during the cycling process. After examination of the causes for capacity loss in Si-Gr cells containing LiPF₆-based electrolyte, Abraham *et al.* found that hydrofluoric acid could be generated through LiPF₆ hydrolysis and the silicon active particles could be corroded significantly, destroying the interface stability and exacerbate undesirable lithium loss.[96] Thus, to further enhance the stability of electrode/electrolyte interface in NCM523/Si-Gr cells, the rate of HF corrosion was reduced through the use of fluoroethylene carbonate (FEC). FEC-derived SEI with greater extent of polymer cross-linking could serve as a superior barrier for HF access to silicon surface, further interfering with the detrimental hydrolytic cycle on electrode/electrolyte interface (Fig. 12g). Additionally, Nguyen's group tried to further promote the stability of electrode/electrolyte interface by optimizing the electrolyte composition.[93] Taking advantage of the blended additives of methyl (2,2,2-trifluoroethyl) carbonate (FEMC) and vinylene carbonate (VC), stable SEI at both high voltage cathode and anode was formed and transportation of dissolved transition metal from the cathode could also be inhibited (Fig. 12h). Apart from constructing tough SEI layer on

electrode/electrolyte interface to suppress the corrosion of HF, designing fluorine-free electrolyte is another way to fulfill the elimination of fluorination and protect the interface integrity (Fig. 12i). Compare with traditional F-rich SEI, the fluorine-free electrolyte formed an O-rich SEI, which could still stabilize the silicon-based anode and support stable cycling in NMC111/Si-Gr full cells.[140] These results are encouraging to further in-depth boost the research toward effective protection of electrode/electrolyte interface.

Electrolyte Volume Factor. Generally, electrolyte is the origin of SEI components and an important factor affecting SEI stability and reversible lithium storage performance. Nevertheless, most of the results in the literature are based on experiments with coin cells, and the electrolyte volume is essentially flooded. Thus, more research on effect of electrolyte volume, especially in practical lithium-ion full cells, should be further thoroughly carried out. Preliminary effort have been made to optimize the volume of electrolyte used in 15 wt% Si-graphite/NMC full cell systems in pouch format.[144] When the ratio of electrolyte volume to pore volume (F) is 1.6 (denoted as F1.6), lithium dendrite could be formed on silicon-graphite anode (Fig. 13a). After 100 cycles, the separator for F1.6 was also dry, and some regions of the electrode with relatively bright and light green in color, similar to the pristine anode, did not contribute to lithium storage process due to lack of electrolyte. No lithium dendrites were observed when volume factors are F2.6 (Fig. 13b) and F3.5 (Fig. 13c). In the cell resistance analysis during discharge for different factor groups, cells with F3.1 had low resistances both in the 4th and 97th cycles (Fig. 13d and e). Thus, optimizing the volume factor in practical battery could effectively enhance the lithium storage behavior.

Aging Behavior. During the aging process, capacity loss which was mainly brought from the passivation of the SEI and associated loss of lithium inventory (LLI) could be easily found. Despite that there was no volume expansion in silicon-graphite electrode during aging, infrequent current bursts could be identified, leading to sudden accelerated SEI passivation.[145] Fig. 15f illustrates the LLI loss and additionally the total capacity loss, in

which the LLI share is non-dominant. Associated discharge of the negative electrode due to LLI would result in battery decay. Besides, measured and simulated voltage decay demonstrates similar characteristics in the SOC range. Side reactions such as growth and repair of the SEI in the positive side could also contribute to the voltage decay significantly. Taking small self-discharge current into account, the SOC can be set below 15% during the aging process. To sum up, by carefully controlling the SOCs of the stored nickel-rich/silicon-graphite cells, premature degradation could be rationally avoided.

Thermal Runaway. Thermal runaway in lithium-ion batteries has become one of the main issues for their utilization in electric vehicles and other energy storage systems.[147-149] However, the roles of positive or negative active materials in thermal runaway are still not thoroughly clarified. To understand the thermal runaway behavior in full cell, accelerating rate calorimetry (ARC) analysis has been conducted by Inoue and his coworker as it could provide an adiabatic self-heating rate as a function of time (Fig. 13g).[146] The curve for the all-inclusive microcell (AIM) was similar to that for NCA except for the behavior at around 160 °C which might be due to an endothermic melting reaction of the separator at around 135 °C. It implied that the positive electrode significantly influenced thermal runaway process in assembled full cell. Furthermore, to suppress the thermal run, they also proposed reliable full battery modified by MgB₂ and AlB₂. The value of the heat flow could be effectively decreased, thus improving the thermal stability.[146] More efforts should be made to promote a deeper understanding and explore feasible additives, electrolyte solvents or stable separator for the restriction of thermal runaway during working process.

6. Advanced Detection Techniques

Advanced detection techniques are conducive to in-depth and thorough analysis of graphite-silicon electrode. The two main characterization trends are: (1) qualitative and quantitative investigation of the chemical composition; (2) analysis of morphology and mechanical properties before and after lithiation/delithiation. Understanding of the chemical composition

of silicon-graphite anode during working process is the basis for understanding its electrochemical behavior. For instance, an XPS depth profile could be applied to effectively analyze the state and the composition of accumulated SEI on the electrode, further revealing the surface stability of designed Si-graphite active materials. In addition to the some basic test like SEM/TEM, several advanced techniques have emerged for further deep analysis of the anode during charge and discharge. Hard X-ray photoelectron spectroscopy (HAXPES) was applied to study the difference in the surface states of silicon-graphite anodes with four different binders (e.g. PVdF, PAH, PAH_{0.2}Na_{0.8} and PANa), among which PAH_{0.2}Na_{0.8} and PANa binders could guarantee uniform and flat layers (Fig. 14a). Apparently, Si 1s spectra could be deconvoluted into elemental silicon (Si₀) at 1839.5 eV and native oxide of SiO₂ (Si⁴⁺) on the particle surface. It was noticeable there was obvious shift of the peak for Si⁴⁺ in PVdF electrode relative to those of PAH_{0.2}Na_{0.8} and PANa, indicating partial charge-up of silicon particles and electric isolation (Fig. 14b).[150] Thus, HAXPES is an effective method to evaluate the dispersion state of silicon, which is affected by the dispersion extent of silicon active material. Operando X-ray tomographic microscopy (XTM) was also applied to study the lithiation dynamics and structural evolution of graphite-silicon composite anodes. During the measurement, X-rays could penetrate the cell in transmission geometry and are converted through a scintillator and magnified with an optical microscope, in which δ/β , representing beam deflection/attenuation, was a tuneable imaging parameter that determines the degree to which the phase is retrieved (Fig. 14c). By observing the cuts through the electrodes, electrode dynamics could be qualitatively recorded, and the arrows pointing outwards visually indicated the expansion direction during lithiation clearly (Fig. 14d).[151] The phase changes in graphite-silicon composite are of great importance for shedding light on the effect of electrode modification. Aiming to further unveil the lithium storage behavior of silicon and graphite in mixed electrode, *in situ* XRD has been used to classify the microstructural changes during working process. Compared with the performance of pure graphite (Gr), the addition

of silicon could relatively reduce the lithiation overpotential of Gr based anode (Fig. 14e). In addition, at least five ordered phases (known as the lithiation stages) could be formed during Li intercalation between the Gr layers. After initial lithiation, Si particles became disordered, and the delithiation of the Si-Gr electrode occurred sequentially, namely, Li was first lost from Gr and then lost from Si (Fig. 14f).[152] Significantly, the content of silicon in Si-graphite anode could also affect the (de)lithiation on graphite. In Fig. 14g, *in-situ* XRD patterns of blended graphite and silicon carbon nano (SCN) composites with various SCN contents (0, 3.5 and 9 wt%) was carried out. As the contents increased from 0 to 9 wt%, structural changes of graphite were retarded as silicon amount increased both at the beginning of discharging and end of charging.[153] Additionally, the plateau length of in the charge process was shorter than that during discharge, which indicated a capacity loss starting from discharging period. Nuclear magnetic resonance (NMR) is a reliable method to obtain information of Li ions in both graphite and silicon and distinguish lithiated states of graphite and silicon separately. To further concrete the effect of SCN, *ex-situ* ^{7}Li NMR spectra were measured on anode with 9 wt% SCN. The spectra of those samples with different state of discharging (SOD) (Fig. 14h) and portions of capacity for both phases of LiC_x and LiSi_y (Fig. 14i) were plotted and analyzed, unveiling that Li ions could be inserted into graphite and silicon simultaneously but more rapidly alloyed with silicon at the beginning of SOD.[153] Moreover, the storage of lithium in Si played an key role in capacity fading, implying that improving lithium ion transport in silicon active material was critical for the improvement of battery performance. Recently, X-ray diffraction computed tomography (XRD-CT) has emerged as time-resolved, facile technique to identify 3D crystallographic heterogeneities in the bulk electrodes. In Fig. 14j, Finegan and coworkers explored its utilization in investigating the dynamic processes of silicon-graphite composite anode in 3D with micrometer-scale resolution. The spatial distribution of crystalline Si, lithiated Li_xSi , and LiC_{12} phases could be clearly presented, in which the presence of crystalline Si cores after lithiation indicated a

reduced energy density of the composite electrode due to insufficient utilization of cell's capacity. However, the resolution of XRD-CT was not enough to visualize the formation of submicrometer cracks that could have occurred near the phase boundary.[154] In order to further understanding the degradation mechanism of silicon-based electrodes, neutron depth profiling (NDP) was proposed to collect information on the extent of electrolyte decomposition products across the thickness of the electrode. Fig. 14k illustrates the energy spectra collected from NDP test of silicon-graphite (SiG) electrodes aged for different cycles. During NDP examination, the ^4He and ^3H particles were emitted, and energy distribution profile obtained for the ^3H signal started at 2727 keV and then overlapped with the ^4He particle signal at 2055 keV.[155] The area below this signal was related to the total lithium content while relative flat plateau of the ^3H signal could be ascribed to uniform distribution of lithium containing species deposited in the SiG electrode (Fig. 14k).[155] Besides, the active material utilization across the electrode could also be determined. As a non-destructive and highly lithium-sensitive technique, NDP significantly enables a depth-resolved quantification way in the analysis of silicon-graphite electrodes. To identify electrochemically inactive regions of the silicon-graphite anode, Raman microspectroscopy combined with mapping was proposed by Ruther and coworkers.[156] As shown in Fig. 14l, after the first cycle, the signal of amorphous silicon (a-Si) (blue) increased at the expense of crystalline silicon (c-Si) (red), and the relative amount of c-Si continuously decreased along with repeated charge/discharge. Surprisingly, some c-Si was still present even after 100 cycles, indicating that some silicon was still electronically isolated and did not contribute to the lithium storage process. To have a deep understanding of the lithiation chemistry of low-cost microsilicon, Shen *et al.* conducted *in situ* electrochemical atomic force microscopy (EC-AFM) test to visualize its surface structural evolution.[157] As shown in Fig. 14m, microsilicon experienced obvious volume change and significant growth of SEI layer, which could be verified by the gradually disappeared outline of particles. Moreover, Han *et al.* further characterized the SEI generation

on the surface of graphite *via in situ* AFM, and found that the SEI layer generated in FEC/DMC-based electrolyte was thick and dense in comparison to that in EC/DMC-based electrolyte.[159] Thus, the composition of electrolyte could sufficiently influence the physicochemical property of electrode/electrolyte interface. In addition, with the aim of shedding light on the early-stage defects which were generally inaccessible by most surface-probing techniques, Notten and coworkers adopted operando full field diffraction X-ray microscopy (FFDXM) to unveil the impact of SEI inhomogeneities on anode stability.[158] Specifically, silicon based electrode and two lithium foils were immersed in electrolyte and utilized as the working electrode, reference electrode and counter electrode, respectively. After X-ray photon diffraction, the structural deformation of silicon based electrode could be precisely imaged, as illustrated in Fig. 14n. Moreover, heterogeneous lithiation was also identified as a result of inhomogeneous thickness of SEI layer and strong variation in lithium ion mobility, which inevitably led to structural defects upon repeated lithiation. These advanced characterizations successfully enable the identification and isolation of factors that result in unsatisfactory lithium storage properties and will enhance the exploration of high-energy LIBs.

7. Conclusion and Perspective

The demand for devices with higher energy and power densities has led to great pressure on researchers to explore novel, environmentally friendly, and low-cost electrode materials. Because of its impressive merits, such as abundant resource, ultrahigh theoretical capacity, and environmental benignity, Si has been receiving a lot of attention as an anodic candidate. After years of exploration, it has been found that totally replacing graphite with Si is an unrealistic short-term strategy. Nevertheless, the synergy effect between Si and graphite could be further exploited, as the hybrid electrode may not only offer enhanced Li storage capacity, but also exhibit prolonged cycling stability, thereby integrating the contribution of the Si active material and graphite matrix in terms of capacity improvement and electrode-integrity

enhancement. Therefore, significant efforts have been made in the past few years in fabricating Si-graphite anodes to keep up with the requirements of various applications. In this review, recent development in Si-graphite anodes was summarized and growing trends were further proposed.

- i. The synthesis methods, Li storage behaviors and application of silicon-graphite composites, including graphite/SiO_x, graphite/Si-M, graphite/nanosilicon, and graphite/microsilicon, were systematically organized. Especially, the graphite/nanosilicon composite anode was classified into three different structures for the first time, *i.e.*, watermelon-like structure, core-shell structure, and quasi-sandwich structure.
- ii. With regard to the Si source, there is an increasing cost concern during the choice of Si precursor for practical production. Generally, bulk Si (more than 10 μm) is around 10 times cheaper than nanosilicon. Notably, after rational porosity engineering and microstructural modification, its tap density and electrochemical performance could still meet the demand.[160] Besides, clay minerals are another low-cost Si source, and it has been used for the formation of 3D porous Si, 2D Si flakes, and 0D nanosilicon.[161] Natural halloysite clay could even be used as the precursor for ultrafine nanosilicon.[162]
- iii. For industrial production of silicon materials, scalability and batch-to-batch consistency are significantly important. Aiming to enhance the consistency, rice husks, with highly consistent pore structures and massive quantities worldwide (96 million tons in 2016) showed great potential to be selected as scalable Si candidates, as silica occupies around 20 wt% of the whole weight.[163] After fabricating with carbon matrix, the conductivity and stability of rice husk-based electrodes could be effectively optimized.[164] Additionally, other natural sources, such as sugar cane bagasse, bamboo, and reed plant, could also be applied in a scalable manner in the production of Si-based anodes.[165] Commercial Si alloys, such as Fe-Si alloy and Al-Si alloy, are also regarded as some of the most promising candidates for Si-based anodes to date, considering that the microsized porous Si obtained through facile acid

etching could maintain good tap density, optimized SEI film, and reliable consistency.[166]

iv. Electrodes with high loading level and areal capacity are essential in further industrial production. After several years of attempts, the cell-level energy density achieved was around 250 Wh kg^{-1} at a price of 200 to 300 US \$ kWh^{-1} . To meet the goals projected by the US Department of Energy Vehicle Technologies Office (350 Wh kg^{-1} and 125 US \$ kWh^{-1}) by 2022, the ratio of electrochemical active materials in batteries should be significantly increased, in addition to the exploration of new battery chemistries with enhanced capacity.[167] Using thick electrode is a reasonable way to maximize the active component ratio at the device level, thereby leading to increased battery energy density as well as decreased cost.[168, 169] Nevertheless, challenges, such as deteriorated reaction kinetics ascribed to the increased charge transfer distance should also be given close attention.

v. Effective ICE enhancement through binder optimization, surface modification, and rational prelithiation has come into being another trend in Si-graphite anode. In particular, prelithiation has recently been widely utilized as an effective method of balancing the excessive Li consumption during side reaction and SEI membrane formation, which suppresses volume change and promotes electrode integrity.[170] Generally, prelithiation could be carried out in four ways: stabilized Li metal powders (SLMP)-induced prelithiation, electrochemical prelithiation, additive-induced prelithiation, and mechanical prelithiation. In the SLMP-based prelithiation, lithium carbonate-coated Li particles are initially dispersed in Si-based anodes. Then the LiCO_3 could be broken under mechanical press, thereby ensuring sufficient contact between Li and the active material.[171, 172] Electrochemical prelithiation is a method of electrode prelithiation in a temporary cell or assembled electrochemical instrument, which is a widely used approach in labs but is infeasible for industrial application.[170] Additive-induced prelithiation is a facile method for ICE enhancement, wherein additives, such as lithium silicate powder and Li_xSi , are used because of their smaller particle size (100 to 200 nm) compared to SLMP, better dispersion in Si-based electrode, and

reduced effects on the volume of the electrode.[173] Nevertheless, Li_xSi additives are sensitive to moisture, and could be stored for several days in a dry atmosphere, but only 6 h in a moist atmosphere.[174] Prelithiation of Si could also be accomplished *via* high-energy ball milling; however, the high reactivity of lithium silicide particles significantly hinders its further exploration.[175]

vi. Other challenges, such as unstable SEI layer, tedious preparation process and high mechanical stress, should be further addressed for practical applications. Furthermore, the relatively undesirable conductivity and volume change still negatively influence the achievement of desirable properties.[176, 177] Delicate structure designation, *e.g.*, porosity engineering, void buffer fabrication, stable carbon coating, and heteroatom modification, can be further improved based on the physical and chemical properties of carbon and Si resources, which are of vital importance for their effective participation in the Li storage.

vii. Graphite with significantly stable electrochemical performance has been effectively used in electrodes as a reliable material or matrix, which is a facile way to increase the overall anode conductivity and mitigate the volume variation during cycling.[178] Up to now, various types of graphite with diameters ranging from 0.4 to 20 μm have been applied in LIBs, such as flake graphite, artificial graphite sphere, and natural bulk graphite. The size and morphology of graphite with different features need to be paid much more attention in the near future, given that small-sized flake graphite is suitable for spraying technique and graphite with a rough surface is more beneficial for CVD process.

viii. Many studies have reported that pitch, a kind of complex polymer mixture, is preferred as the binder polymer for Si-graphite electrode assembly owing to its low-cost, abundance, and facile encapsulation property.[179] Depending on production techniques, temperature, and origin of raw materials, pitch exhibits significantly different physical and chemical properties, heavily influencing the final performance of electrodes.[180] Thus, more efforts should be made to fully exploit the properties of pitch prior to electrode preparation.

Furthermore, it is crucial to figure out which component in the pitch mixture plays more important role during charge and discharge processes.

ix. When Si-based anodes are maintained at an open-circuit state, the cells generally undergo a slow self-discharge process, during which the lithium lost from the anode reacts with the electrolyte. Moreover, the terminal phase of lithium silicide could be easily influenced. When the temperature is higher than 100 °C, a Li₂₁Si₅ phase can be formed at the end of lithiation, whereas Li₁₅Si₄ can be formed at a relatively lower temperature (less than 85 °C) thereby demonstrating a decreased lithium storage capacity. In the near future, more efforts should be made to further understand the detailed processes and develop rational ways to effectively suppress the undesired capacity loss.

Therefore, the silicon-graphite based anodes combined with desirable integrity, acceptable cost, facile fabrication and reliable lithium storage capability are promising candidate to meet the increasing energy demand. Although significant improvements have been made in recent years, nonnegligible bottlenecks still exist and need to be paid more attention. With the investigation carried out purposefully and continuously by researchers worldwide, advanced LIBs could certainly be achieved with satisfactory energy storage performance.

Author Information:

Corresponding Author

*E-mail: smyung@sejong.ac.kr (S.-T. Myung) , yksun@hanyang.ac.kr (Y.-K. Sun)

ORCID

Yang-Kook Sun: 0000-0002-0117-0170

Seung-Taek Myung: 0000-0001-6888-5376

Declaration of interests

The authors declare that they have no known competing financial interests or personal relationships that could have appeared to influence the work reported in this paper

Acknowledgements

This work was supported by the Global Frontier R&D Programme (2013M3A6B1078875) of the Center for Hybrid Interface Materials (HIM) funded by the Ministry of Science; ICT & Future Planning and by the Human Resources Development programme (no. 20184010201720) of a Korea Institute of Energy Technology Evaluation and Planning (KETEP) grant funded by the Ministry of Trade, Industry, and Energy of the Korean government.

References

- [1] Y.K. Sun, S.T. Myung, B.C. Park, J. Prakash, I. Belharouak, K. Amine, High-energy cathode material for long-life and safe lithium batteries, *Nat. Mater.* 8 (2009) 320-324.
- [2] W.J. Kwak, Rosy, D. Sharon, C. Xia, H. Kim, L.R. Johnson, P.G. Bruce, L.F. Nazar, Y.K. Sun, A.A. Frimer, M. Noked, S.A. Freunberger, D. Aurbach, Lithium-oxygen batteries and related systems: potential, status, and future, *Chem. Rev.* 120 (2020) 6626-6683.
- [3] B. Dunn, H. Kamath, J.M. Tarascon, Electrical energy storage for the grid: a battery of choices, *Science* 334 (2011) 928-935.
- [4] Y.K. Sun, Z.H. Chen, H.J. Noh, D.J. Lee, H.G. Jung, Y. Ren, S. Wang, C.S. Yoon, S.T. Myung, K. Amine, Nanostructured high-energy cathode materials for advanced lithium batteries, *Nat. Mater.* 11 (2012) 942-947.
- [5] A. Yoshino, The birth of the lithium-ion battery, *Angew. Chem.-Int. Edit.* 51 (2012) 5798-5800.
- [6] J.Y. Hwang, S.T. Myung, Y.K. Sun, Sodium-ion batteries: present and future, *Chem. Soc. Rev.* 46 (2017) 3529-3614.

- [7] Z.H. Liu, Q. Yu, Y.L. Zhao, R.H. He, M. Xu, S.H. Feng, S.D. Li, L. Zhou, L.Q. Mai, Silicon oxides: a promising family of anode materials for lithium-ion batteries, *Chem. Soc. Rev.* 48 (2019) 285-309.
- [8] X.H. Liu, J.Y. Huang, In situ TEM electrochemistry of anode materials in lithium ion batteries, *Energy Environ. Sci.* 4 (2011) 3844-3860.
- [9] C.K. Chan, H.L. Peng, G. Liu, K. McIlwrath, X.F. Zhang, R.A. Huggins, Y. Cui, High-performance lithium battery anodes using silicon nanowires, *Nat. Nanotechnol.* 3 (2008) 31-35.
- [10] J.Y. Wang, W.L. Huang, Y.S. Kim, Y.K. Jeong, S.C. Kim, J. Heo, H.K. Lee, B.F. Liu, J. Nah, Y. Cui, Scalable synthesis of nanoporous silicon microparticles for highly cyclable lithium-ion batteries, *Nano Res.* 13 (2020) 1558-1563.
- [11] F. Wang, C.S. Song, B.X. Zhao, L. Sun, H.B. Du, One-pot solution synthesis of carbon-coated silicon nanoparticles as an anode material for lithium-ion batteries, *ChemComm* 56 (2020) 1109-1112.
- [12] X. Su, Q.L. Wu, J.C. Li, X.C. Xiao, A. Lott, W.Q. Lu, B.W. Sheldon, J. Wu, Silicon-Based Nanomaterials for Lithium-Ion Batteries: A Review, *Adv. Energy Mater.* 4 (2014) 1300882.
- [13] S.S. Zhu, J.B. Zhou, Y. Guan, W.L. Cai, Y.Y. Zhao, Y.C. Zhu, L.Q. Zhu, Y.C. Zhu, Y.T. Qian, Hierarchical Graphene-Scaffolded Silicon/Graphite Composites as High Performance Anodes for Lithium-Ion Batteries, *Small* 14 (2018) 1802457.
- [14] L. Zhang, C.R. Wang, Y.H. Dou, N.Y. Cheng, D.D. Cui, Y. Du, P.R. Liu, M. Al-Mamun, S.Q. Zhang, H.J. Zhao, A Yolk-Shell Structured Silicon Anode with Superior Conductivity and High Tap Density for Full Lithium-Ion Batteries, *Angew. Chem.-Int. Edit.* 58 (2019) 8824-8828.

- [15] L. Zhang, R. Rajagopalan, H.P. Guo, X.L. Hu, S.X. Dou, H.K. Liu, A Green and Facile Way to Prepare Granadilla-Like Silicon-Based Anode Materials for Li-Ion Batteries, *Adv. Funct. Mater.* 26 (2016) 440-446.
- [16] H. Shang, Z.C. Zuo, L. Yu, F. Wang, F. He, Y.L. Li, Low-Temperature Growth of All-Carbon Graphdiyne on a Silicon Anode for High-Performance Lithium-Ion Batteries, *Adv. Mater.* 30 (2018) 1801459.
- [17] B. Zhu, G.L. Liu, G.X. Lv, Y. Mu, Y.L. Zhao, Y.X. Wang, X.Q. Li, P.C. Yao, Y. Deng, Y. Cui, J. Zhu, Minimized lithium trapping by isovalent isomorphism for high initial Coulombic efficiency of silicon anodes, *Sci. Adv.* 5 (2019) eaax0651.
- [18] Y.C. Hu, B. Yu, X.P. Qi, B.M. Shi, S. Fang, Z.L. Yu, J.Y. Yang, The preparation of graphite/silicon@carbon composites for lithium-ion batteries through molten salts electrolysis, *J Mater Sci* 55 (2020) 10155-10167.
- [19] J.R. Szczech, S. Jin, Nanostructured silicon for high capacity lithium battery anodes, *Energy Environ. Sci.* 4 (2011) 56-72.
- [20] Y. Jin, B. Zhu, Z.D. Lu, N. Liu, J. Zhu, Challenges and Recent Progress in the Development of Si Anodes for Lithium-Ion Battery, *Adv. Energy Mater.* 7 (2017) 1700715.
- [21] S.O. Kim, A. Manthiram, A facile, low-cost synthesis of high-performance silicon-based composite anodes with high tap density for lithium-ion batteries, *J. Mater. Chem. A* 3 (2015) 2399-2406.
- [22] J. Zhang, Y.H. Liang, Q. Zhou, Y. Peng, H.B. Yang, Enhancing electrochemical properties of silicon-graphite anodes by the introduction of cobalt for lithium-ion batteries, *J. Power Sources* 290 (2015) 71-79.
- [23] J.H. Lee, W.J. Kim, J.Y. Kim, S.H. Lim, S.M. Lee, Spherical silicon/graphite/carbon composites as anode material for lithium-ion batteries, *J. Power Sources* 176 (2008) 353-358.

- [24] T.S. Mu, Z.G. Zhang, Q. Li, S.F. Lou, P.J. Zuo, C.Y. Du, G.P. Yin, Scalable submicron/micron silicon particles stabilized in a robust graphite-carbon architecture for enhanced lithium storage, *J. Colloid Interface Sci.* 555 (2019) 783-790.
- [25] C.H. Gan, C.K. Zhang, W.D. Wen, Y.K. Liu, J. Chen, Q.S. Xie, X.T. Luo, Enhancing Delithiation Reversibility of $\text{Li}_{15}\text{Si}_4$ Alloy of Silicon Nanoparticles-Carbon/Graphite Anode Materials for Stable-Cycling Lithium Ion Batteries by Restricting the Silicon Particle Size, *ACS Appl. Mater. Interfaces* 11 (2019) 35809-35819.
- [26] D. Sui, Y.Q. Xie, W.M. Zhao, H.T. Zhang, Y. Zhou, X.T. Qin, Y.F. Ma, Y. Yang, Y.S. Chen, A high-performance ternary Si composite anode material with crystal graphite core and amorphous carbon shell, *J. Power Sources* 384 (2018) 328-333.
- [27] Z. Yan, J.C. Guo, High-performance silicon-carbon anode material via aerosol spray drying and magnesiothermic reduction, *Nano Energy* 63 (2019) 103845.
- [28] Y. Yang, Z.X. Wang, Y. Zhou, H.J. Guo, X.H. Li, Synthesis of porous Si/graphite/carbon nanotubes@C composites as a practical high-capacity anode for lithium-ion batteries, *Mater. Lett.* 199 (2017) 84-87.
- [29] Z.L. Wang, Z.M. Mao, L.F. Lai, M. Okubo, Y.H. Song, Y.J. Zhou, X. Liu, W. Huang, Sub-micron silicon/pyrolyzed carbon@natural graphite self-assembly composite anode material for lithium-ion batteries, *Chem. Eng. J.* 313 (2017) 187-196.
- [30] I. Sultana, M.M. Rahman, S. Mateti, V.G. Ahmadabadi, A.M. Glushenkov, Y. Chen, K-ion and Na-ion storage performances of $\text{Co}_3\text{O}_4\text{-Fe}_2\text{O}_3$ nanoparticle-decorated super P carbon black prepared by a ball milling process, *Nanoscale* 9 (2017) 3646-3654.
- [31] J.T. Xu, I.Y. Jeon, J.M. Seo, S.X. Dou, L.M. Dai, J.B. Baek, Edge-Selectively Halogenated Graphene Nanoplatelets (XGnPs , X = Cl, Br, or I) Prepared by Ball-Milling and Used as Anode Materials for Lithium-Ion Batteries, *Adv. Mater.* 26 (2014) 7317-7323.

- [32] W.L. An, B.A. Gao, S.X. Mei, B. Xiang, J.J. Fu, L. Wang, Q.B. Zhang, P.K. Chu, K.F. Huo, Scalable synthesis of ant-nest-like bulk porous silicon for high-performance lithium-ion battery anodes, *Nat. Commun.* 10 (2019) 1447.
- [33] X.T. Li, D.D. Yang, X.C. Hou, J.H. Shi, Y. Peng, H.B. Yang, Scalable preparation of mesoporous Silicon@C/graphite hybrid as stable anodes for lithium-ion batteries, *J. Alloys Compd.* 728 (2017) 1-9.
- [34] J. Wang, W. Bao, L. Ma, G.Q. Tan, Y.F. Su, S. Chen, F. Wu, J. Lu, K. Amine, Scalable Preparation of Ternary Hierarchical Silicon Oxide-Nickel-Graphite Composites for Lithium-Ion Batteries, *Chemsuschem* 8 (2015) 4073-4080.
- [35] L.Z. Qian, J.L. Lan, M.Y. Xue, Y.H. Yu, X.P. Yang, Two-step ball-milling synthesis of a Si/SiO_x/C composite electrode for lithium ion batteries with excellent long-term cycling stability, *RSC Adv.* 7 (2017) 36697-36704.
- [36] S.Q. Huang, L.Z. Cheong, D.Y. Wang, C. Shen, Nanostructured Phosphorus Doped Silicon/Graphite Composite as Anode for High-Performance Lithium-Ion Batteries, *ACS Appl. Mater. Interfaces* 9 (2017) 23672-23678.
- [37] M. Cabello, E. Gucciardi, A. Herrán, D. Carriazo, A. Villaverde, T. Rojo, Towards a High-Power Si@graphite Anode for Lithium Ion Batteries through a Wet Ball Milling Process, *Molecules* 25 (2020) 2494.
- [38] W.P. Liu, H.R. Xu, H.Q. Qin, Y.L. Lv, G.S. Zhu, X.X. Lei, F. Lin, Z.J. Zhang, L.H. Wang, Rapid coating of asphalt to prepare carbon-encapsulated composites of nano-silicon and graphite for lithium battery anodes, *J Mater Sci* 55 (2020) 4382-4394.
- [39] W. Liu, P. Gao, Y.Y. Mi, J.T. Chen, H.H. Zhou, X.X. Zhang, Fabrication of high tap density LiFe_{0.6}Mn_{0.4}PO₄/C microspheres by a double carbon coating-spray drying method for high rate lithium ion batteries, *J. Mater. Chem. A* 1 (2013) 2411-2417.

- [40] M.R. Su, Z.X. Wang, H.J. Guo, X.H. Li, S.L. Huang, W. Xiao, L. Gan, Enhancement of the Cyclability of a Si/Graphite@Graphene composite as anode for Lithium-ion batteries, *Electrochim. Acta* 116 (2014) 230-236.
- [41] S. Chae, M. Ko, S. Park, N. Kim, J. Ma, J. Cho, Micron-sized Fe-Cu-Si ternary composite anodes for high energy Li-ion batteries, *Energy Environ. Sci.* 9 (2016) 1251-1257.
- [42] M. Li, X.H. Hou, Y.J. Sha, J. Wang, S.J. Hu, X. Liu, Z.P. Shao, Facile spray-drying/pyrolysis synthesis of core-shell structure graphite/silicon-porous carbon composite as a superior anode for Li-ion batteries, *J. Power Sources* 248 (2014) 721-728.
- [43] N. Kim, S. Chae, J. Ma, M. Ko, J. Cho, Fast-charging high-energy lithium-ion batteries via implantation of amorphous silicon nanolayer in edge-plane activated graphite anodes, *Nat. Commun.* 8 (2017) 812.
- [44] S. Jeong, J.P. Lee, M. Ko, G. Kim, S. Park, J. Cho, Etched Graphite with Internally Grown Si Nanowires from Pores as an Anode for High Density Li-Ion Batteries, *Nano Lett.* 13 (2013) 3403-3407.
- [45] S.Y. Lim, Amorphous-silicon nanoshell on artificial graphite composite as the anode for lithium-ion battery, *Solid State Sci.* 93 (2019) 24-30.
- [46] Q. Xu, J.Y. Li, J.K. Sun, Y.X. Yin, L.J. Wan, Y.G. Guo, Watermelon-Inspired Si/C Microspheres with Hierarchical Buffer Structures for Densely Compacted Lithium-Ion Battery Anodes, *Adv. Energy Mater.* 7 (2017) 1601481.
- [47] M. Ko, S. Chae, J. Ma, N. Kim, H.W. Lee, Y. Cui, J. Cho, Scalable synthesis of silicon-nanolayer-embedded graphite for high-energy lithium-ion batteries, *Nature Energy* 1 (2016) 16113.
- [48] S.H. Choi, G. Nam, S. Chae, D. Kim, N. Kim, W.S. Kim, J. Ma, J. Sung, S.M. Han, M. Ko, H.W. Lee, J. Cho, Robust Pitch on Silicon Nanolayer-Embedded Graphite for Suppressing Undesirable Volume Expansion, *Adv. Energy Mater.* 9 (2019) 1803121.

- [49] H.P. Jia, X.L. Li, J.H. Song, X. Zhang, L.L. Luo, Y. He, B.S. Li, Y. Cai, S.Y. Hu, X.C. Xiao, C.M. Wang, K.M. Rosso, R. Yi, R. Patel, J.G. Zhang, Hierarchical porous silicon structures with extraordinary mechanical strength as high-performance lithium-ion battery anodes, *Nat. Commun.* 11 (2020) 1474.
- [50] Z.J. Fan, J. Yan, T. Wei, G.Q. Ning, L.J. Zhi, J.C. Liu, D.X. Cao, G.L. Wang, F. Wei, Nanographene-Constructed Carbon Nanofibers Grown on Graphene Sheets by Chemical Vapor Deposition: High-Performance Anode Materials for Lithium Ion Batteries, *ACS Nano* 5 (2011) 2787-2794.
- [51] X.R. Wang, G. Yushin, Chemical vapor deposition and atomic layer deposition for advanced lithium ion batteries and supercapacitors, *Energy Environ. Sci.* 8 (2015) 1889-1904.
- [52] I.C. Kim, D. Byun, S. Lee, J.K. Lee, Electrochemical characteristics of copper silicide-coated graphite as an anode material of lithium secondary batteries, *Electrochim. Acta* 52 (2006) 1532-1537.
- [53] L.B. Hu, H. Wu, S.S. Hong, L.F. Cui, J.R. McDonough, S. Bohy, Y. Cui, Si nanoparticle-decorated Si nanowire networks for Li-ion battery anodes, *ChemComm* 47 (2011) 367-369.
- [54] H. Kim, J. Cho, Superior Lithium Electroactive Mesoporous Si@Carbon Core-Shell Nanowires for Lithium Battery Anode Material, *Nano Lett.* 8 (2008) 3688-3691.
- [55] I.C. Kim, D. Byun, J.K. Lee, Electrochemical characteristics of silicon-metals coated graphites for anode materials of lithium secondary batteries, *J. Electroceramics* 17 (2006) 661-665.
- [56] S.Y. Kim, J. Lee, B.H. Kim, Y.J. Kim, K.S. Yang, M.S. Park, Facile Synthesis of Carbon-Coated Silicon/Graphite Spherical Composites for High-Performance Lithium-Ion Batteries, *ACS Appl. Mater. Interfaces* 8 (2016) 12109-12117.

- [57] Y. Yang, Z.X. Wang, G.C. Yan, H.J. Guo, J.X. Wang, X.H. Li, Y. Zhou, R. Zhou, Pitch carbon and LiF co-modified Si-based anode material for lithium ion batteries, Ceram. Int. 43 (2017) 8590-8595.
- [58] Z.L. Hu, Z.Q. Zhang, J. Mao, Silicon and reduced graphene oxide employed as additives to enhance the performances of artificial graphite anode for lithium-ion battery, Fuller. Nanotub. Carbon Nanostructures 27 (2019) 887-894.
- [59] T. Zhang, J. Gao, L.J. Fu, L.C. Yang, Y.P. Wu, H.Q. Wu, Natural graphite coated by Si nanoparticles as anode materials for lithium ion batteries, J. Mater. Chem. 17 (2007) 1321-1325.
- [60] F.S. Li, Y.S. Wu, J. Chou, N.L. Wu, A dimensionally stable and fast-discharging graphite-silicon composite Li-ion battery anode enabled by electrostatically self-assembled multifunctional polymer-blend coating, ChemComm 51 (2015) 8429-8431.
- [61] Y.C. Hsu, C.C. Hsieh, W.R. Liu, Synthesis of double core-shell carbon/silicon/graphite composite anode materials for lithium-ion batteries, Surf. Coat. Technol. 387 (2020) 125528.
- [62] H. Wiggers, Y.H. Sehlleier, F. Kunze, L.S. Xiao, S.M. Schnurre, C. Schulz, Self-assembled nano-silicon/graphite hybrid embedded in a conductive polyaniline matrix for the performance enhancement of industrial applicable lithium-ion battery anodes, Solid State Ion 344 (2020) 115117.
- [63] C.M. Xiao, P. He, J.G. Ren, M. Yue, Y.Y. Huang, X.Q. He, Walnut-structure Si-G/C materials with high coulombic efficiency for long-life lithium ion batteries, RSC Adv. 8 (2018) 27580-27586.
- [64] X.L. Li, P.F. Yan, X.C. Xiao, J.H. Woo, C.M. Wang, J. Liua, J.G. Zhang, Design of porous Si/C-graphite electrodes with long cycle stability and controlled swelling, Energy Environ. Sci. 10 (2017) 1427-1434.

- [65] M.S. Park, S. Rajendran, Y.M. Kang, K.S. Han, Y.S. Han, J.Y. Lee, Si-Ni alloy-graphite composite synthesized by arc-melting and high-energy mechanical milling for use as an anode in lithium-ion batteries, *J. Power Sources* 158 (2006) 650-653.
- [66] S. Jeong, X.L. Li, J.M. Zheng, P.F. Yan, R.G. Cao, H.J. Jung, C.M. Wang, J. Liu, J.G. Zhang, Hard carbon coated nano-Si/graphite composite as a high performance anode for Li-ion batteries, *J. Power Sources* 329 (2016) 323-329.
- [67] S.S. Suh, W.Y. Yoon, D.H. Kim, S.U. Kwon, J.H. Kim, Y.U. Kim, C.U. Jeong, Y.Y. Chan, S.H. Kang, J.K. Lee, Electrochemical behavior of SiO_x anodes with variation of oxygen ratio for Li-ion batteries, *Electrochim. Acta* 148 (2014) 111-117.
- [68] LM. Wei, Z.Y. Hou, H. Wei, Preparation, Porous sandwiched graphene/silicon anodes for lithium storage, *Electrochim. Acta* 229 (2017) 445-451.
- [69] Y. Zheng, H.J. Seifert, H. Shi, Y. Zhang, C. Kubel, W. Pfleging, 3D silicon/graphite composite electrodes for high-energy lithium-ion batteries, *Electrochim. Acta* 317 (2019) 502-508.
- [70] R.S. Gao, J. Tang, X.L. Yu, S. Tang, K. Ozawa, T. Sasaki, L.C. Qin, In situ synthesis of MOF-derived carbon shells for silicon anode with improved lithium-ion storage, *Nano Energy* 70 (2020).
- [71] N. Kim, H. Park, N. Yoon, J.K. Lee, Zeolite-Templated Mesoporous Silicon Particles for Advanced Lithium-Ion Battery Anodes, *ACS Nano* 12 (2018) 3853-3864.
- [72] Q. Xu, J.K. Sun, Y.X. Yin, Y.G. Guo, Facile Synthesis of Blocky SiO_x/C with Graphite-Like Structure for High-Performance Lithium-Ion Battery Anodes, *Adv. Funct. Mater.* 28 (2018) 1705235.
- [73] H. Uono, B.C. Kim, T. Fuse, M. Ue, J.I. Yamaki, Optimized structure of silicon/carbon/graphite composites as an anode material for Li-ion batteries, *J. Electrochem. Soc.* 153 (2006) A1708-A1713.

- [74] M.R. Su, Z.X. Wang, H.J. Guo, X.H. Li, S.L. Huang, L. Gan, Silicon, flake graphite and phenolic resin-pyrolyzed carbon based Si/C composites as anode material for lithium-ion batteries, *Adv Powder Technol* 24 (2013) 921-925.
- [75] R. Zhou, H.J. Guo, Y. Yang, Z.X. Wang, X.H. Li, Y. Zhou, N-doped carbon layer derived from polydopamine to improve the electrochemical performance of spray-dried Si/graphite composite anode material for lithium ion batteries, *J. Alloys Compd.* 689 (2016) 130-137.
- [76] P. Li, J.Y. Hwang, Y.K. Sun, Nano/Microstructured Silicon-Graphite Composite Anode for High-Energy-Density Li-Ion Battery, *ACS Nano* 13 (2019) 2624-2633.
- [77] M. Ashuri, Q.R. He, Y.Z. Liu, S. Emani, L.L. Shaw, Synthesis and performance of nanostructured silicon/graphite composites with a thin carbon shell and engineered voids, *Electrochim. Acta* 258 (2017) 274-283.
- [78] X.X. Li, G.Q. Zhang, L. Zhang, M.L. Zhong, X.J. Yuan, Silicon/Graphite/Carbon Nanotubes Composite as Anode for Lithium Ion Battery, *Int. J. Electrochem. Sci.* 10 (2015) 2802-2811.
- [79] M. Wetjen, D. Pritzl, R. Jung, S. Solchenbach, R. Ghadimi, H.A. Gasteiger, Differentiating the Degradation Phenomena in Silicon-Graphite Electrodes for Lithium-Ion Batteries, *J. Electrochem. Soc.* 164 (2017) A2840-A2852.
- [80] F. Jeschull, Y. Surace, S. Zürcher, G. Lari, M.E. Spahr, P. Novak, S.S. Trabesinger, Graphite Particle-Size Induced Morphological and Performance Changes of Graphite–Silicon Electrodes, *J. Electrochem. Soc.* (2020) 100535.
- [81] M.H. Parekh, V.P. Parikh, P.J. Kim, S. Misra, Z.M. Qi, H.Y. Wang, V.G. Pol, Encapsulation and networking of silicon nanoparticles using amorphous carbon and graphite for high performance Li-ion batteries, *Carbon* 148 (2019) 36-43.

- [82] S. Kim, Y.K. Jeong, Y. Wang, H. Lee, J.W. Choi, A "Sticky" Mucin-Inspired DNA-Polysaccharide Binder for Silicon and Silicon-Graphite Blended Anodes in Lithium-Ion Batteries, *Adv. Mater.* 30 (2018) 1707594.
- [83] K.G. Gallagher, D.W. Dees, A.N. Jansen, D.P. Abraham, S.H. Kang, A Volume Averaged Approach to the Numerical Modeling of Phase-Transition Intercalation Electrodes Presented for LixC₆, *J. Electrochem. Soc.* 159 (2012) A2029-A2037.
- [84] M. Yoshio, H.Y. Wang, K. Fukuda, Spherical carbon-coated natural graphite as a lithium-ion battery-anode material, *Angew. Chem.-Int. Edit.* 42 (2003) 4203-4206.
- [85] M.T. McDowell, S.W. Lee, W.D. Nix, Y. Cui, 25th Anniversary Article: Understanding the Lithiation of Silicon and Other Alloying Anodes for Lithium-Ion Batteries, *Adv. Mater.* 25 (2013) 4966-4984.
- [86] M.T. McDowell, S.W. Lee, J.T. Harris, B.A. Korgel, C.M. Wang, W.D. Nix, Y. Cui, In Situ TEM of Two-Phase Lithiation of Amorphous Silicon Nanospheres, *Nano Lett.* 13 (2013) 758-764.
- [87] Z.D. Zeng, N.A. Liu, Q.S. Zeng, S.W. Lee, W.L. Mao, Y. Cui, In situ measurement of lithiation-induced stress in silicon nanoparticles using micro-Raman spectroscopy, *Nano Energy* 22 (2016) 105-110.
- [88] F.F. Shi, Z.C. Song, P.N. Ross, G.A. Somorjai, R.O. Ritchie, K. Komvopoulos, Failure mechanisms of single-crystal silicon electrodes in lithium-ion batteries, *Nat. Commun.* 7 (2016) 11886.
- [89] M. Wetjen, S. Solchenbach, D. Pritzl, J. Hou, V. Tileli, H.A. Gasteiger, Morphological Changes of Silicon Nanoparticles and the Influence of Cutoff Potentials in Silicon-Graphite Electrodes, *J. Electrochem. Soc.* 165 (2018) A1503-A1514.
- [90] S.B. Son, L. Cao, T. Yoon, A. Cresce, S.E. Hafner, J. Liu, M. Groner, K. Xu, C.M. Ban, Interfacially Induced Cascading Failure in Graphite-Silicon Composite Anodes, *Adv. Sci.* 6 (2019) 1801007.

- [91] X.H. Liu, L. Zhong, S. Huang, S.X. Mao, T. Zhu, J.Y. Huang, Size-Dependent Fracture of Silicon Nanoparticles During Lithiation, *ACS Nano* 6 (2012) 1522-1531.
- [92] A.L. Michan, G. Divitini, A.J. Pell, M. Leskes, C. Ducati, C.P. Grey, Solid Electrolyte Interphase Growth and Capacity Loss in Silicon Electrodes, *J. Am. Chem. Soc.* 138 (2016) 7918-7931.
- [93] D.T. Nguyen, J. Kang, K.M. Nam, Y. Paik, S.W. Song, Understanding interfacial chemistry and stability for performance improvement and fade of high-energy Li-ion battery of $\text{LiNi}_{0.5}\text{Co}_{0.2}\text{Mn}_{0.3}\text{O}_2$ //silicon-graphite, *J. Power Sources* 303 (2016) 150-158.
- [94] T. Jaumann, J. Balach, M. Klose, S. Oswald, U. Langklotz, A. Michaelis, J. Eckerta, L. Giebelera, SEI-component formation on sub 5 nm sized silicon nanoparticles in Li-ion batteries: the role of electrode preparation, FEC addition and binders, *Phys. Chem. Chem. Phys.* 17 (2015) 24956-24967.
- [95] N. Dupre, P. Moreau, E. De Vito, L. Quazuguel, M. Boniface, A. Bordes, C. Rudisch, P. Bayle-Guillemaud, D. Guyomard, Multiprobe Study of the Solid Electrolyte Interphase on Silicon-Based Electrodes in Full-Cell Configuration, *Chem. Mat.* 28 (2016) 2557-2572.
- [96] J. Barenco, I.A. Shkrob, J.A. Gilbert, M. Klett, D.P. Abraham, Capacity Fade and Its Mitigation in Li-Ion Cells with Silicon-Graphite Electrodes, *J. Phys. Chem. C* 121 (2017) 20640-20649.
- [97] Y.R. Ren, J.N. Ding, N.Y. Yuan, S.Y. Jia, M.Z. Qu, Z.L. Yu, Preparation and characterization of silicon monoxide/graphite/carbon nanotubes composite as anode for lithium-ion batteries, *J. Solid State Chem.* 16 (2012) 1453-1460.
- [98] H.J. Xue, Y.Q. Wu, Y.G. Zou, Y.B. Shen, G. Liu, Q. Li, D.M. Yin, L.M. Wang, J. Ming, Unraveling Metal Oxide Role in Exfoliating Graphite: New Strategy to Construct High-Performance Graphene-Modified SiO_x -Based Anode for Lithium-Ion Batteries, *Adv. Funct. Mater.* 30 (2020) 1910657.

- [99] W.J. He, T.F. Zhang, J.M. Jiang, C.L. Chen, Y.D. Zhang, N. Liu, H. Dou, X.G. Zhang, Efficient Synthesis of N-Doped SiO_x/C Composite Based on the Defect-Enriched Graphite Flake for Lithium-Ion Battery, ACS Appl. Energy Mater. 3 (2020) 4394-4402.
- [100] J. Yang, Y. Takeda, N. Imanishi, C. Capiglia, J.Y. Xie, O. Yamamoto, SiO_x-based anodes for secondary lithium batteries, Solid State Ion 152 (2002) 125-129.
- [101] Y.S. Hu, R. Demir-Cakan, M.M. Titirici, J.O. Muller, R. Schlogl, M. Antonietti, J. Maier, Superior storage performance of a Si@SiO_x/C nanocomposite as anode material for lithium-ion batteries, Angew. Chem.-Int. Edit. 47 (2008) 1645-1649.
- [102] W. Luo, X.Q. Chen, Y. Xia, M. Chen, L.J. Wang, Q.Q. Wang, W. Li, J.P. Yang, Surface and Interface Engineering of Silicon-Based Anode Materials for Lithium-Ion Batteries, Adv. Energy Mater. 7 (2017).
- [103] H. Ming, J.Y. Qiu, S.T. Zhang, M. Li, X.Y. Zhu, L.M. Wang, J. Ming, Constructing Dense SiO_x@Carbon Nanotubes versus Spinel Cathode for Advanced High-Energy Lithium-Ion Batteries, Chemelectrochem 4 (2017) 1165-1171.
- [104] J. Wang, H.L. Zhao, J.C. He, C.M. Wang, J. Wang, Nano-sized SiO_x/C composite anode for lithium ion batteries, J. Power Sources 196 (2011) 4811-4815.
- [105] L. Zhang, J.W. Deng, L.F. Liu, W.P. Si, S. Oswald, L.X. Xi, M. Kundu, G.Z. Ma, T. Gemming, S. Baunack, F. Ding, C.L. Yan, O.G. Schmidt, Hierarchically Designed SiO_x/SiO_y Bilayer Nanomembranes as Stable Anodes for Lithium Ion Batteries, Adv. Mater. 26 (2014) 4527-4532.
- [106] M.S. Munde, A. Mehonic, W.H. Ng, M. Buckwell, L. Montesi, M. Bosman, A.L. Shluger, A.J. Kenyon, Intrinsic Resistance Switching in Amorphous Silicon Suboxides: The Role of Columnar Microstructure, Sci. Rep. 7 (2017) 9274.
- [107] Y. Zhang, G.N. Guo, C. Chen, Y.C. Jiao, T.T. Li, X. Chen, Y.C. Yang, D. Yang, A.G. Dong, An affordable manufacturing method to boost the initial Coulombic efficiency of disproportionated SiO lithium-ion battery anodes, J. Power Sources 426 (2019) 116-123.

- [108] W. Wu, M. Wang, R. Wang, D.W. Xu, H.B. Zeng, C.Y. Wang, Y.L. Cao, Y.H. Deng, Magnesio-mechanochemical reduced SiO_x for high-performance lithium ion batteries, *J. Power Sources* 407 (2018) 112-122.
- [109] C.S. Yoon, M.H. Choi, B.B. Lim, E.J. Lee, Y.K. Sun, Review-High-Capacity $\text{Li Ni}_{1-x}\text{Co}_{x/2}\text{Mn}_{x/2}\text{O}_2$ ($x=0.1, 0.05, 0$) Cathodes for Next-Generation Li-Ion Battery, *J. Electrochem. Soc.* 162 (2015) A2483-A2489.
- [110] J.B. Park, J.S. Ham, M.S. Shin, H.K. Park, Y.J. Lee, S.M. Lee, Synthesis and electrochemical characterization of anode material with titanium-silicon alloy solid core/nanoporous silicon shell structures for lithium rechargeable batteries, *J. Power Sources* 299 (2015) 537-543.
- [111] T. Li, Y.L. Cao, X.P. Ai, H.X. Yang, Cycleable graphite/FeSi₆ alloy composite as a high capacity anode material for Li-ion batteries, *J. Power Sources* 184 (2008) 473-476.
- [112] Y. Chen, J.F. Qian, Y.L. Cao, H.X. Yang, X.P. Ai, Green Synthesis and Stable Li-Storage Performance of FeSi₂/Si@C Nanocomposite for Lithium-Ion Batteries, *ACS Appl. Mater. Interfaces* 4 (2012) 3753-3758.
- [113] Z. Edfouf, F. Cuevas, M. Latroche, C. Georges, C. Jordy, T. Hezeque, G. Caillon, J.C. Jumas, M.T. Sougrati, Nanostructured Si/Sn-Ni/C composite as negative electrode for Li-ion batteries, *J. Power Sources* 196 (2011) 4762-4768.
- [114] Z.Q. Zhang, X. Han, L.C. Li, P.F. Su, W. Huang, J.Y. Wang, J.F. Xu, C. Li, S.Y. Chen, Y. Yang, Tailoring the interfaces of silicon/carbon nanotube for high rate lithium-ion battery anodes, *J. Power Sources* 450 (2020).
- [115] N. Harpak, G. Davidi, D. Schneier, S. Menkin, E. Mados, D. Golodnitsky, E. Peled, F. Patolsky, Large-Scale Self-Catalyzed Spongelike Silicon Nano-Network-Based 3D Anodes for High-Capacity Lithium-Ion Batteries, *Nano Lett.* 19 (2019) 1944-1954.
- [116] J.H. Cho, X.L. Li, S.T. Picraux, The effect of metal silicide formation on silicon nanowire-based lithium-ion battery anode capacity, *J. Power Sources* 205 (2012) 467-473.

- [117] P. Wang, Y. NuLi, J. Yang, Y. Zheng, Carbon-coated Si-Cu/graphite Composite as Anode Material for Lithium-ion Batteries, *Int. J. Electrochem. Sci.* 1 (2006) 122-129.
- [118] L. Gan, H.J. Guo, Z.X. Wang, X.H. Li, W.J. Peng, J.X. Wang, S.L. Huang, M.R. Su, A facile synthesis of graphite/silicon/graphene spherical composite anode for lithium-ion batteries, *Electrochim. Acta* 104 (2013) 117-123.
- [119] W. Liu, Y.M. Zhong, S.Y. Yang, S.S. Zhang, X.Y. Yu, H.Q. Wang, Q.Y. Li, J. Li, X. Cai, Y.P. Fang, Electrospray synthesis of nano-Si encapsulated in graphite/carbon microplates as robust anodes for high performance lithium-ion batteries, *Sustain. Energy Fuels* 2 (2018) 679-687.
- [120] D. Lee, A. Kondo, S. Lee, S. Myeong, S. Sun, I. Hwang, T. Song, M. Naito, U. Paik, Controlled swelling behavior and stable cycling of silicon/graphite granular composite for high energy density in lithium ion batteries, *J. Power Sources* 457 (2020) 228021.
- [121] J. Wu, W.M. Tu, Y. Zhang, B.L. Guo, S.S. Li, Y. Zhang, Y.D. Wang, M. Pan, Poly-dopamine coated graphite oxide/silicon composite as anode of lithium ion batteries, *Powder Technol.* 311 (2017) 200-205.
- [122] A. Yin, L. Yang, Z. Zhuang, Q. Feng, Z. Liu, T. Chen, F. Tu, Q. Peng, L. Luo, G. Tang, A novel silicon graphite composite material with core-shell structure as an anode for lithium ion batteries, *Energy Storage* 4 (2020) e132.
- [123] M. Sohn, D.G. Lee, H.I. Park, C. Park, J.H. Choi, H. Kim, Microstructure Controlled Porous Silicon Particles as a High Capacity Lithium Storage Material via Dual Step Pore Engineering, *Adv. Funct. Mater.* 28 (2018) 1800855.
- [124] W. Wang, Z. Favors, C. Li, C. Liu, R. Ye, C. Fu, K. Bozhilov, J. Guo, M. Ozkan, C.S. Ozkan, Silicon and Carbon Nanocomposite Spheres with Enhanced Electrochemical Performance for Full Cell Lithium Ion Batteries, *Sci. Rep.* 7 (2017) 44838.
- [125] T. Jaumann, M. Gerwig, J. Balach, S. Oswald, E. Brendler, R. Hauser, B. Kieback, U. Eckert, L. Giebel, E. Kroke, Dichlorosilane-derived nano-silicon inside hollow carbon

spheres as a high-performance anode for Li-ion batteries, *J. Mater. Chem. A* 5 (2017) 9262-9271.

[126] P. Guan, W. Zhang, C.Y. Li, N. Han, X.C. Wang, Q.F. Li, G.J. Song, Z. Peng, J.J. Li, L. Zhang, X.Y. Zhu, Low-cost urchin-like silicon-based anode with superior conductivity for lithium storage applications, *J. Colloid Interface Sci.* 575 (2020) 150-157.

[127] M. Ge, X. Fang, J. Rong, C. Zhou, Review of porous silicon preparation and its application for lithium-ion battery anodes, *Nanotechnology* 24 (2013) 422001.

[128] W.T. Yang, H.J. Ying, S.L. Zhang, R.N. Guo, J.L. Wang, W.Q. Han, Electrochemical performance enhancement of porous Si lithium-ion battery anode by integrating with optimized carbonaceous materials, *Electrochim. Acta* 337 (2020) 135687.

[129] Q. Xu, J.K. Sun, J.Y. Li, Y.X. Yin, Y.G. Guo, Scalable synthesis of spherical Si/C granules with 3D conducting networks as ultrahigh loading anodes in lithium-ion batteries, *Energy Stor. Mater.* 12 (2018) 54-60.

[130] H. Wang, J. Xie, S.C. Zhang, G.S. Cao, X.B. Zhao, Scalable preparation of silicon@graphite/carbon microspheres as high-performance lithium-ion battery anode materials, *RSC Adv.* 6 (2016) 69882-69888.

[131] J. Li, J.T. Wang, J.Y. Yang, X.L. Ma, S.G. Lu, Scalable synthesis of a novel structured graphite/silicon/pyrolyzed-carbon composite as anode material for high-performance lithium-ion batteries, *J. Alloys Compd.* 688 (2016) 1072-1079.

[132] J. Lai, H.J. Guo, Z.X. Wang, X.H. Li, X.P. Zhang, F.X. Wu, P. Yue, Preparation and characterization of flake graphite/silicon/carbon spherical composite as anode materials for lithium-ion batteries, *J. Alloys Compd.* 530 (2012) 30-35.

[133] Y.N. Jo, Y. Kim, J.S. Kim, J.H. Song, K.J. Kim, C.Y. Kwag, D.J. Lee, C.W. Park, Y.J. Kim, Si-graphite composites as anode materials for lithium secondary batteries, *J. Power Sources* 195 (2010) 6031-6036.

- [134] B. Liu, P. Huang, Q. Zhang, Q.Z. Huang, Z.Y. Xie, Rational-design micro-nanostructure of porous carbon film/silicon nanowire/graphite microsphere composites for high-performance lithium-ion batteries, *J Mater Sci* 55 (2020) 12165-12176.
- [135] Z.X. Yang, Y. Du, G.L. Hou, Y.G. Ouyang, F. Ding, F.L. Yuan, Nanoporous silicon spheres preparation via a controllable magnesiothermic reduction as anode for Li-ion batteries, *Electrochim. Acta* 329 (2020) 135141.
- [136] F. Aupperle, G.G. Eshetu, K.W. Eberman, A. Xiaoa, J.-S. Bridel, E. Figgemeier, Realizing a high-performance $\text{LiNi}_{0.6}\text{Mn}_{0.2}\text{Co}_{0.2}\text{O}_2$ /silicon-graphite full lithium ion battery cell via a designer electrolyte additive, *J. Mater. Chem. A* (2020) 19573-19587.
- [137] L. De Sutter, G. Berckmans, M. Marinaro, M. Wohlfahrt-Mehrens, M. Berecibar, J. Van Mierlo, Mechanical behavior of Silicon-Graphite pouch cells under external compressive load: Implications and opportunities for battery pack design, *J. Power Sources* 451 (2020) 227774.
- [138] S. Karuppiyah, C. Keller, P. Kumar, P.-H. Jouneau, D. Aldakov, J.-B. Ducros, G. Lapertot, P. Chenevier, C. Haon, A Scalable Silicon Nanowires-Grown-On-Graphite Composite for High Energy Lithium Batteries, *ACS Nano* (2020) 12006-12015.
- [139] Y. Son, N. Kim, T. Lee, Y. Lee, J. Ma, S. Chae, J. Sung, H. Cha, Y. Yoo, J. Cho, Calendering-Compatible Macroporous Architecture for Silicon-Graphite Composite toward High-Energy Lithium-Ion Batteries, *Adv. Mater.* 37 (2020) 2003286.
- [140] G. Hernandez, A.J. Naylor, Y.C. Chien, D. Brandell, J. Mindemark, K. Edstrom, Elimination of Fluorination: The Influence of Fluorine-Free Electrolytes on the Performance of $\text{LiNi}_{1/3}\text{Mn}_{1/3}\text{Co}_{1/3}\text{O}_2$ /Silicon-Graphite Li-Ion Battery Cells, *ACS Sustain. Chem. Eng.* 8 (2020) 10041-10052.
- [141] A. Ratner, R. Beaumont, I. Masters, Dynamic Mechanical Compression Impulse of Lithium-Ion Pouch Cells, *Energies* 13 (2020) 2105.

- [142] Y.S. Hu, R. Demir - Cakan, M.M. Titirici, J.O. Müller, R. Schlögl, M. Antonietti, J. Maier, Superior storage performance of a Si@SiO_x/C nanocomposite as anode material for lithium-ion batteries, *Angew. Chem. Int. Ed.* 47 (2008) 1645-1649.
- [143] J. Cannarella, C.B. Arnold, Stress evolution and capacity fade in constrained lithium-ion pouch cells, *J. Power Sources* 245 (2014) 745-751.
- [144] S.J. An, J.L. Li, C. Daniel, H.M. Meyer, S.E. Trask, B.J. Polzin, D.L. Wood, Electrolyte Volume Effects on Electrochemical Performance and Solid Electrolyte Interphase in Si-Graphite/NMC Lithium-Ion Pouch Cells, *ACS Appl. Mater. Interfaces* 9 (2017) 18799-18808.
- [145] I. Zilberman, J. Sturm, A. Jossen, Reversible self-discharge and calendar aging of 18650 nickel-rich, silicon-graphite lithium-ion cells, *J. Power Sources* 425 (2019) 217-226.
- [146] T. Inoue, K. Mukai, Roles of positive or negative electrodes in the thermal runaway of lithium-ion batteries: accelerating rate calorimetry analyses with an all-inclusive microcell, *Electrochimica Acta* 77 (2017) 28-31.
- [147] X. Liu, D.S. Ren, H.J. Hsu, X.N. Feng, G.L. Xu, M.H. Zhuang, H. Gao, L.G. Lu, X.B. Han, Z.Y. Chu, J.Q. Li, X.M. He, K. Amine, M.G. Ouyang, Thermal Runaway of Lithium-Ion Batteries without Internal Short Circuit, *Joule* 2 (2018) 2047-2064.
- [148] D.P. Finegan, E. Darcy, M. Keyser, B. Tjaden, T.M.M. Heenan, R. Jervis, J.J. Bailey, R. Malik, N.T. Vo, O.V. Magdysyuk, R. Atwood, M. Drakopoulos, M. DiMichiel, A. Rack, G. Hinds, D.J.L. Brett, P.R. Shearing, Characterising thermal runaway within lithium-ion cells by inducing and monitoring internal short circuits, *Energy Environ. Sci.* 10 (2017) 1377-1388.
- [149] S. Koch, A. Fill, K.P. Birke, Comprehensive gas analysis on large scale automotive lithium-ion cells in thermal runaway, *J. Power Sources* 398 (2018) 106-112.
- [150] Z.J. Han, K. Yamagiwa, N. Yabuuchi, J.Y. Son, Y.T. Cui, H. Oji, A. Kogure, T. Harada, S. Ishikawa, Y. Aoki, S. Komaba, Electrochemical lithiation performance and

characterization of silicon-graphite composites with lithium, sodium, potassium, and ammonium polyacrylate binders, *Phys. Chem. Chem. Phys.* 17 (2015) 3783-3795.

[151] P. Pietsch, D. Westhoff, J. Feinauer, J. Eller, F. Marone, M. Stampaoni, V. Schmidt, V. Wood, Quantifying microstructural dynamics and electrochemical activity of graphite and silicon-graphite lithium ion battery anodes, *Nat. Commun.* 7 (2016) 12909.

[152] K.P.C. Yao, J.S. Okasinski, K. Kalaga, J.D. Almer, D.P. Abraham, Operando Quantification of (De)Lithiation Behavior of Silicon-Graphite Blended Electrodes for Lithium-Ion Batteries, *Adv. Energy Mater.* 9 (2019) 1803380.

[153] H. Jung, K.S. Kim, S.E. Park, J. Park, The structural and electrochemical study on the blended anode with graphite and silicon carbon nano composite in Li ion battery, *Electrochim. Acta* 245 (2017) 791-795.

[154] D.P. Finegan, A. Vamvakeros, L. Cao, C. Tan, T.M.M. Heenan, S.R. Daemi, S.D.M. Jacques, A.M. Beale, M. Di Michiel, K. Smith, D.J.L. Brett, P.R. Shearing, C.M. Ban, Spatially Resolving Lithiation in Silicon-Graphite Composite Electrodes via in Situ High-Energy X-ray Diffraction Computed Tomography, *Nano Lett.* 19 (2019) 3811-3820.

[155] M. Wetjen, M. Trunk, L. Werner, R. Gernhauser, B. Markisch, Z. Revay, R. Gilles, H.A. Gasteiger, Quantifying the Distribution of Electrolyte Decomposition Products in Silicon-Graphite Electrodes by Neutron Depth Profiling, *J. Electrochem. Soc.* 165 (2018) A2340-A2348.

[156] R.E. Ruther, K.A. Hays, S.J. An, J.L. Li, D.L. Wood, J. Nanda, Chemical Evolution in Silicon-Graphite Composite Anodes Investigated by Vibrational Spectroscopy, *ACS Appl. Mater. Interfaces* 10 (2018) 18641-18649.

[157] S.Q. Huang, L.Z. Cheong, S.W. Wang, D.Y. Wang, C. Shen, In-situ study of surface structure evolution of silicon anodes by electrochemical atomic force microscopy, *Appl. Surf. Sci.* 452 (2018) 67-74.

- [158] C.G. Chen, T. Zhou, D.L. Danilov, L. Gao, S. Benning, N. Schon, S. Tardif, H. Simons, F. Hausen, T.U. Schulli, R.A. Eichel, P.H.L. Notten, Impact of dual-layer solid-electrolyte interphase inhomogeneities on early-stage defect formation in Si electrodes, *Nat. Commun.* 11 (2020) 3283.
- [159] C. Shen, S.W. Wang, Y. Jin, W.Q. Han, In Situ AFM Imaging of Solid Electrolyte Interfaces on HOPG with Ethylene Carbonate and Fluoroethylene Carbonate-Based Electrolytes, *ACS Appl. Mater. Interfaces* 7 (2015) 25441-25447.
- [160] Z.L. Zhang, Y.H. Wang, W.F. Ren, Q.Q. Tan, Y.F. Chen, H. Li, Z.Y. Zhong, F.B. Su, Scalable Synthesis of Interconnected Porous Silicon/Carbon Composites by the Rochow Reaction as High-Performance Anodes of Lithium Ion Batteries, *Angew. Chem.-Int. Edit.* 53 (2014) 5165-5169.
- [161] Q.Z. Chen, S.H. Liu, R.L. Zhu, D.C. Wu, H.Y. Fu, J.X. Zhu, H.P. He, Clay minerals derived nanostructured silicon with various morphology: Controlled synthesis, structural evolution, and enhanced lithium storage properties, *J. Power Sources* 405 (2018) 61-69.
- [162] X.Y. Zhou, L.L. Wu, J. Yang, J.J. Tang, L.H. Xi, B. Wang, Synthesis of nano-sized silicon from natural halloysite clay and its high performance as anode for lithium-ion batteries, *J. Power Sources* 324 (2016) 33-40.
- [163] H.J. Kim, J.H. Choi, J.W. Choi, Rice husk-originating silicon-graphite composites for advanced lithium ion battery anodes, *Nano Converg.* 4 (2017) 24.
- [164] Y.C. Zhang, Y. You, S. Xin, Y.X. Yin, J. Zhang, P. Wang, X.S. Zheng, F.F. Cao, Y.G. Guo, Rice husk-derived hierarchical silicon/nitrogen-doped carbon/carbon nanotube spheres as low-cost and high-capacity anodes for lithium-ion batteries, *Nano Energy* 25 (2016) 120-127.
- [165] W.U. Rehman, H.F. Wang, R.Z.A. Manj, W. Luo, J.P. Yang, When Silicon Materials Meet Natural Sources: Opportunities and Challenges for Low-Cost Lithium Storage, *Small* (2019) 1904508.

- [166] J.M. Su, C.C. Zhang, X. Chen, S.Y. Liu, T. Huang, A.S. Yu, Carbon-shell-constrained silicon cluster derived from Al-Si alloy as long-cycling life lithium ion batteries anode, *J. Power Sources* 381 (2018) 66-71.
- [167] Y.D. Kuang, C.J. Chen, D. Kirsch, L.B. Hu, Thick Electrode Batteries: Principles, Opportunities, and Challenges, *Adv. Energy Mater.* 9 (2019) 1901457.
- [168] H. Li, L. Peng, D.B. Wu, J. Wu, Y.J. Zhu, X.L. Hu, Ultrahigh-Capacity and Fire-Resistant LiFePO₄-Based Composite Cathodes for Advanced Lithium-Ion Batteries, *Adv. Energy Mater.* 9 (2019) 1802930.
- [169] R. Elango, A. Demortiere, V. De Andrade, M. Morcrette, V. Seznec, Thick Binder-Free Electrodes for Li-Ion Battery Fabricated Using Templating Approach and Spark Plasma Sintering Reveals High Areal Capacity, *Adv. Energy Mater.* 8 (2018) 1703031.
- [170] H.J. Kim, S. Choi, S.J. Lee, M.W. Seo, J.G. Lee, E. Deniz, Y.J. Lee, E.K. Kim, J.W. Choi, Controlled Prelithiation of Silicon Monoxide for High Performance Lithium-Ion Rechargeable Full Cells, *Nano Lett.* 16 (2016) 282-288.
- [171] Y.X. Sun, H.M. Guan, Z.H. Jiang, Z.B. Wang, Study on Prelithiation Technology of Hard Carbon Electrode Using Stable Metal Lithium Powder, *J. Electrochem. Energy Convers. Storage* 16 (2019) 021007.
- [172] Q.R. Pan, P.J. Zuo, T.S. Mu, C.Y. Du, X.Q. Cheng, Y.L. Ma, Y.Z. Gao, G.P. Yin, Improved electrochemical performance of micro-sized SiO-based composite anode by prelithiation of stabilized lithium metal powder, *J. Power Sources* 347 (2017) 170-177.
- [173] J. Zhao, Z.D. Lu, N.A. Liu, H.W. Lee, M.T. McDowell, Y. Cui, Dry-air-stable lithium silicide-lithium oxide core-shell nanoparticles as high-capacity prelithiation reagents, *Nat. Commun.* 5 (2014) 5088.
- [174] J. Zhao, Z.D. Lu, H.T. Wang, W. Liu, H.W. Lee, K. Yan, D. Zhuo, D.C. Lin, N. Liu, Y. Cui, Artificial Solid Electrolyte Interphase-Protected Li_xSi Nanoparticles: An Efficient

and Stable Prelithiation Reagent for Lithium-Ion Batteries, *J. Am. Chem. Soc.* 137 (2015) 8372-8375.

[175] X.M. Li, F.E. Kersey-Bronec, J. Ke, J.E. Cloud, Y.L. Wang, C.L. Ngo, S. Pylypenko, Y.G. Yang, Study of Lithium Silicide Nanoparticles as Anode Materials for Advanced Lithium Ion Batteries, *ACS Appl. Mater. Interfaces* 9 (2017) 16071-16080.

[176] M.G. Jeong, H.L. Du, M. Islam, J.K. Lee, Y.K. Sun, H.G. Jung, Self-Rearrangement of Silicon Nanoparticles Embedded in Micro Carbon Sphere Framework for High-Energy and Long-Life Lithium Ion Batteries, *Nano Lett.* 17 (2017) 5600-5606.

[177] C. Chae, H.J. Noh, J.K. Lee, B. Scrosati, Y.K. Sun, A High-Energy Li-Ion Battery Using a Silicon-Based Anode and a Nano-Structured Layered Composite Cathode, *Adv. Funct. Mater.* 24 (2014) 3036-3042.

[178] J. Ming, Z. Cao, W. Wahyudi, M.L. Li, P. Kumar, Y.Q. Wu, J.Y. Hwang, M.N. Hedhili, L. Cavallo, Y.K. Sun, L.J. Li, New Insights on Graphite Anode Stability in Rechargeable Batteries: Li Ion Coordination Structures Prevail over Solid Electrolyte Interphases, *ACS Energy Lett.* 3 (2018) 335-340.

[179] H. Hu, M.B. Wu, Heavy oil-derived carbon for energy storage applications, *J. Mater. Chem. A* 8 (2020) 7066-7082.

[180] V.C. Hoang, M. Hassan, V.G. Gomes, Coal derived carbon nanomaterials-Recent advances in synthesis and applications, *Appl. Mater. Today* 12 (2018) 342-358.

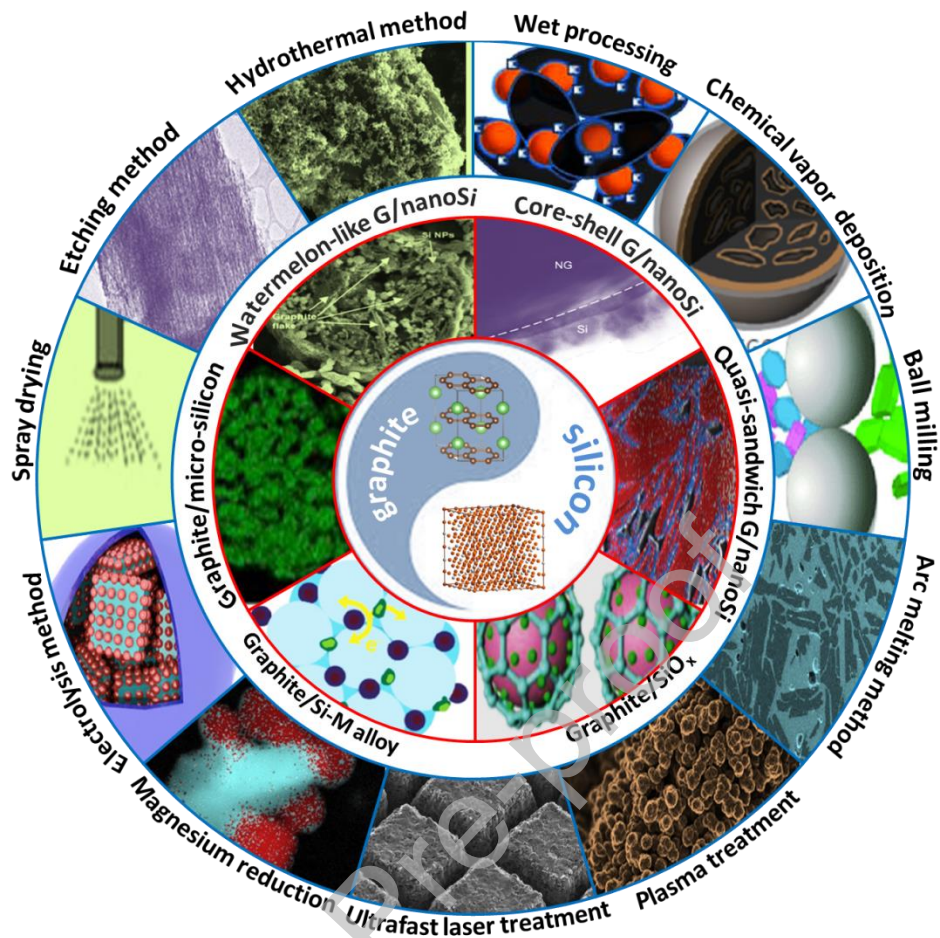


Fig. 1 Overview of Si-graphite composite electrode in lithium ion battery

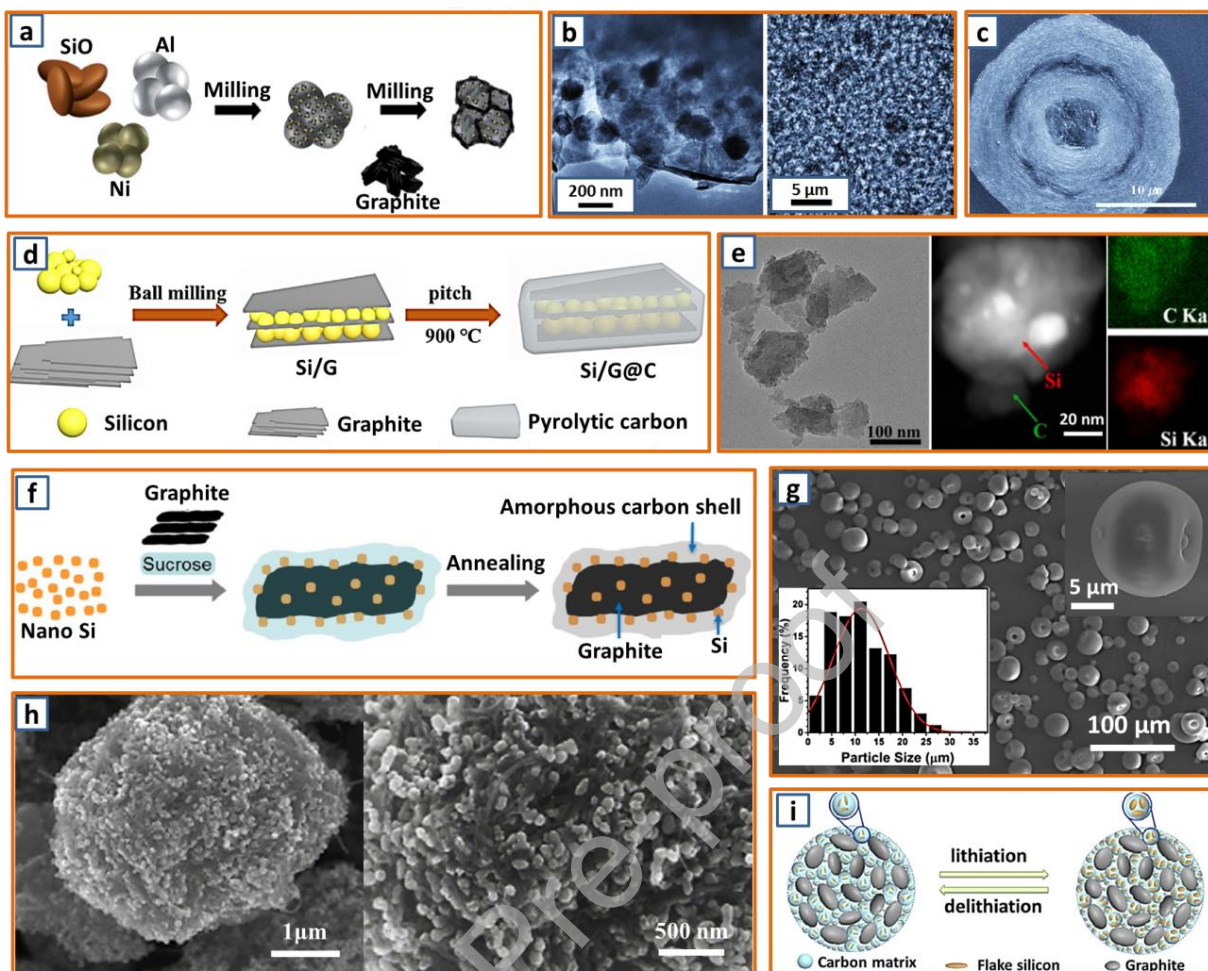


Fig. 2 Preparation of Si-graphite composite anodes through ball milling (a-e) and spraying method (f-i). (a) Schematic diagram of the formation of $\text{Si-NiSi}_2\text{-Al}_2\text{O}_3@\text{C}$ composites *via* the ball milling method. Reproduced with permission.[21] Copyright 2014, Royal Society of Chemistry. (b) TEM images of mechanically milled Si-based anode powders. Reproduced with permission.[22] Copyright 2015, Elsevier. (c) Cross-sectional SEM images of the Si/graphite/carbon composite sphere. Reproduced with permission.[23] Copyright 2008, Elsevier. (d) Schematic illustration of the preparation process of the $\text{Si}/\text{G}@\text{C}$ composites. Reproduced with permission.[24] Copyright 2019, Elsevier. (e) TEM image of the mechanically milled silicon nanoparticles and HADDF images of SiNPs-C composite with elemental mapping. Reproduced with permission.[25] Copyright 2019, American Chemical Society. (f) Schematic of the synthesis process of the SiGC composite. Reproduced with

permission.[26] Copyright 2018, Elsevier. (g) SEM image of the Si-based particles obtained from aerosol spray drying with particle size distribution inserted. Reproduced with permission.[27] Copyright 2019, Elsevier. (h) SEM image of the nanosilicon/CNT/pitch/graphite-based sphere. Reproduced with permission.[28] Copyright 2017, Elsevier. (i) Schematic illustration for the design of the hierarchically structured Si/C@NGs composite with Si embedded in between the natural graphite and encapsulated with an amorphous carbon shell. Reproduced with permission.[29] Copyright 2017, Elsevier.

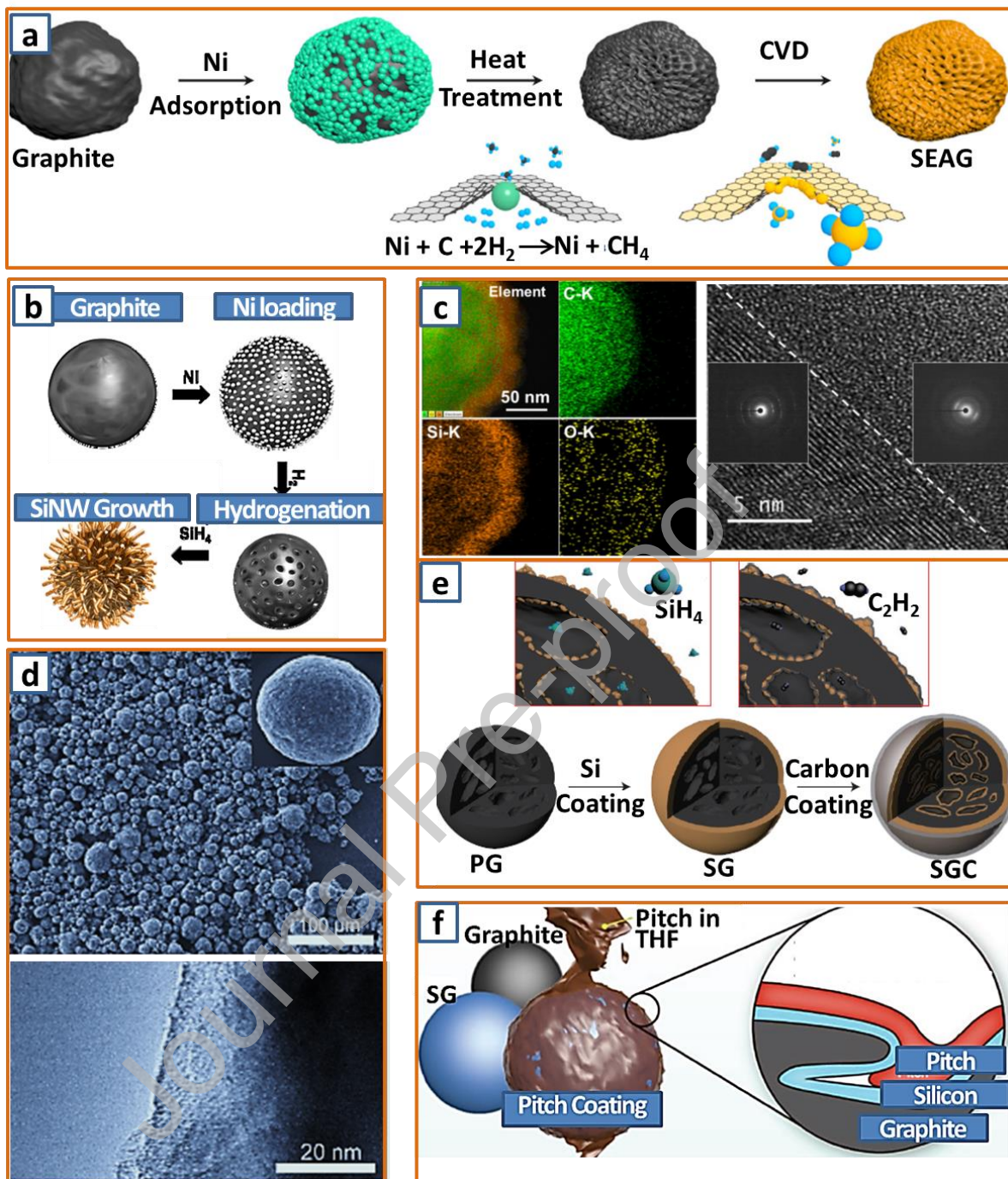


Fig. 3 Synthesis of Si-graphite anode *via* chemical vapor deposition strategy. (a) Fabrication of edge-plane activated graphite/Si nanolayer through CVD. Reproduced with permission.[43] Copyright 2017, Nature. (b) Schematic view for the synthesis process of Si nanowires internally grown in porous graphite. Reproduced with permission.[44] Copyright 2013, American Chemical Society. (c) Elemental mapping of G@a-Si and corresponding HR-

TEM images showing the interfacial region. Reproduced with permission.[45] Copyright 2019, Elsevier. (d) SEM and HRTEM of the carbon-coated nanosilicon/flake graphite microspheres. Reproduced with permission.[46] Copyright 2017, Wiley. (e) Schematic of the fabrication process of the Si-nanolayer-embedded graphite/carbon hybrids. Reproduced with permission.[47] Copyright 2016, Nature. (f) Schematic illustration of the pitch-coated Si-graphite composite fabricated *via* the CVD process. Reproduced with permission.[48] Copyright 2019, Wiley.

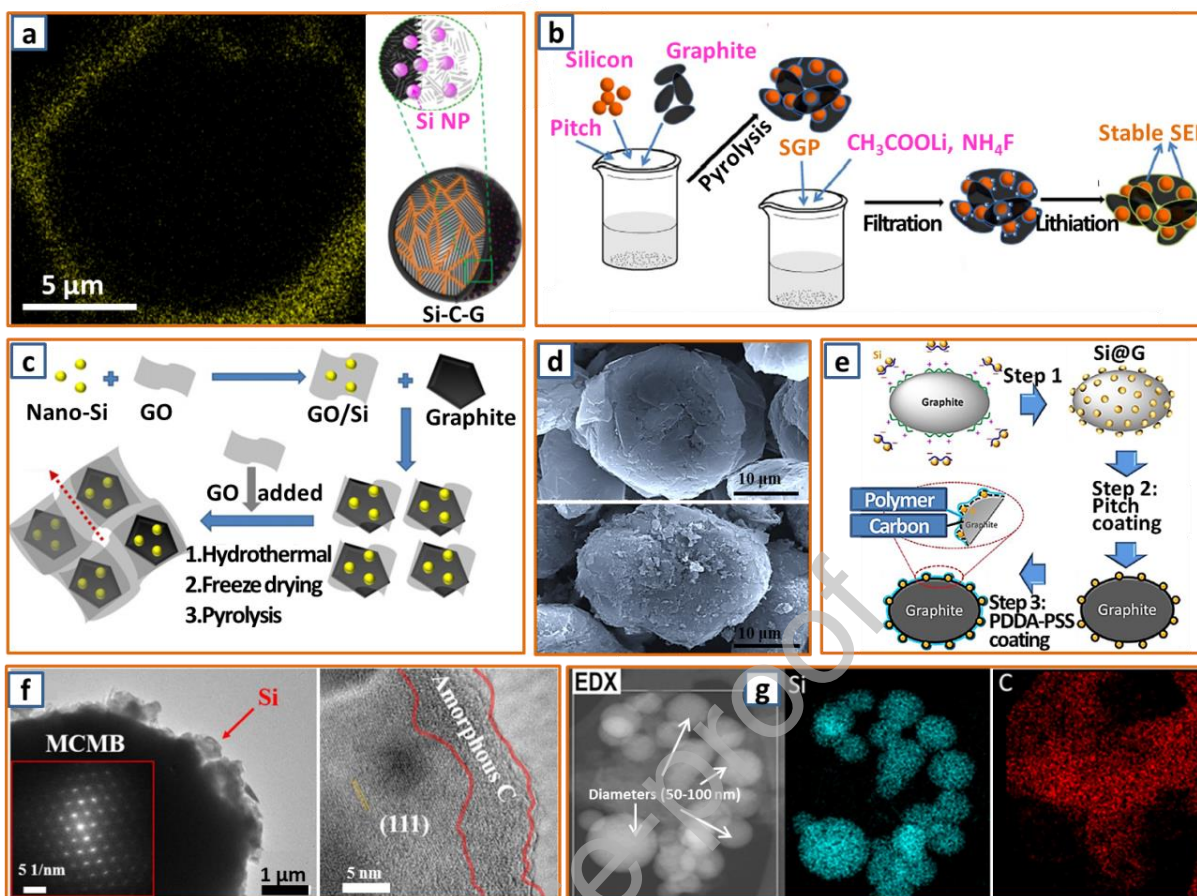


Fig. 4 Preparation of Si-graphite anode through wet process. (a) Illustration and cross-sectional elemental mapping of the Si-C-G composite. Reproduced with permission.[56] Copyright 2016, American Chemical Society. (b) Schematic illustration of the synthesis of the Si/graphite/carbon/LiF composite. Reproduced with permission.[57] Copyright 2017, Elsevier. (c) Schematic illustration for preparation of the G/Si/rGO aerogel. Reproduced with permission.[58] Copyright 2019, Marcel Dekker Inc. (d) SEM micrographs of the pristine and nanosilicon-coated graphite. Reproduced with permission.[59] Copyright 2007, Royal Society of Chemistry. (e) Schematics of the synthesis process of the polymer-based carbon/Si@graphite powder. Reproduced with permission.[60] Copyright 2015, Royal Society of Chemistry. (f) TEM images of designed Si/G/C composite. Reproduced with permission.[61] Copyright 2020, Elsevier. (g) EDX measurements of the obtained

Si/graphite/PANI nanocomposite. Reproduced with permission.[62] Copyright 2019, Elsevier.

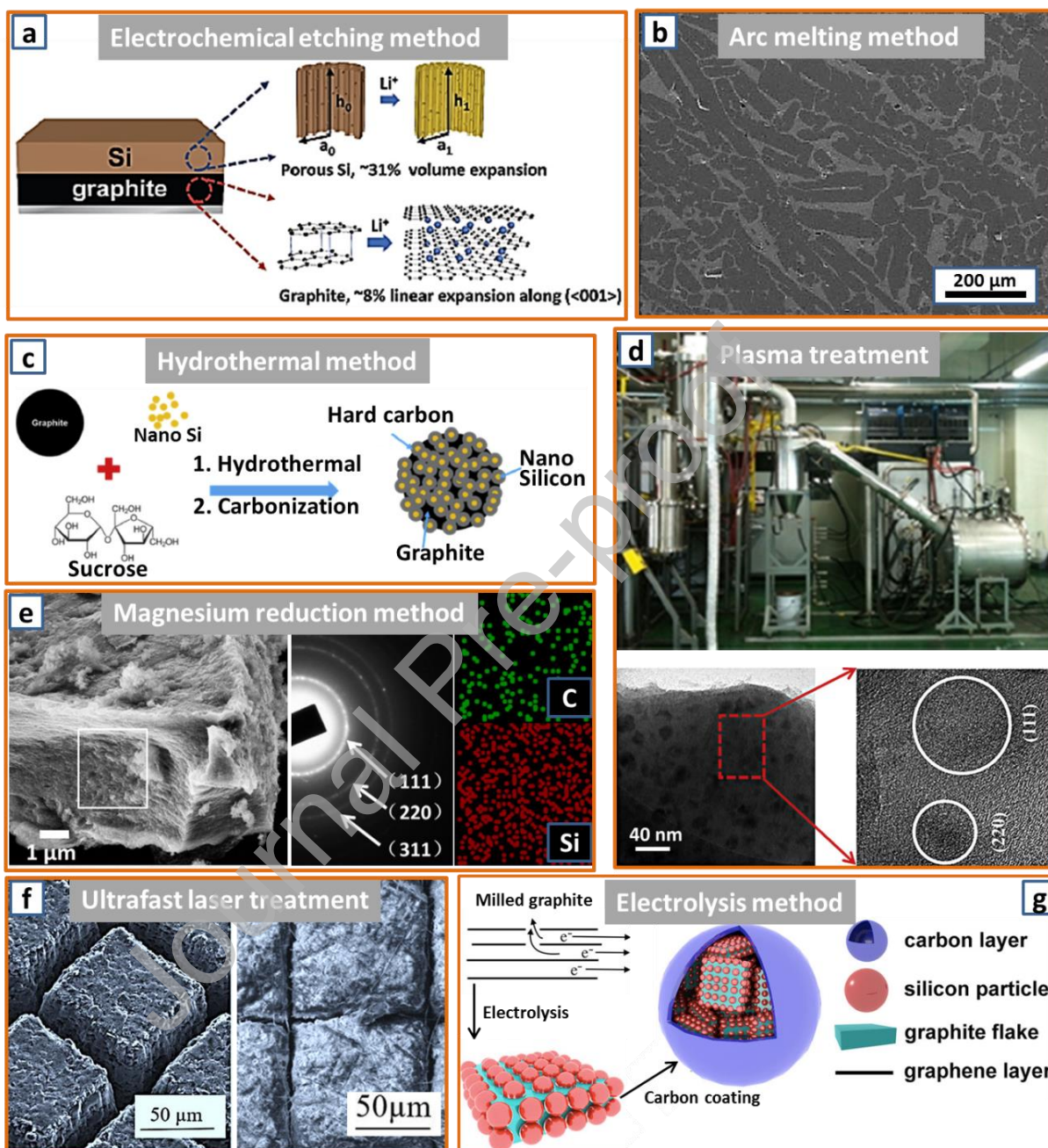


Fig. 5 Other methods for the synthesis of Si-graphite anode. (a) Schematic design of the porous Si/C-graphite electrode. Reproduced with permission.[64] Copyright 2017, Royal Society of Chemistry. (b) SEM image of the Si alloy before its combination with graphite. Reproduced with permission.[65] Copyright 2006, Elsevier. (c) Schematic illustration of the

synthesis of the interconnected HC-nSi/G. Reproduced with permission.[66] Copyright 2016, Elsevier. (d) The synthesis apparatus and TEM of the granulated SiO_x nanoparticles. Reproduced with permission.[67] Copyright 2014, Elsevier. (e) Cross-sectional SEM image, corresponding electron diffraction and elemental mapping images of PG-Si.[68] Copyright 2017, Elsevier. (f) SEM image of the ultrafast laser-generated submicron Si/graphite electrode before (left) and after (right) cycling. Reproduced with permission.[69] Copyright 2019, Elsevier. (g) Schematic diagram of the preparation of graphite/Si@carbon composites. Reproduced with permission.[18] Copyright 2020, Springer.

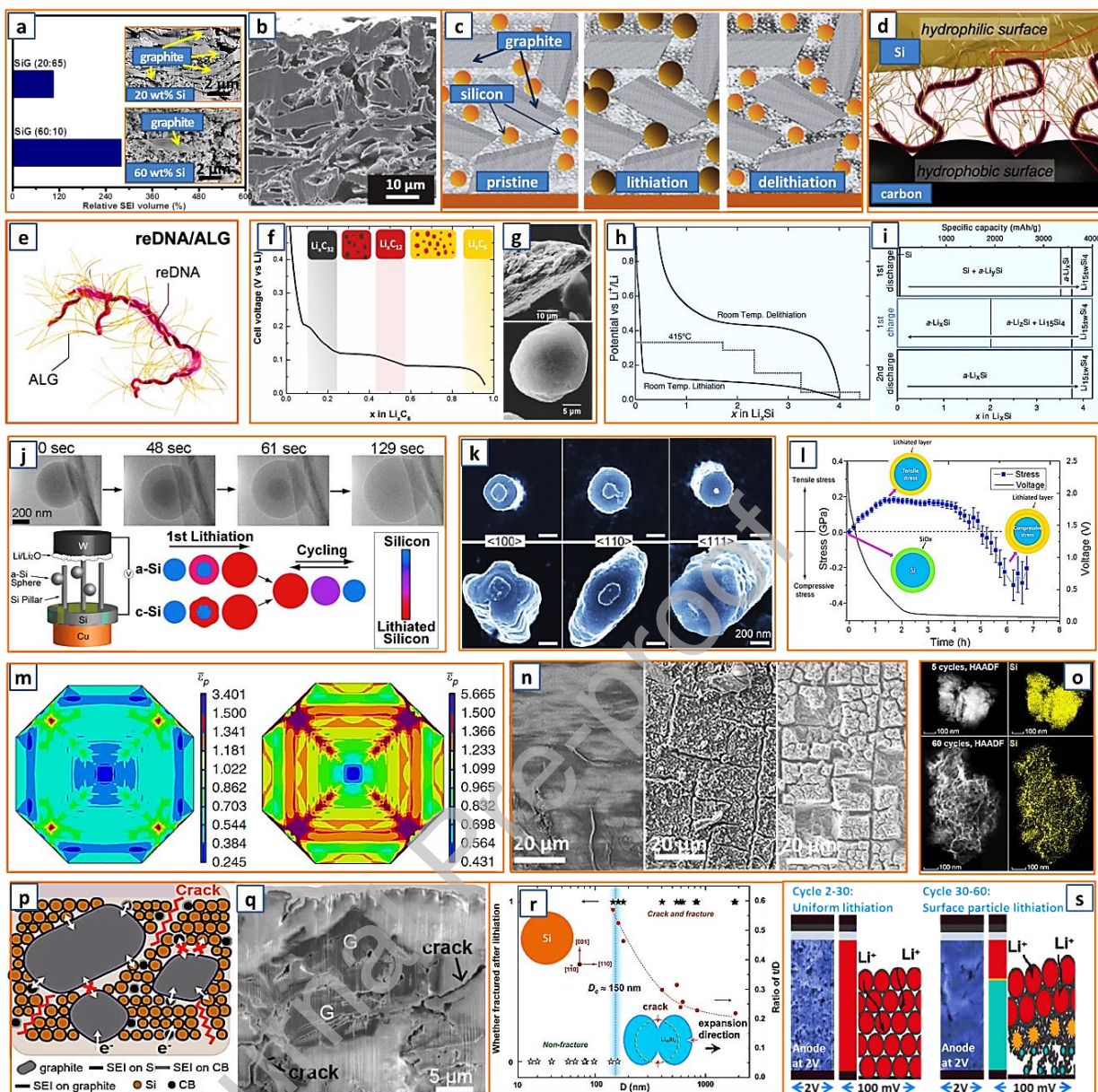


Fig. 6 Lithium storage behavior of Si-graphite anodes. (a) Relative SEI volume and inserted SEM images of Si-graphite composites with different silicon ratios. Reproduced with permission.[79] Copyright 2017, Electrochemical Society. (b) Cross-section images of Si-graphite composite with 5 wt% silicon. Reproduced with permission.[80] Copyright 2020, Electrochemical Society. (c) Illustration of structure change during lithiation of delithiation. Reproduced with permission.[81] Copyright 2019, Elsevier. (d) The proposed reDNA/ALG hybrid binder at Si/carbon interfaces, and (e) the schematic microstructure of reDNA/ALG. Reproduced with permission.[82] Copyright 2018, Wiley. (f) Potential profile of lithiated

graphite consists of multiple single and two-phase regions. Reproduced with permission.[83] Copyright 2012, Electrochemical Society. (g) Structural morphology of graphite particles. Reproduced with permission.[84] Copyright 2003, Wiley. (h) Coulometric titration curve for the Li-Si system at 415 °C (dotted line) and galvanostatic charge/discharge of a Si powder electrode at room temperature (solid line), and (i) the schematic summary of the phases formed as a function of specific capacity. Reproduced with permission.[85] Copyright 2013, Wiley. (j) In situ TEM test of the lithiation of a single a-Si sphere, and corresponding summary of the lithiation behaviors of a-Si and c-Si. Reproduced with permission.[86] Copyright 2013, American Chemical Society. (k) Anisotropic lateral expansion upon lithiation of crystalline Si. Reproduced with permission.[85] Copyright 2013, Wiley. (l) The calculated stress in Si nanoparticles. Reproduced with permission.[87] Copyright 2016, Elsevier. (m) Equivalent strain in fully lithiated (left) and delithiated (right) silicon, and (n) the surface morphology of silicon electrodes after 3, 8 and 50 cycles. Reproduced with permission.[88] Copyright 2016, Nature. (o) HAADF images of silicon particles after 5 and 60 cycles. Reproduced with permission. [89] Copyright 2018, Electrochemical Society. (p) Cross-sectional electron pathway and (q) SEM images of G-Si electrode after 100 cycles. Reproduced with permission.[90] Copyright 2018, Wiley. (r) The relationship between particle diameter and structural fracture. Reproduced with permission.[91] Copyright 2012, American Chemical Society. (s) Lithium ion diffusion in the increasingly dense anode structure. Reproduced with permission.[92] Copyright 2016, American Chemical Society.

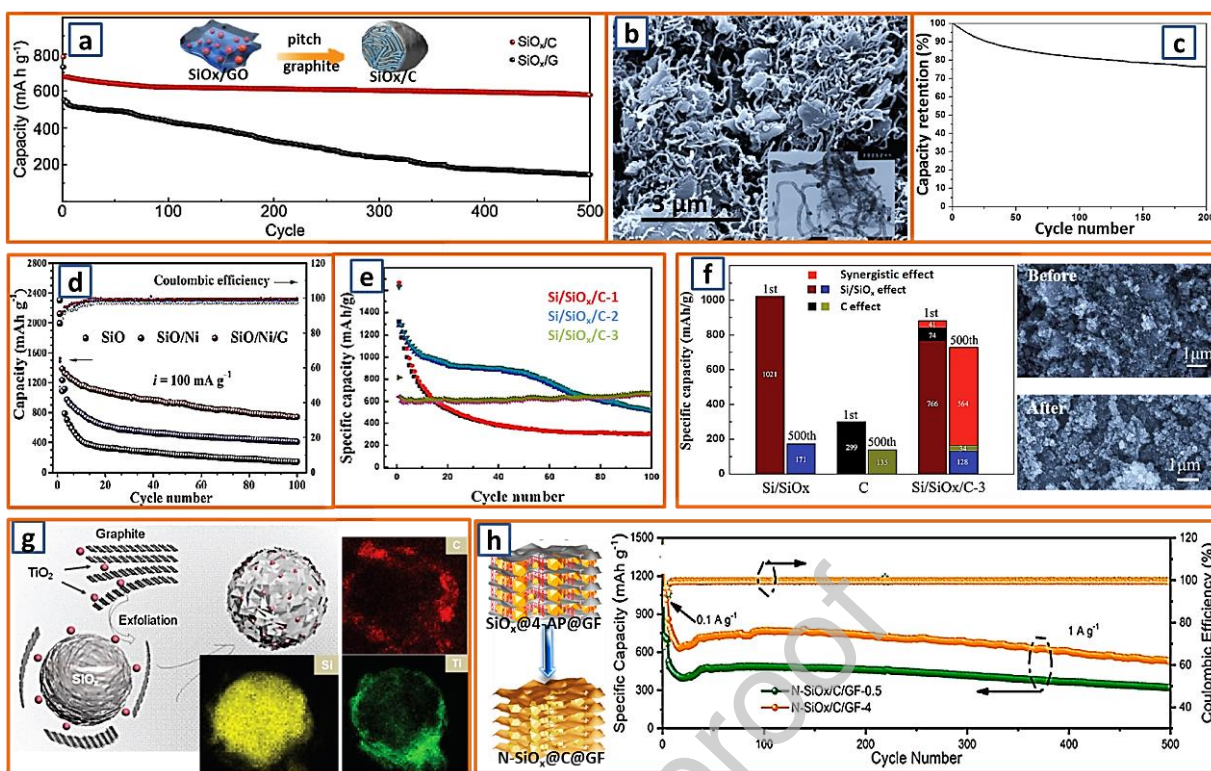


Fig. 7 Graphite/SiO_x ($0 < x < 2$) and its lithium storage performance. (a) Cycling performance of the SiO_x/C anodes at the mass loading of 3.5 mg cm^{-2} . Reproduced with permission.[72] Copyright 2017, Wiley. (b) SEM image of the CNTs-coated SiO/G with TEM image inserted. Reproduced with permission.[97] Copyright 2012, Springer. (c) Cycling retention of the full cell with graphite/SiO_x and Li(NiCoMn)O₂ as its anode and cathode, respectively. Reproduced with permission.[67] Copyright 2014, Elsevier. (d) Capacity and coulombic efficiency of SiO, SiO/Ni, and SiO/Ni/graphite electrodes over 100 cycles. Reproduced with permission.[34] Copyright 2015, Wiley. (e) The cycling performance of Si/SiO_x/C series, and (f) the 1st and 500th reversible charge specific capacities of Si/SiO_x, C, and Si/SiO_x/C-3 electrodes calculated based on experimental values with SEM images of Si/SiO_x/C-3 electrodes before and after cycling. Reproduced with permission.[35] Copyright 2017, Royal Society of Chemistry. (g) Schematic illustration of the exfoliation and self-assembly coating process towards SiO_x/TiO₂@MLG and its corresponding EDX mapping. Reproduced with permission.[98] Copyright 2020, Wiley. (h) Formation of N-SiO_x/C/GF composites and long-

term cycling performances of N-SiO_x/C/GF-0.5 and N-SiO_x/C/GF-4 electrodes. Reproduced with permission.[99] Copyright 2020, American Chemical Society.

Journal Pre-proof

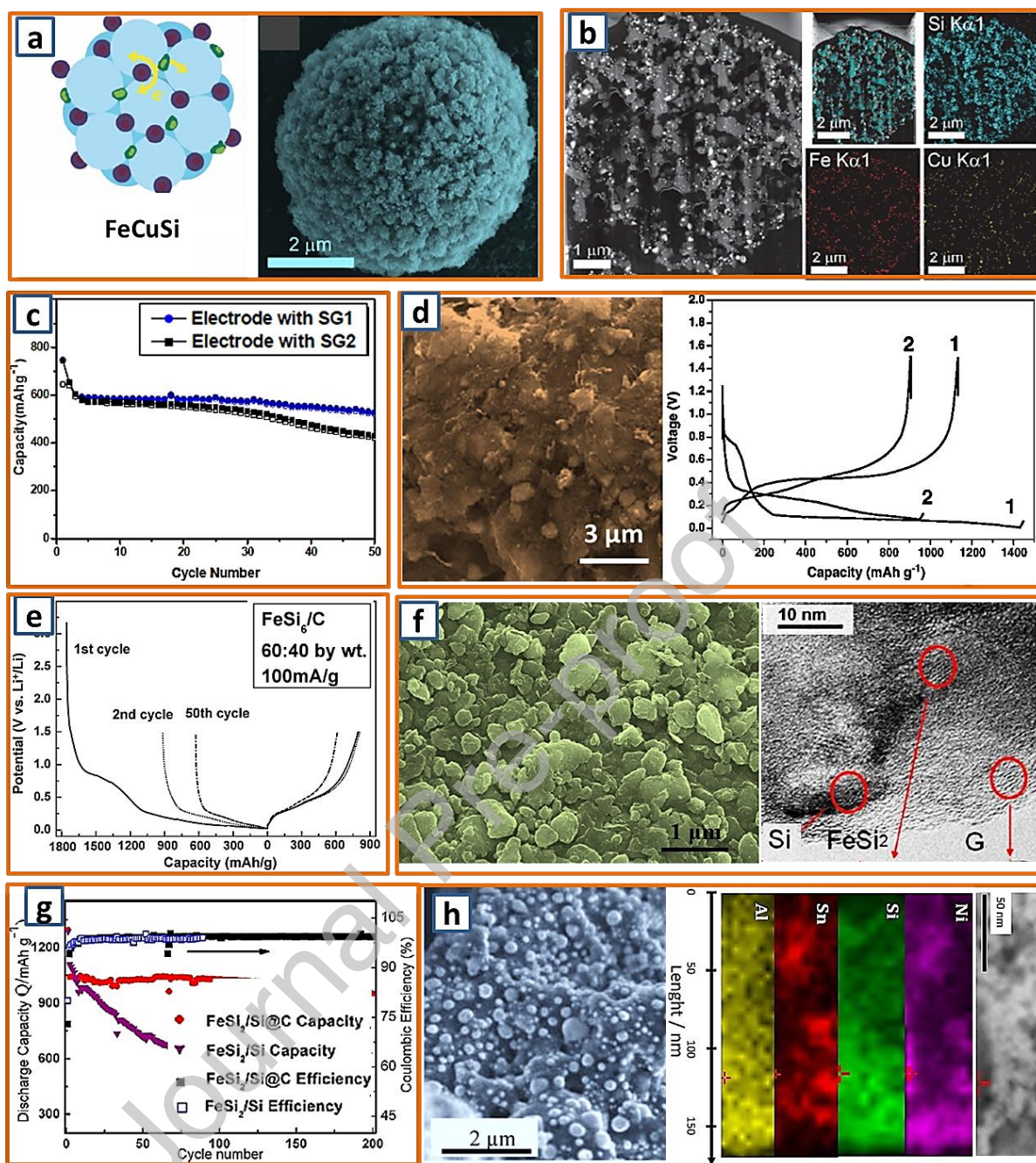


Fig. 8 Graphite/Si-metal composite and its lithium storage performance. (a) Schematic illustrations of FeCuSi, and (b) its HAADF-STEM image and EDS mapping in a cross-sectional view. Reproduced with permission.[41] Copyright 2016, Royal Society of Chemistry. (c) Charge/discharge performance of blended electrodes containing C/Si composite and graphite with two different particle sizes (SG1 or SG2). Reproduced with permission.[110] Copyright 2015, Elsevier. (d) Morphology and charge/discharge profile of the Si-Ni (6:1) alloy and graphite composite. Reproduced with permission.[65] Copyright

2006, Elsevier. (e) The discharge-charge profiles of the FeSi₆/C composite electrode. Reproduced with permission.[111] Copyright 2008, Elsevier. (f) SEM and TEM images of FeSi₂/Si@C composite and (g) its cycling performance. Reproduced with permission.[112] Copyright 2012, American Chemical Society. (h) SEM image of nanostructured Ni_{0.14}Sn_{0.17}Si_{0.32}Al_{0.037}C_{0.346} composite and EDX chemical mapping of complex matrix. Reproduced with permission.[113] Copyright 2011, Elsevier.

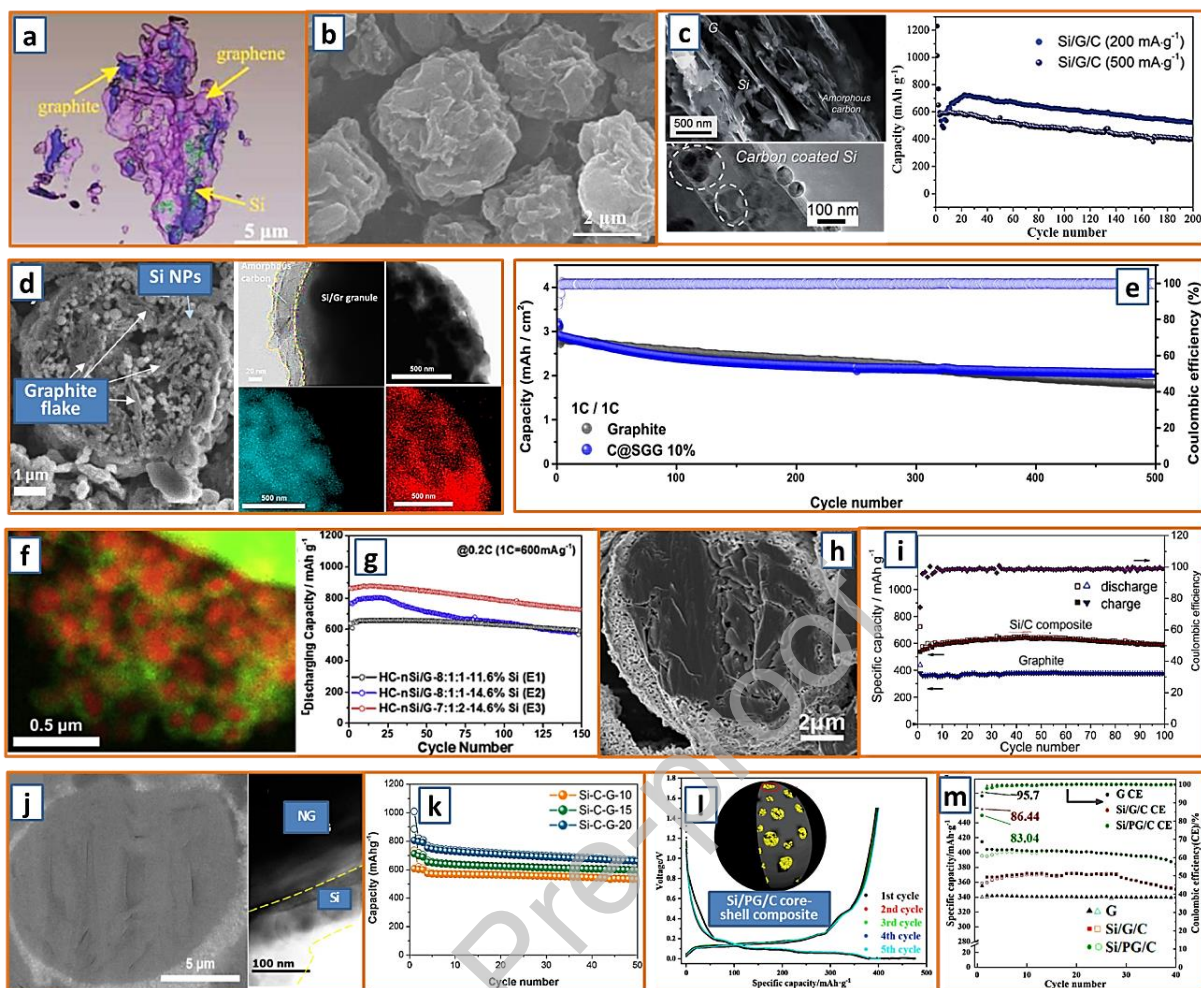


Fig. 9 The application of graphite/nanosilicon anodes with watermelon-like structure (a-e) and core-shell structure (f-m) in lithium ion batteries. (a) 3D microstructures of the Si/G/GF composite. Reproduced with permission.[13] Copyright 2018, Wiley. (b) Microstructure of the graphite/Si@reGO composite. Reproduced with permission.[118] Copyright 2013, Elsevier. (c) Cycling capacities of Si/G/C at 200 mA g⁻¹ and 500 mA g⁻¹, respectively. Reproduced with permission.[119] Copyright 2018, Royal Society of Chemistry. (d) SEM image of the cross-section of C@SGG and its TEM image with EDS-mapping. (e) Cycling performance of the full cells prepared with LCO/C@SGG with graphite at 1C rate. Reproduced with permission.[120] Copyright 2020, Elsevier. (f) Energy-dispersive X-ray spectroscopy elemental maps (green: carbon, red: Si) and (g) cycling performance of HC-nSi/G. Reproduced with permission.[121] Copyright 2016, Elsevier. (h) Cross profile of the

novel core-shell porous Si/C composite and (i) its corresponding cycling performance. Reproduced with permission.[42] Copyright 2013, Elsevier. (j) Core-shell images and (k) cycling performance of the Si-C-G anode. Reproduced with permission.[56] Copyright 2016, American Chemical Society. (l) The galvanostatic charge/discharge voltage profiles and (m) cycling performance of Si/PG/C. Reproduced with permission.[122] Copyright 2020, Wiley.

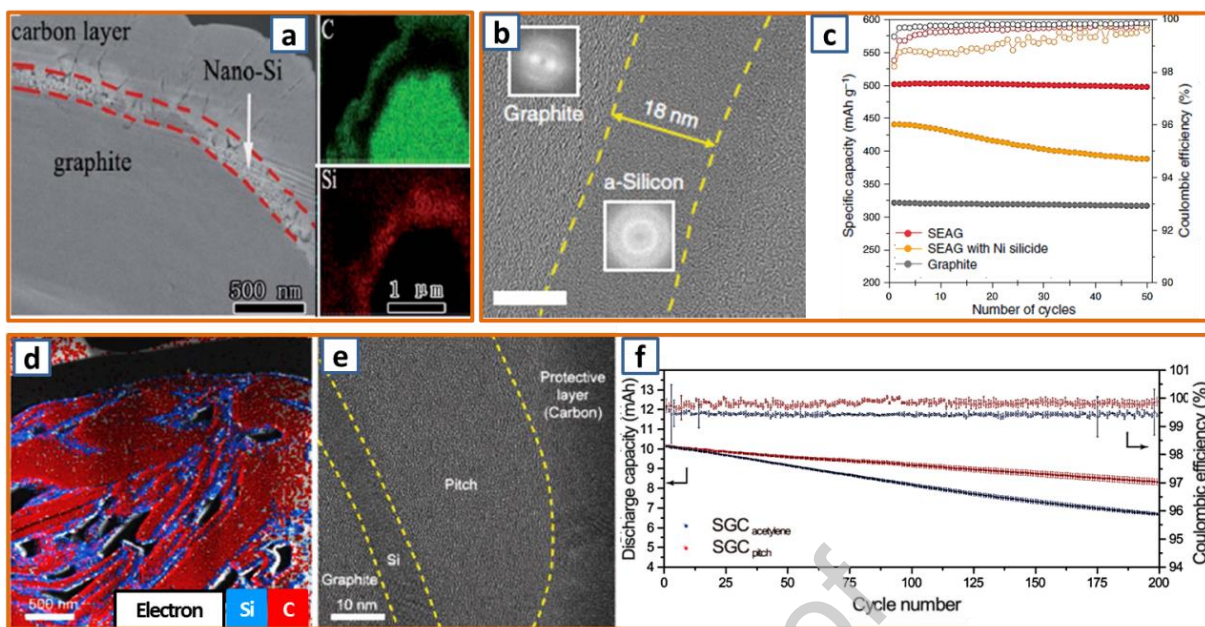


Fig. 10 The application of graphite/nanosilicon composite with quasi-sandwich structure in lithium ion battery. (a) Quasi-sandwich structure of the Si-G/C composite. Reproduced with permission.[63] Copyright 2018, Royal Society of Chemistry. (b) Quasi-sandwich structure of graphite/Si layer/carbon anode and (c) its charge/discharge properties. Reproduced with permission.[43] Copyright 2017, Nature. (d) EDS mapping, (e) HR-TEM image, and (f) electrochemical performance of the SGC_{pitch} anode. Reproduced with permission.[48] Copyright 2018, Wiley.

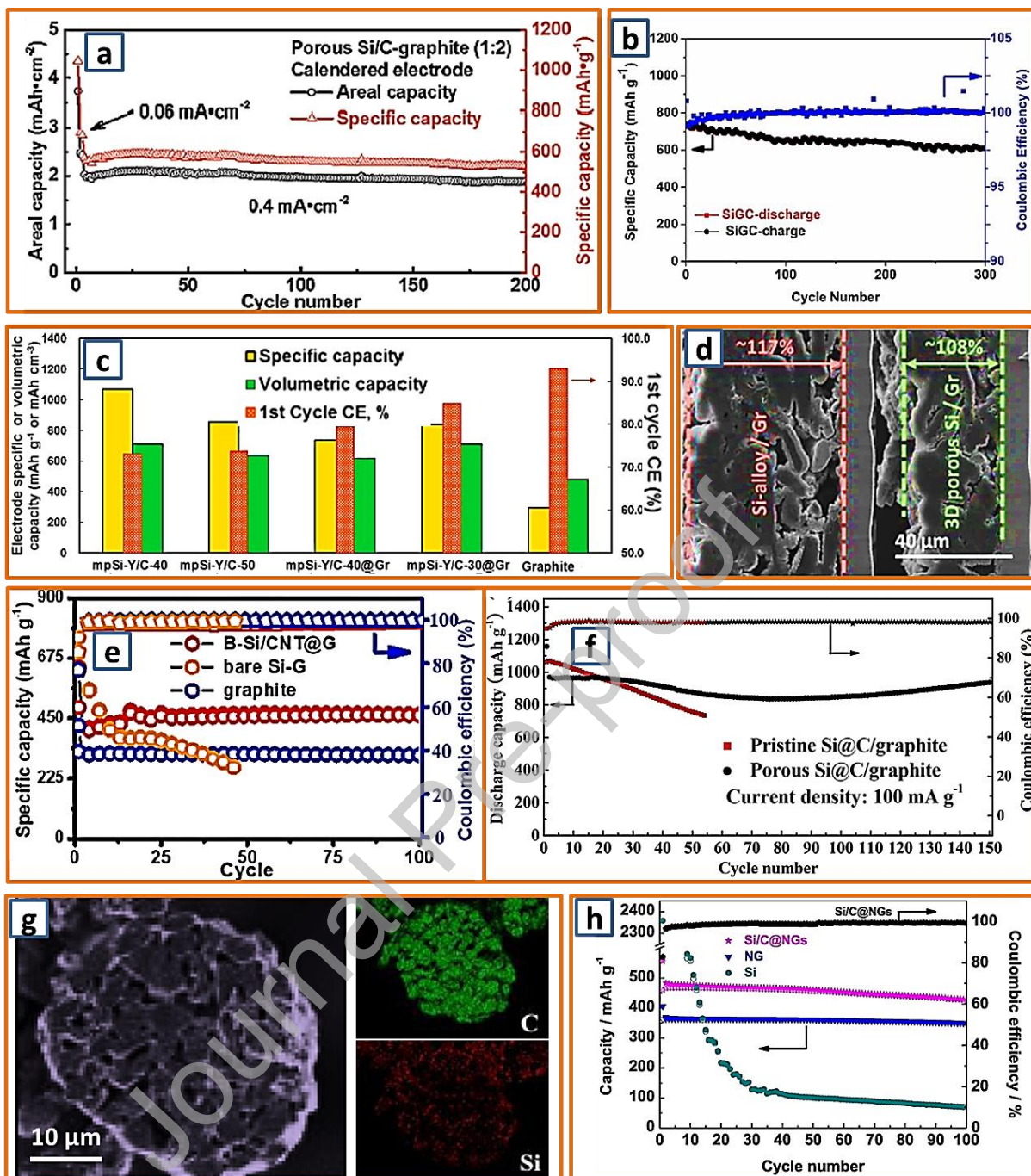


Fig. 11 The lithium storage performance of graphite/microsilicon. (a) Long-term cycling of the electrode with a porous Si/C to graphite ratio of 1:2. Reproduced with permission.[64] Copyright 2017, Royal Society of Chemistry. (b) Cycling performance of SiGC composite. Reproduced with permission.[26] Copyright 2018, Elsevier. (c) Electrode specific and volumetric capacities, and 1st cycle coulombic efficiencies of the mesoporous Si-based composites. Reproduced with permission.[71] Copyright 2018, American Chemical Society.

(d) Cross-sectional SEM image of Si-alloy/Gr and 3D porous Si/Gr electrodes. Reproduced with permission.[123] Copyright 2018, Wiley. (e) Cycling performance of B-Si/CNT@G, bare Si-G, and graphite. Reproduced with permission.[76] Copyright 2019, American Chemical Society. (f) Cycle performance of porous Si@C/G and pristine Si@C/G electrodes. Reproduced with permission.[33] Copyright 2017, Elsevier. (g) STEM images of Si/C@NGs composite with elemental mapping and (h) its cycling performance at 0.1 A g^{-1} . Reproduced with permission.[29] Copyright 2016, Elsevier.

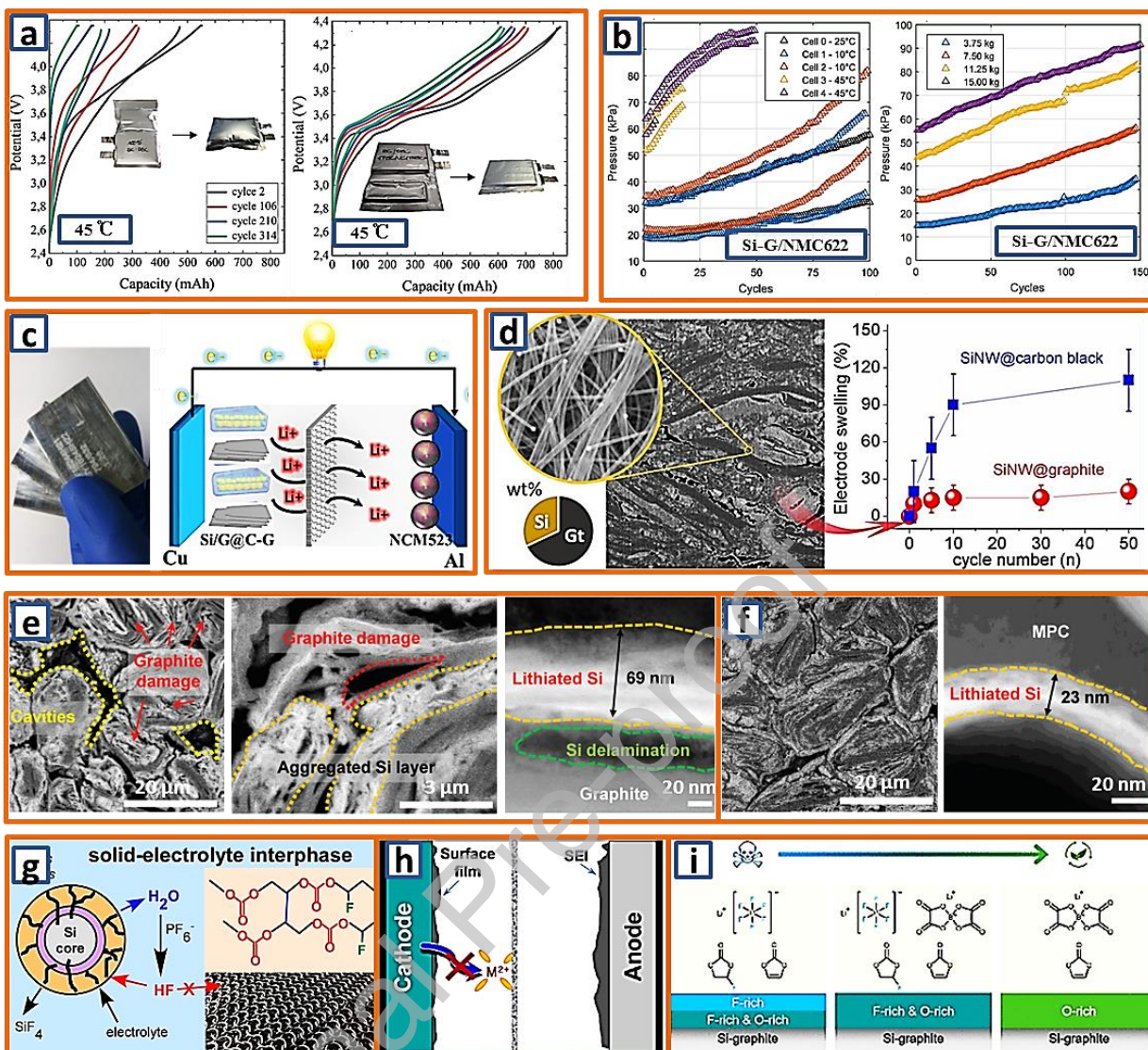


Fig. 12 Current issues in material aspect. (a) Potential vs. capacity profiles of NMC622/Si-Gr pouch cells cycled at high temperature in base electrolyte (left) and TEOSCN(1 wt%) modified electrolyte (right). Reproduced with permission.[136] Copyright 2020, Royal Society of Chemistry. (b) Influence of different cycling conditions on the mechanical behavior of Si-G/NMC622 cells. Reproduced with permission.[137] Copyright 2020, Elsevier. (c) The photo and schematic image of the Si/G@C-G and NCM523 full cell. Reproduced with permission.[24] Copyright 2019, Elsevier. (d) Microstructure and suppressed electrode swelling of Gt-SiNW composite anode. Reproduced with permission.[138] Copyright 2020, American Chemical Society. Cross-sectional SEM and TEM images of (e) CSG and (f) MPC and Li⁺ diffusion in Si delamination. (g) Solid-electrolyte interphase (SEI) formation. (h) SEI film on anode. (i) F-rich, F-rich & O-rich, and O-rich Si-graphite structures.

C/Si@MPC-G electrodes. Reproduced with permission.[139] Copyright 2020, Wiley. (g) The schematic protection of silicon particle by poly-FEC-derived SEI layer. Reproduced with permission.[96] Copyright 2017, American Chemical Society. (h) Schematic illustration for interfacial stability of full-cells cycled in with blended additives of FEMC-VC. Reproduced with permission.[93] Copyright 2016, Elsevier. (i) Influence of fluorine-free electrolytes on silicon-graphite anode. Reproduced with permission.[140] Copyright 2020, American Chemical Society.

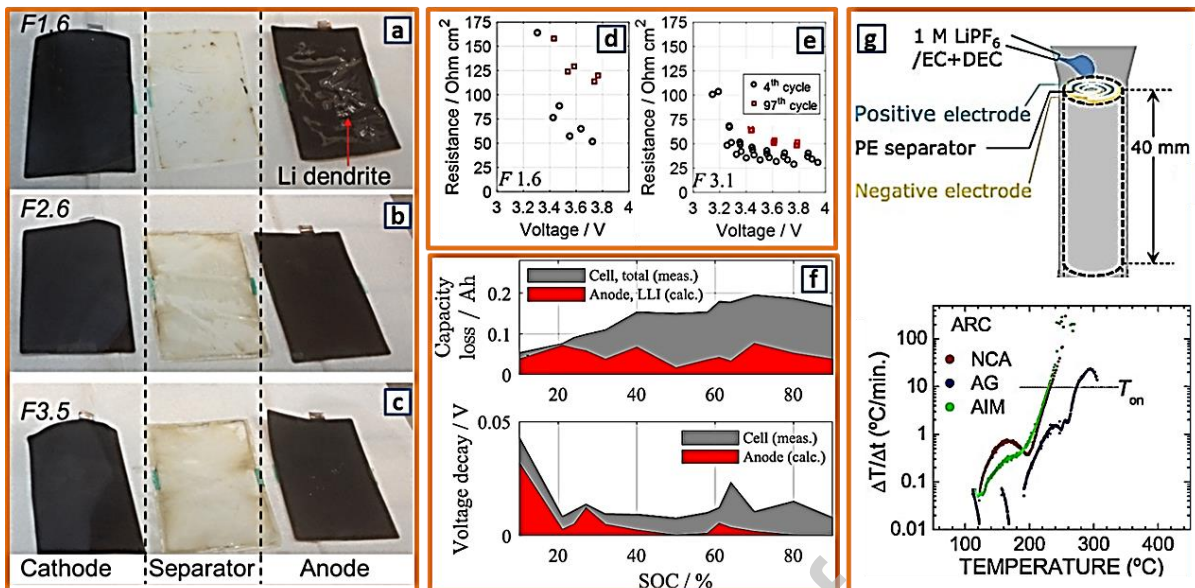


Fig. 13 Current issues in battery assemble aspect. (a-c) Images of Si-graphite/NMC pouch cells with different electrolyte volume (F1.6, F2.6, and F3.5) after 100 cycles. (d,e) Resistance of Si-graphite/NMC532 cells at fourth and 97th cycle with different electrolyte volume. Reproduced with permission.[144] Copyright 2017, American Chemical Society. (f) Measured total capacity loss and voltage decay 18650 nickel-rich/Si-graphite full cell. Reproduced with permission.[145] Copyright 2019, Elsevier. (g) Schematic structure of the microcell and its corresponding temperature dependence of $\Delta T/\Delta t$. Reproduced with permission.[146] Copyright 2017, Elsevier.

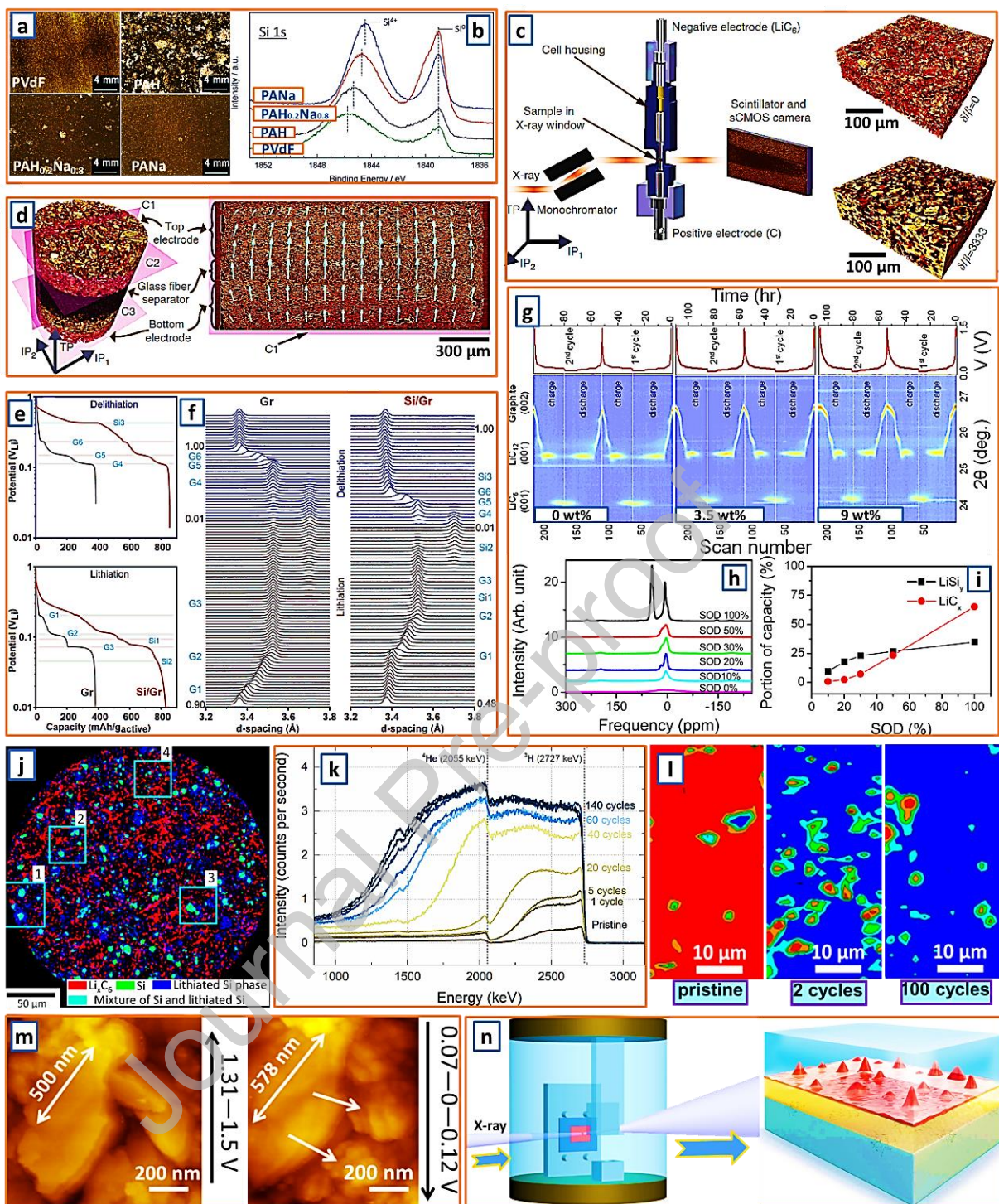


Fig. 14 Advanced detection techniques in Si-graphite characterization. (a) Morphology images and (b) Si 1s HAXPES spectra of the surface of the Si-graphite composite electrodes with 10 wt% PVdF, PAH, PAH_{0.2}Na_{0.8} and PANa binders. Reproduced with permission.[150] Copyright 2015, Royal Society of Chemistry. (c) Sketch of the electrochemical cell and the measurement setup of operando tomography, including a coordinate system indicating the two IP detectors. (d) Schematic diagram of the electrode structure and the X-ray tomography setup. (e) Delithiation and Lithiation curves. (f) XRD patterns. (g) Operando XRD patterns showing the evolution of peaks over time. (h) NMR spectra. (i) Portion of capacity vs SOD. (j) EDS mapping. (k) RBS spectra. (l) EDS maps. (m) AFM topography. (n) Schematic of the AFM-XRD setup.

IP directions and the TP direction. (d) Schematic of the two electrodes, the separator (black) and the cuts C1, C2, and C3 (purple), and the corresponding vertical cut with superimposed vector field. Reproduced with permission.[151] Copyright 2016, Nature. (e) Electrode potential *versus* capacity (normalized to the total mass of active materials) and (f) operando XRD spectra (in the 3.2-3.8 Å d-spacing range) during lithiation and delithiation of the Gr and the Si-Gr cells. Reproduced with permission.[152] Copyright 2019, Wiley. (g) *In-situ* XRD patterns during 1st and 2nd cycle of blended electrodes with different nanosilicon contents. (h) NMR spectrum of blended anode with different state of discharging during discharging process. (i) Calculated portion of capacities of LiC_x(red) and LiSi_y(black) from *ex-situ* NMR spectra of samples (silicon content, 9 wt%) with different SODs. Reproduced with permission.[153] Copyright 2017, Elsevier. (j) X-ray diffraction computed tomography taken at the beginning of the charge step showing a phase-distribution map of LiC₁₂ (red), crystalline Si (green), and lithium silicides Li_xSi (blue). Reproduced with permission.[154] Copyright 2019, American Chemical Society. (k) Neutron depth profiling spectra of SiG electrodes. Reproduced with permission.[155] Copyright 2018, Electrochemical Society. (l) Raman maps of Si-Gr anodes taken before cycling (pristine), after 2 cycles, and after 100 cycles. Reproduced with permission.[156] Copyright 2018, American Chemical Society. (m) *In situ* AFM images of microsilicon during lithiation. Reproduced with permission.[157] Copyright 2018, Elsevier. (n) Operando electrochemical cell configuration and schematic multilevel interface probed by FFDXM. Reproduced with permission.[158] Copyright 2020, nature.

Table 1. Summary of the preparation of various silicon-graphite anodes in LIB

Name	Silicon source	Graphite source	Silicon ratio	Synthesis strategy	Ref.
Si–NiSi ₂ –Al ₂ O ₃ @C	SiO (325 mesh)	Commercial graphite	27.3%	Ball milling	[21]
Fe-Cu-Si/Graphite	Nanosilicon	Natural graphite	<i>ca.</i> 7%	Spraying method	[41]
AG@a-Si	Silane gas	MCMB graphite	4.7%	Chemical deposition vapor	[45]
Porous Si/C-graphite	Microsilicon	MCMB graphite	25%	Electrochemical etching	[64]
Nanosilicon-C@G	Nanosilicon	Spherical graphite	15%	Wet process	[56]
Si/C microsphere	Nanosilicon	Flake graphite	12.5%	Spraying method	[46]
Si/graphite/PANI	Amine-functionalized Si NPs	Carboxyl-functionalized graphite	60%	Wet process	[62]
Edge activated graphite/Si	Silane gas	Spherical graphite	10%	Chemical vapor deposition	[43]
mpSi-Y/C-30@Gr	Microsilicon	--	42%	Magnesium reduction	[71]
SiO _x /GO/FG@Ptich	SiO _x	Artificial graphite (22.8 μm)	30% (SiO _x)	Ball milling	[72]
SiO _x /Graphite	SiO _x	--	3% (SiO _x)	Plasma treatment	[67]
Si@amorphous carbon/graphite	Al-Si alloy (10 μm)	Commercial graphite	13.58%	Ball milling	[33]
Walnut-structure Si–G/C	Nanosilicon	Spherical graphite	<i>ca.</i> 20%	Wet process	[63]
LiF and pitch comodified silicon/graphite	Nanosilicon (30 nm)	Flake graphite (1μm)	14.6%	Wet process	[57]
Silicon/carbon/graphite composites	Microsilicon (0.8 um)	Graphite (30 μm)	15%	Ball milling	[73]
Phenolic resin-pyrolyzed carbon based Si/C	Nanosilicon (30 nm)	Flake graphite (0.5 μm)	15%	Wet process	[74]

Table 1 (continued)

Name	Silicon source	Graphite source	Silicon ratio	Synthesis strategy	Ref.
Double core-shell Si/G/C	Si wastes from solar plants	MCMB graphite	30%	Wet process	[61]
Silicon-metal-graphite	Silane gas	Flake graphite (6.0 μm)	3.0%	Chemical vapor deposition	[55]
Copper silicide-coated graphite	Silane gas	Commercial graphite (6.0 μm)	3.1%	Chemical vapor deposition	[52]
Spray-dried Si/graphite	Nano sphere silicon	Flake graphite	36.3%	Spraying method	[75]
Si/graphite/amorphous carbon	Nanosilicon	Natural graphite (<i>ca.</i> 20 μm)	8%	Spraying method	[42]
Natural graphite coated by Si nanoparticles	Nanosilicon	Natural graphite	10%	Wet process	[59]
Nano/microstructured silicon-graphite	Microsilicon (5 μm)	Commercial graphite	8.5%	Ball milling	[76]
Nanostructured silicon/graphite	Microsilicon	Commercial graphite	<i>ca.</i> 10%	Ball Milling	[77]
Micrometer-sized silicon	Microsilicon (0.5 μm)	Commercial graphite	22%	Ball milling	[78]
Si@G electrodes	Nanosilicon	Commercial graphite	30%	Ball milling	[37]
Porous Si/graphite/carbon nanotube@C	Nanosilicon (30 nm)	Flake graphite	33%	Spraying method	[28]
Porous Si/C-graphite	Si wafer	MCMB graphite	<i>ca.</i> 30%	Electrochemical etching	[64]
Si-Ni alloy-graphite composite	Si wafer	Graphite (17 μm)	--	Arc melting method	[65]
HC-nSi/G	Nanosilicon (<i>ca.</i> 50 nm)	Graphite (10 μm)	14.6%	Hydrothermal method	[66]
Graphite/silicon@carbon	Silica (20–30 nm)	Commercial graphite	--	Electrolysis method	[18]
3D silicon/graphite composite	Nanosilicon (100 nm)	Graphite (15 μm)	20%	Ultrafast laser treatment	[69]
Graphite/Si nanowire composite	Silane gas	MCMB graphite	20%	Chemical vapor deposition	[44]

Table 2. Summary of the lithium storage performance of typical silicon-graphite anodes

Name	ICE	Current	Capacity	Cut voltage	Retention	Ref.
Pitch/Si layer-graphite	90.9%	0.1 C	523 mAh/g	0.005–1.5 V	81.9% /200 cycles	[48]
Graphene-scaffolded silicon/graphite	75.6%	75 mA/g	559 mAh/g	0.005–1.5 V	90% /100 cycles	[13]
Spherical Si/C granules	90.8%	45 mA/g	471 mAh/g	0.005–1.0 V	86%/500 cycles	[129]
Silicon@graphite/carbon microsphere	74%	200 mA/g	587 mAh/g	0.01–1.5 V	90%/300 cycles	[130]
Graphite/silicon/pyrolyzed carbon	77.9%	0.1 C	637.7 mAh/g	0.005–2.5 V	89.5% /100 cycles	[131]
Natural graphite coated by Si nanoparticles	65.7%	0.2 C	567 mAh/g	0.01–2 V	96.4% /20 cycles	[59]
Ternary Si/graphite/pyrolytic carbon	80%	100 mA/g	818 mAh/g	0.01–1.5 V	83.6% /300 cycles	[26]
Flake graphite/silicon/carbon	69.7%	60 mA/g	602.7 mAh/g	0.02–1.5 V	92%/20 cycles	[132]
Silicon nanolayer-embedded graphite	92%	0.5 C	525 mAh/g	0.005–1.5 V	96%/100 cycles	[47]
Polymer carbon coated Si-on-graphite	98%	0.1 C	450 mAh/g	0–1.5 V	95%/200 cycles	[60]
Si-graphite composite	87%	140 mA/g	568 mAh/g	0.008–1.5 V	78%/30 cycles	[133]
Spherical silicon/graphite/carbon	86%	0.2 mA/cm ²	700 mAh/g	0.02–1.5V	93%/50 cycles	[23]
Walnut-structured Si–G/C	90.6%	500 mA/g	687.7 mAh/g	0.001–1.5 V	81% /1200 cycles	[63]
LiF and pitch modified Si/graphite	83%	100 mA/g	630 mAh/g	0.01–2 V	82.3% /100 cycles	[57]
Silicon/carbon/graphite composite	81.5%	0.3 mA/cm ²	708 mAh/g	0–1.5 V	77.5% /20 cycles	[73]
Hard carbon coated nanosilicon/graphite	ca. 80%	120 mA/g	638.6 mAh/g	0.005–1.5V	92.1% /150 cycles	[66]
Silicon coated natural graphite	72.7%	37.2 mA/g	458.8 mAh/g	0–2V	85.4% /50 cycles	[68]
Copper silicide-coated graphite	83%	0.2 C	480 mAh/g	0–2V	87%/30 cycles	[52]
Spray-dried Si/graphite	78.1%	300 mA/g	741.2 mAh/g	0.01–2 V	82.4% /100 cycles	[75]

Table 2 (continued)

Name	ICE	Current	Capacity	Cut voltage	Retention	Ref.
Silicon/graphite/amorphous carbon	75.2%	100 mA/g	ca.600 mAh/g	0.01–1 V	94.9% /100 cycles	[42]
Graphite/silicon/graphene	74.5%	50 mA/g	575.1 mAh/g	0.01–2 V	73.1% /50 cycles	[118]
Sub-micron silicon/C @natural graphite	82.8%	100 mA/g	428.1 mAh/g	0.01–1.5 V	82.8% /100 cycles	[29]
Porous carbon/silicon nanowire/graphite	82.1%	0.2 C	530 mAh/g	0.1–3 V	70%/100 cycles	[134]
Nanosilicon/graphite/CNT	81%	100 mA/g	863.2 mAh/g	0.01–2 V	81.3% /100 cycles	[28]
SiNWs-G	91%	0.2 C	1014 mAh/cm ³	0.005–1.4 V	ca. 100% /100 cycles	[44]
Si/graphite@graphene	78%	100 mA/g	800 mAh/g	0.01–2 V	83.4% /20 cycles	[40]
Nanosilicon in G/C microplates	56.3%	500 mA/g	400 mAh/g	0.05–3 V	66.7% /200 cycles	[119]
Nanosilicon/graphite/commercial CNT	93%	350 mA/g	1363 mAh/g	0.02–1.5 V	86%/35 cycles	[78]
Bulk silicon/graphite/pitch	86.4%	140 mA/g	530 mAh/g	0.008–1.5 V	78%/30 cycles	[133]
Nanosilicon/graphite/pitch	86%	0.2 mA/cm ²	700 mAh/g	0.02–1.5 V	92.8% /50 cycles	[23]
l-rSi/Gr	78.5%	0.1 C	670 mAh/g	0.01–3 V	65%/200 cycles	[135]
Graphite/silicon@carbon	87.4%	120 mA/g	580 mAh/g	0.005–2 V	80%/200 cycles	[18]
30 wt% Si-C/graphite	84%	0.5 mA/cm ²	756 mAh/g	0.01–1.2 V	90%/200 cycles	[27]
AG@a-Si-90	93.8%	1.3 A/g	384 mAh/g	0.001–1.5 V	83%/200 cycles	[45]
Si/graphite/PANI	86.2%	1.25 A/g	2000 mAh/g	0.02–2.0 V	76%/500 cycles	[62]
Double core-shell Si/G/C	87.8%	0.2 C	847 mAh/g	0.05–1.5 V	79%/500 cycles	[61]
Si@G electrodes	77%	250 mA/g	850 mAh/g	0.05–0.9 V	84%/100 cycles	[37]
SiNPs-C/G	67.2%	100 mA/g	505 mAh/g	0.01–2 V	91.5% /500 cycles	[25]
Si/C-AG	64%	500 mA/g	445 mAh/g	0.01–1.5 V	94%/200 cycles	[128]

Graphical Abstract

